Linear and nonlinear study of drift waves in nonthermal distributed electrons

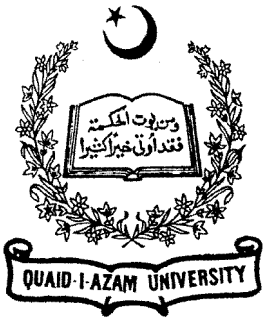

By

Javed Iqbal

Department of Mathematics
Quaid-i-Azam University, Islamabad
PAKISTAN
2017

Contents

1 Introduction **7**

2 Toroidal ITG Driven Vortices in Nonuniform Magnetoplasma **18**

2.1 Preamble 18

2.2 Mathematical Formulation 19

2.3 Linear Analysis 23

2.4 Stationary Solutions 27

2.5 Conclusion 32

3 Tripolar Vortices in ITG Mode in Nonuniform Magnetoplasma **33**

3.1 Introduction 33

3.2 Model Equations 35

3.3 Tripolar Vortices 38

3.4 Conclusions 46

4 Sheared Driven Ion Acoustic Vortex Formation in Two-Electron-Temperature Plasma **47**

4.1 Introduction 47

4.2 Nonlinear Model Equations 48

4.3 Derivation of Dispersion Relation 51
4.4 Nonlinear Analysis 53
4.5 Summary 58

5 Electron acoustic soliton in magneto-rotating e-p-i plasma 59

5.1 Introduction 59
5.2 Derivation of Linear Dispersion Relation 60
5.3 Derivation of kdV Equation 64
5.3.1 Solution of KdV Equation 68
5.4 Discussion of Results 69
5.5 Conclusion 75
5.6 Future Work 76

List of Figures

2-1 Plot of real part of frequency versus k_y, for various values of $\kappa = 3$(solid line), $\kappa = 4$ (dotted line), and $\kappa = 6$ (dashed line). 25

2-2 Plot of Imaginary part of wave frequency versus k_y, for numerous values of $\kappa = 3$(solid line), $\kappa = 4$ (dotted line), and $\kappa = 6$ (dashed line) 26

2-3 Vortex chains profile obtained from Eq. (2.30) for the tokamak parameters. 31

3-1 Fig.1. (colored online only) A shadowgraph of 3D view of the normalized electrostatic potential for $\kappa = 3$ case for other plasma parameters given in the text. 45

3-2 Shadow graph of 3D view of the normalized potential for $\kappa -> \infty$ case in which the electrons follow classical Bolzmann type distribution with the same other parameters as taken in Fig.3-1. 46

4-1 Plot of normalized growth rate as a function of $k_z\rho_i$ for the parameters described in the text. The black solid line is for $\alpha = 0.22$ and the red one is for $\alpha = 0.1$. 52

4-2 The plot of potential ϕ in the contour form in (x, ξ) plane is shown for the mach number $M = u/c_s = 0.98$, with $S_i = 0.1$. The normalization used for the distances is with ρ_i. 57

4-3 The dipolar vortex in 2D is plotted for $\alpha = 0.1$ (in red color) and $\alpha = 0.9$ (black color) for $M = 0.98$. 58

5-1 Plot of normalized EAW phase speed λ with β in the presence (dashed curves) and in the absence (solid curves) of magneto-rotating effects at different positron concentrations. The other parameters are $\sigma = 0.7$, $\rho = 10$, $\theta = 10^{\circ}$, $l_x = 0.3$, $\Gamma_0 = 0.1$. 66

5-2 Variation of normalized EAW phase speed λ with various parameters. Left most plot, ($\sigma = 0.7$, $\rho = 10$, $\theta = 10^{\circ}, R = 0.3, \beta = 0.3$, $\Gamma_0 = 0.1$) middle plot,($\alpha = 0.1$, $\sigma = 0.1, \rho = 10$, $\theta = 10^{\circ}, R = 0.3, \beta = 0.3$, $l_x = 0.3$), Right most plot, ($\alpha = 0.1$, $\sigma = 0.1$, $\theta = 10^{\circ}, R = 0.3, \beta = 0.3$, $l_x = 0.3, \Gamma_0 = 0.1$). 67

5-3 (a) Variation of coefficients A, B with β parameter in the presence of positrons (dashed curves $R = 0.3$, $\Gamma_0 = 0.1$) and (solid curves $R = 0$). The other parameters are $\alpha = 0.2$, $\sigma = 0.7$, $\rho = 10$, $\theta = 10^{\circ}$, $l_x = 0.3$. (b) Variation of coefficients A, B with β parameter in the presence of positrons (dashed curves $R = 0.3$, $\Gamma_0 = 0.1$) and (solid curves $R = 0$). The other parameters are $\alpha = 0$, $\sigma = 0.7$, $\rho = 10$, $\theta = 10^{\circ}$, $l_x = 0.3$. 70

5-4 (a) Variation of hump type EA soliton structure with Γ_0(rotation frequency). The other parameters are $\alpha = 0.1$, $\sigma = 0.7$, $\rho = 10$, $\theta = 10^{\circ}$, $R = 0.3$, $\beta = 0.4$, $l_x = 0.3$, $u = 0.01$. (b) Variation of dip type EA soliton structure with Γ_0(rotation frequency). The other parameters are $\alpha = 0.1$, $\sigma = 0.7$, $\rho = 10$, $\theta = 10^{\circ}$, $R = 0.3$, $\beta = 0.25$, $l_x = 0.3$, $u = 0.01$. 71

5-5 (a) Variation of hump type EA soliton structure with R(electron rotation frequency). The other parameters are $\alpha = 0.1$, $\sigma = 0.7$, $\rho = 10$, $\theta = 10^{\circ}$, $\Gamma_0 = 0.1$, $\beta = 0.4$, $l_x = 0.3$, $u = 0.01$. (b) Variation of dip type EA soliton structure with Γ_0(rotation frequency). The other parameters are $\alpha = 0.1$, $\sigma = 0.7$, $\rho = 10$, $\theta = 10^{\circ}$, $\Gamma_0 = 0.1$, $\beta = 0.25$, $l_x = 0.3$, $u = 0.01$. 72

5-6 (a) Variation of hump type EA soliton structure with l_x(obliqueness of wave propagation along magnetic field). The other parameters are $\alpha = 0.1$, $\sigma = 0.7$, $\rho = 10$, $\theta = 10^{\circ}$, $\Gamma_0 = 0.1$, $\beta = 0.4$, $R = 0.3$, $u = 0.01$. (b) Variation of dip type EA soliton structure with l_x(obliqueness of wave propagation along magnetic field). The other parameters are $\alpha = 0.1$, $\sigma = 0.7$, $\rho = 10$, $\theta = 10^{\circ}$, $\Gamma_0 = 0.1$, $\beta = 0.25$, $R = 0.3$, $u = 0.01$. 72

5-7 (a) Variation of hump type EA soliton structure with α parameter in the presence (dashed curves $R = 0.3$, $\Gamma_0 = 0.1$) and in the absence (solid curves $R = 0$) of magneto-rotating effects. The other parameters are $\sigma = 0.7$, $\beta = 0.4$, $\rho = 10$, $u = 0.01$, $\theta = 10^{\circ}$, $l_x = 0.3$. (b) Variation of dip type EA soliton structure with α parameter in the presence (dashed curves $R = 0.3$, $\Gamma_0 = 0.1$) and in the absence (solid curves $R = 0$) of magneto-rotating effects. The other parameters are $\sigma = 0.7$, $\beta = 0.25$, $\rho = 10$, $u = 0.01$, $\theta = 10^{\circ}$, $l_x = 0.3$. 73

5-8 (a) Variation of hump type EA soliton structure with σ parameter in the presence (dashed curves $R = 0.3$, $\Gamma_0 = 0.1$) and in the absence (solid curves $R = 0$) of magneto-rotating effects. The other parameters are $\alpha = 0.1$, $\beta = 0.4$, $\rho = 10$, $u = 0.01$, $\theta = 10^\circ$, $l_x = 0.3$. (b) Variation of dip type EA soliton structure with α parameter in the presence (dashed curves $R = 0.3$, $\Gamma_0 = 0.1$) and in the absence (solid curves $R = 0$) of magneto-rotating effects. The other parameters are $\alpha = 0.1$, $\beta = 0.25$, $\rho = 10$, $u = 0.01$, $\theta = 10^\circ$, $l_x = 0.3$. 74

5-9 (a) Variation of hump type EA soliton structure with ρ parameter in the presence (dashed curves $R = 0.3$, $\Gamma_0 = 0.1$) and in the absence (solid curves $R = 0$) of magneto-rotating effects. The other parameters are $\alpha = 0.1$, $\beta = 0.4$, $\sigma = 0.7$, $u = 0.01$, $\theta = 10^\circ$, $l_x = 0.3$. (b) Variation of dip type EA soliton structure with ρ parameter in the presence (dashed curves $R = 0.3$, $\Gamma_0 = 0.1$) and in the absence (solid curves $R = 0$) of magneto-rotating effects. The other parameters are $\alpha = 0.1$, $\beta = 0.25$, $\sigma = 0.7$, $u = 0.01$, $\theta = 10^\circ$, $l_x = 0.3$. 75

Chapter 1

Introduction

The rapid urbanization and growing population has resulted in a still increasing need for energy, considering the rising energy demand and the constrained availability of energy resources, one needs more efficient utilization of energy and to develop new technologies as a long term solution. Taking into account the environmental requirements and the need to invest in a sustainable energy economy, new viable energy sources must be exploited. The power reactors based on the process of nuclear fusion may provide an almost unlimited supply of energy in the future. It has been over five decades that the scientists and engineers are trying to achieve controlled nuclear fusion reactions on earth for the future energy needs of the man kind. In this regard fusion physicists are involved extensively in designing fusion devices which can confine hot thermonuclear plasma. It is a well established fact that nuclear fusion reactions are occurring in stars, e.g., sun is a massive fusion reactor. The fundamental principle of this process is quite simple: If two light nuclei fuse together under specific reaction conditions, this results in the reduction of the total mass and a consequent release of energy in the form of kinetic energy of the reaction products. However, because the nuclei are positively charged, there is strong Coulomb repulsion between them. To achieve nuclear fusion reactions, we have to bring the two

nuclei at a distance in which strong nuclear force overcomes the repulsive barrier. Various types of schemes have been devised among which, perhaps the most suitable scheme is the magnetic confinement fusion (MCF). In the said scheme suitable ions, e.g., Hydrogen isotopes, are heated up to thermonuclear fusion temperatures of the order of 10^8 K, and are confined by the use of different magnetic field configurations. There are two major issues associated with controlled fusion reactions on earth, namely, heating of fusion fuel to very high temperatures, and the confinement of such hot fuel long enough to achieve considerable fusion reactions. These requirements can be presented mathematically by the well known Lawson criterion which states, in its simplest form, that the product of number density (n) and confinement time (τ) must satisfy the condition: $n\tau > 10^{14}$ sec/cm^3 for a deuteron (D) and triton (T) plasma at 10 keV temperatures [1]. One of the primary objective in all MCF schemes is to confine very hot plasma for sufficiently long time so as to satisfy the Lawson criterion. However, in most of fusion devices, the observed confinement time, due to various plasma instabilities, is much smaller than that demanded by the said criterion and, hence, both the particle and energy loss have been detected. Moreover, the experimentally measured losses have been much larger than theoretical predictions which points toward some additional (anomalous) losses that have not been properly taken into account. For correct interpretation and predictions for the behavior of present and future fusion devices like ITER, it is important to examine and understand the associated anomalous transport in the confining magnetic field. It is generally believed that in MCF plasma devices, e.g., tokamaks or stellarators, the ion-temperature-gradient (ITG) driven drift-wave instability is the source of anomalous transport. The ITG mode is also known as η_i-mode, where $\eta_i = d_x(\ln T_i)/d_x(\ln n_i)$ with T_i and n_i denoting, respectively, the ion temperature and density. Physically, the unstable η_i-mode arises due to free energy stored in the form of ion temperature (density) gradient. It has been found, as in Ref. [2], that $\eta_i = 2/3$ represents a threshold value

of instability, moreover, for a short wavelength case $\eta_i > 0.902$ is required for instability, whereas $\eta_i = 2$ corresponds to a hard threshold condition for anomalous transport.

In 1957, Tserkovnikov [3] discovered the ITG mode of instability and, later on, Rudakov and Sagdeev [4] performed a local analysis and derived instability criterion in the presence of ITGs. The later investigation was then further extended by Pogutse [5] by considering inhomogeneous magnetoplasma with sheared-ion flows and accounting for kinetic ion effects. Coppi *et al.*, [6] on the other hand, assumed that both the electrons and ions are adiabatic and, using the slab geometry, obtained a Weber type equation with eigenvalue condition for unstable η_i mode. By considering kinetic-ion effects, Kadomtsev and Pogutse [7] obtained a critical value of $\eta_i \sim 1$ for marginal stability that was later confirmed numerically by Waltz et al. [8]. Hinton and Horton [9] accomplished nonlinear analysis of collisional drift mode by using the two-fluid model, these results were found to be in agreement with some laboratory experiments.

Coppi and Spight [10] modelled the ITG driven drift wave instability differently and is termed as ion mixing mode (IM) mode. When a neutral gas is injected in tokamak plasmas through a stable discharge and the rate of density rises, this phenomenon can only be explained through this IM mode [10], Antonsen et al. [11]. Horton et al., [12] and Coppi and Pegoraro [13], showed that this instability is usually caused by the magnetic field curvature. For toroidal geometry, the numerical simulations of the ITG driven mode by Guzdar et al. [14] has indicated a threshold η_{ic} value by including the Landau resonance. The properties of the ITG mode with the magnetic shear effect have been investigated by Hahm and Tang [15].

We can divide ITG driven mode in two main types, namely, slab type and interchange mode. The slab type is the result of coupling of drift and ion acoustic wave that is determined by the local ion temperature gradients. Whereas, the interchange mode, also called toroidal branch, is determined in the presence of bad curvature of magnetic field

lines in the finite ion temperature gradient [16]. It has been reported that the anomalous thermal transport observed in stellarators and tokamaks are caused by the turbulence of the said branches of the ITG driven mode. When the magnetic field curvature is weaker than magnetic shear, the slab type ITG-driven instability is dominated which is the major source for the anomalous thermal transport [17, 18].

The investigations of the ITG mode is an important topic in the studies of fusion plasmas [19]. The effect of η_i on toroidal modes have also been investigated by Kadomtsev [20], moreover, ballooning mode formalism [6] is also employed for the description of these modes. The presence of a toroidal mode determined by toroidal η_i effects alone was first mentioned by Horton et al. [9], and was subsequently studied extensively by Horton and Braginskii in [21, 22]. Several studies have been carried out to understand the toroidal-ion-temperature-gradient (TITG) driven mode and it has been shown that an instability arises in inhomogeneous applied magnetic field. Shukla and Weiland [23] and Shukla [24] derived the group of equations for the nonlinear coupled TITG and showed that these coupled modes were self organized and give rise to dipolar type of vortices [26]. The existence of such type of vortices has been realized in experiments [27] as well as in numerical simulations [28, 29].

The satellite observations of space plasmas, during the last two decades, have shown a universal existence of ion and electron extent that are far away form their equilibrium site [30, 31]. These particles with suprathermal behavior can adequately be represented by the so called kappa distributions, which comprises the core as Maxwellian and power law for the high-energy tail, e.g., Vasyliunas [32], way back in 1968, fitted OGO1 and OGO2 solar wind data using kappa distributions. The distribution was an empirical fit for the detected particles. From that point forward, suprathermal distributions for linear as well as nonlinear structures was extensively embraced by various researchers [33, 34] for the regimes of ion and dust-acoustic.

Non-Maxwellian distribution of electrons have also been found to exist in toroidal fusion devices, e.g., the electron cyclotron heating (ECH) experiments on stellarators and tokamaks illustrate the existence of a superthermal tail in the electron distribution function. These experiments also show a disagreement between the linear theory of microwave absorption and the experimental observations [35].

Although the distribution function of electrons is Maxwellian in the Q-machine, it is non-Maxwellian in the case of radio frequency (RF) discharge. Consequently, the generalized Lorentzian (kappa) distribution function is required to simulate the electron distribution function in these devices. The Maxwellian distribution is a special case of more general kappa distribution, i.e., $\kappa \rightarrow \infty$ [36].

In tokamak fusion devices, under the influence of the toroidal electric field, electrons will experience a driving force, and due to the decrease of the Coulomb collision frequency there is an increase in their kinetic energy. Electric field will continuously accelerate those electrons having energy higher than some critical value (v_{cr}) [37], such accelerated electrons are named as runaway electrons. As runaway electrons are continuously accelerated in the parallel direction of the toroidal magnetic field, the formerly Maxwellian electron distribution function start to form a runaway particle tail. This results in a strong anisotropic velocity distribution [38]. The free energy due to the non-Maxwellian component can be exchanged via resonant interaction between electrons and plasma oscillations. Above a certain threshold, the Parail–Pogutes instability can be excited and limit either the runaway energy or the runaway confinement [39, 40]. In toroidal fusion devices the nonlinear vortex structures can play significant role in particle transport, for instance, the vortices may provide the transportation of heat flux along the magnetic field.

The existence of coherent vortical structures, which are believed to be the building blocks in turbulent physical situations, is a characteristic feature of two-dimensional or

quasi-two dimensional flows, such as planetary atmospheres and oceans, laboratory experiments with rotating and/or stratified fluids and strongly magnetized plasmas. These structures have a life time much longer than their period of rotation [41]. Monopoles are not steadily propagating since they couple to linear waves and, hence, are considered to be long-lived and have importance for flow dynamics [42]. The interaction of monopole and dipole generates a tripole. Tripole includes a core of central vortex which is rotating clockwise and two opposite polarity satellite vortices, are easily excited in rotating fluids [43, 44]. Such structures carry angular momentum but no linear momentum. Experimental evidences with explicit solution have been put forward by Kinzner and Khvoles [45], whereas the same are studied in the presence of magnetic and velocity (and background) shear flow by Chakrabarti et al. [47]. Strong monopolar structures, quasi-stationary solutions, are developed into tripolar-like structures when propagating essentially perpendicular to the density gradient [48]. Double immersed dipolar type shapes, called quadrupolar vortices, are a result of shear in magnetic field or in the flows [47]. The vortices discussed above play a vital role in transport of particles and energy in astrophysical objects as well as in laboratory plasmas.

As discussed earlier, the ITG mode was studied a long time ago by Rudakov and Sagdeev in 1961. Additional effects, for example, magnetic curvature, parallel compressibility have been investigated by Rudakov, Jerman etc. [19, 49]. In slab geometry, the ITG modes couple with ion acoustic modes and, hence, destabilize the local temperature gradient. In toroidal geometry the η_i-mode becomes unstable by magnetic curvature effect, and, is effective even in the limit $k_{\|} \to 0$ [50]. Experimental observations on the Alcator C tokamak suggested that η_i instability can be correlated to anomalous transport [49]. In electrostatic limit, the η_i mode propagation is along the ion diamagnetic drift. In the ion fluid limit, $\eta_i = 0$, while for instability threshold ITG mode in sheared slab geometry, $L_n/L_T = \eta_i \approx 1$ [8]. In toroidal geometry, the ITG mode is driven by ion

curvature drift rather than its parallel motion and the threshold could be in the range of $1 \leq \eta_i \leq 2$ [14].

The particle distributions, modeled as kappa distributions, having high energy tails are numerously detected in astronomical plasmas. The presence of non-Maxwellian distribution have insightful effects on transport phenomena and propagation of waves. Such distributions fit to the data obtained in satellite-based experiments [32, 51]. Space plasmas, e.g., solar wind, terrestrial magnetospheres and interstellar medium comprehend a significant degree of non-thermal particles [52]. The ITG mode has been investigated for different non-Maxwellian distributions in the linear regime, and the study concludes that the phase velocity modifies in the presence of nonthermal electrons [53]. The study has been further extended by including dust contaminated plasma with charge fluctuating effect in Ref. [54]. More recently, Mirza et al.[55] considered ITG driven vortices in inhomogeneous magnetoplasma with nonthermal electrons. The present investigation is an extension of [55] to tripolar vortices in non-Maxwellian plasmas.

In different plasma systems such as in the magneto-tail, in auroral ionosphere, in the Earth's bow shock region, magnetosphere and in the laboratory produced plasmas, hot and cold population of electrons have been observed ([57, 56] and the references therein). Hence this topic has got lot of attention among researchers around the globe [58]. Based upon the space data and theoretical models , different non-thermal distributions have been proposed, e.g., κ distribution [32], Cairn's distribution [59] etc. A lot of research has been devoted to investigate the superthermality effects on the linear and nonlinear wave propagation [60, 61]. The effect of nonthermal electrons on acoustic solitary wave formation has been discussed by several authors: namely, Gill *et al.* [62], has discussed the ion-acoustic type solitary wave propagation in the presence of suprathermal electrons and the formation of double layer using reductive perturbation method (RPM). Saini *et al.* [64]. The authors, El-Tantawy et al., [65] discussed the solitary wave propagation in

non-extensive electron positron and ion plasma.

Shan et al., [66] studied vortex formation by the ion acoustic and drift wave in the presence of nonthermal electrons. This work was further extended by Adnan *et al.* [67]. The role of nonthermal hot electrons on the linear/nonlinear (ITG mode driven vortices) behavior of ITG driven mode has been explored, respectively, by Batool *et al.* [53] and Zakir *et al.* [54].

Recently, Rufai *et al.*[68] studied ion-acoustic and super soliton formation in the presence of two types of electrons, i.e., the Cairn's type for energetic electrons and Maxwellian type for the inertialess electrons in the presence of dynamic cold ions. It was shown that the presence of hot electrons extends the limit of Mach number supersonic level. In this regard, we have extended the work of Rufai et al., by including ions shear flow in the parallel direction, and investigated the effect of hot electrons on formation of dipolar and street type vortices. We have also found the modified behavior of the shear flow instability in the presence of highly energetic electrons.

Coriolis force plays a dominant role in cosmic phenomena, rotating plasma in laboratory devices as well as in space plasmas [69, 70]. Most of the astrophysical plasma environments (for instance, neutron stars, pulsars, quasars, black-hole magnetospheres, etc.) and in toroidal devices, the magnetized plasma rotates quite rapidly and, hence, the Coriolis effect plays a significant role in plasma dynamics. The physics of such plasma system can be coined in terms of noninertial (rotating) frames. Under such observations, the effect of Coriolis force on the linear wave propagation in an ideal lower ionosphere has been studied, which is of great importance in the structure of rotating magnetic stars, the star cycle, and sunspot development [71, 72]. In nature, the formation of a star into a neutron star under the conservation laws of angular momentum and magnetic flux decreases with the rotational inertia and causes the presence of frozen-in force lines leading to a rapidly rotating and highly magnetized plasma. Such plasma environments

are enriched in electrons, positrons and ions. One of the aim of the present work is to model such a plasma system to study nonlinear wave propagation in a magneto-rotating plasma.

Many authors have investigated the effect of Coriolis force on wave evolution in both unmagnetized and magnetized plasmas [71, 73] and it has been established that the Coriolis force has an effective magnetic-field-like influence in a rotating plasma [74]. The Coriolis force effects on the pulsar radiation have been investigated in Ref. [75] where it is observed that an increase in rotation causes the soliton radiation known as pulsar radiation. The study of astrophysical plasma has shown that the formation of nebulons is governed by the rotation of the body. In the Refs. [76, 77] the authors have explored the magneto-rotating e-p-i plasma and have shown that the rotation and magnetic field make the solitary waves more spiky. It has been further shown that the rotational effects bifurcate the region of compressive and rarefactive solitary waves [71, 74]. In most of these studies the propagation of ion- and dust-acoustic solitary waves in magneto-rotating plasmas have been analyzed. Quite recently, we have studied the effects of magnetic field on the electron acoustic solitary waves (EASW's) in a rotating electron–positron ions with dynamic electrons with finite temperature and mass, nonthermal electron-positrons and stationary massive positive ions and have obtained interesting new results. The EASW's formation is due to the temperature anisotropy of electrons, and depends on the difference of temperature, the cold electrons provide the inertia and the hot electrons develop the required pressure for the restoring force to excite EAW. Similarly, for the ion acoustic waves (IAW) in pure electron-ion plasma, the inertia is provided by the massive ions and inertialess electrons which gives the restoring force [78]. Furthermore, in the dynamics of EASW's the ions form a stationary background because of its large mass.

In most of the astrophysical plasma positrons are frequently observed, resulting in electron-positron-ion plasmas. The origin of these energetic particles in space plasmas

is the cosmic rays and solar wind. The introduction of positrons leads to significant modification in restoring force [79, 80]. Even in the tokamak plasma systems, a small percentage of positrons also exists, which are generated, due to the collisions of run-away electrons with plasma species [81]. Their presence has also been reported in the UK based tokamak, namely, the joint European Torus (JET) [82]. Mostly, the electrons and positrons in astrophysical plasma environments are highly energetic [83] and are often described with the high energy tail distribution functions. The interaction of high energy cosmic protons as well as collisions of heavy nuclei molecules of the upper atmosphere which produces nonthermal electrons/positrons which are collisionless [84]). Moreover, such particles also exist in the magneto-tail of the earth's sheath boundary layer region, this nonthermal population of plasma particles is formed when the outflows of hot electron-positron plasma from pulsars enter into an interstellar cold, low density electron-ion plasma [78]. In neutron stars, pulsars, black-hole magnetospheres, earth's magnetosphere, etc., the EAWs, when nonlinearly coupled forms various types of nonlinear structures such as solitons, shocks, double layers, electron holes, etc. [85]. Electron-positron-ion plasma also exists in the early universe, pulsars magnetosphere, in the active galactic nuclei, solar atmosphere, quasars, in the rapidly rotating and highly magnetized plasmas [86].

In recent years, a lot of interesting work has been reported in which various properties of linear and nonlinear electrostatic EAWs have been studied, such as EASWs and shock waves in a dissipative, nonplanar space plasma in the presence of nonthermal hot electrons, and negative potential solitary waves [87] etc. Further, spherical EASWs in plasma with superthermal electrons have been investigated by Borhanian *et al.* [88] and it is shown that with an increase in the nonthermal population parameter the amplitude of the solitary waves also increases. Mamun *et al.* [89], have considered the obliquely propagating EA solitary waves in magnetized nonthermal hot electrons, obeying vor-

tex type distribution in the presence of stationary ions as a background in electron-ion plasma. On the other hand, Singh and Lakhina [90] have investigated the problem of excitation of EAWs in the magnetosphere and found that the frequency and the growth rate of EAW gets reduced in the presence of hot background electrons. Lakhina *et al.* [63, 91] proposed a general model to study ion(electron) acoustic solitons/double layers in multi-component space plasmas. Dike *et al.* [72]., have investigated nonlinear EA solitary waves in plasmas having non-Maxwellian kappa-distributed hot electrons. However, in all of these analysis the influence of nonthermal positron component and magneto-rotating effects have not been considered. In our recent work [84] we have included the nonthermal electrons and positrons components in our study on the EASWs and we found that in the presence of positrons the polarity of these solitary waves can switch. As in nature, most of the astrophysical plasmas are magnetized in rotating frames, therefore, its natural to extend the investigations of EASWs under magneto-rotating effects to have a more realistic picture. Thus, in order to model the magneto-rotating effects and that of the presence of hot positron and electrons on the linear/nonlinear electrostatic EAWs in the laboratory and in astrophysical space plasmas, we have incorporated a magneto-rotating electron-positron-ion plasma. The plasma considered here consists of nonthermal electrons and positrons which are nonthermal alongwith cold dynamic electrons and heavy ions to provide a stationary background for the EAWs to exist.

Chapter 2

Toroidal ITG Driven Vortices in Nonuniform Magnetoplasma

2.1 Preamble

In MCF devices, among other instabilities, the ion-temperature-gradient (ITG) driven drift wave instability is believed to be one of the major candidates responsible for anomalous transport of particles. This instability is also known as ITG mode or, simply the η_i mode of instability, where $\eta_i \equiv \frac{L_n}{L_T} = \frac{d_x \ln T_{i0}}{d_x \ln n_{i0}}$ is the ratio of density and temperature gradient scale lengths. The source of available free energy for ITG instability is the ion-temperature gradients. The importance of ion temperature gradient modes in burning fusion plasmas is well known, to the best of our knowledge the ITG mode was first discovered by Tserkovnikov [3]. It was then investigated in detail by Rudakov and Sagdeev [4] using local analysis for a flat density profile to explain the origin of fluctuations and associated cross field anomalous transport in tokamak plasmas. In toroidal geometry, η_i mode has been been considered by Coppi *et al.*, [92]. The existence of a toroidal η_i mode was first pointed out by Horton et al. [12], and subsequently several others studies were

made [93, 94], where it was shown that an instability arises in the presence of inhomogeneous applied magnetic field for $\eta_i > 1.4$. Shukla and Weiland [24, 95] derived the nonlinear set of equations for the coupled ITG and toroidal-ion-temperature-gradient (TITG) modes, and it was shown that nonlinearly interacting ITG and TITG modes self-organizes in the form of dipolar vortices [25, 26].

In this Chapter, we shall examine the nonlinear properties of the low-frequency electrostatic toroidal ITG-driven mode for inhomogeneous magnetized plasma in the presence of nonthermal electron population and obtain the dipolar and vortex chains type vortices. We derive here a set of nonlinear equations that govern the dynamics of low-frequency (i.e., $\omega \ll \omega_{ci}$, where ω_{ci} is the ion gyro-frequency) TITG driven mode in the presence of equilibrium density, temperature, and magnetic field gradients. In the nonlinear case, solutions in the form of dipolar vortices and vortex streets are presented for a plasma comprising of Maxwellian ions and nonthermal electrons in the presence of external magnetic field. By using Braginskii's transport equations for the ions and kappa distributed electrons, new set of mode coupling equations are derived. The results have been applied for tokamak plasmas and the scale lengths, over which the nonlinear vortex structures gets modified, have been derived in the presence of kappa distributed electrons.

2.2 Mathematical Formulation

Consider an electron-ion plasma in an inhomogeneous externally applied magnetic field $\mathbf{B}_0$ ($B_0(x)\hat{z}$, where $\hat{z}$ defines a unit vector in the z-direction) and B_0 is the strength of magnetic field. The equilibrium ion-temperature gradient $\nabla T_{i0}(x)$, ion-density gradient $\nabla n_{i0}(x)$ and magnetic field gradients $\nabla B_0(x)$ are along the x-axis. For low-frequency of TITG mode, we assume that the wave frequency $\omega \ll \omega_{ci} (= eB_0/m_i c$, where, ω_{ci} is the ion-gyrofrequency, e is the magnitude of electronic charge, m_i is the mass of ion,

and c is the speed of light). Here we consider electrostatic case for which $\mathbf{E} = -\nabla\phi$, where $\mathbf{E}$ denotes the electric field and ϕ represents the electrostatic potential. Using the drift-approximation (valid for low-frequency modes, i.e., $\omega \ll \omega_{ci}$), the perpendicular component of ion-fluid velocity can be expressed as

$$\begin{aligned}\mathbf{v}_{i\perp} \simeq & \frac{c}{B_0}\hat{z} \times \nabla\phi + \frac{c}{eB_0 n_i}\hat{\mathbf{z}} \times \nabla\left(n_i T_i\right) \\ & - \frac{c}{B_0\omega_{ci}}\left[\partial_t + \left(\mathbf{v}_E + \mathbf{v}_{Di}\right)\cdot\nabla\right]\nabla_\perp\phi \,,\end{aligned}$$

$$\mathbf{v}_i = \mathbf{v}_E + \mathbf{v}_{Di} + \mathbf{v}_{pi} \,, \tag{2.1}$$

where $\mathbf{v}_E$ is the well known $\mathbf{E} \times \mathbf{B}$ drift velocity of the ionic fluid, $\mathbf{v}_{Di}$ is the ion-diamagnetic drift velocity and $\mathbf{v}_{pi}$ is the ion-polarization drift velocity. For toroidal ITG (TITG) mode, we ignore the parallel to $\mathbf{B}_0$ ion dynamics, i.e., $v_{iz} = 0$, which means that the dynamics of nonlinear TITG mode is considered by ignoring the coupling of ion-sound waves. The perturbed ion number density can be calculated with the help of ion continuity equation in drift-approximation as follows

$$\frac{\partial n_i}{\partial t} + \nabla \cdot n_i\left(\mathbf{v}_E + \mathbf{v}_{Di} + \mathbf{v}_{pi}\right) = 0. \tag{2.2}$$

The ion temperature perturbation can be estimated using ion energy balance equation

$$\frac{3}{2}\left[\partial_t + \mathbf{v}_i \cdot \nabla\right] T_i + T_i \nabla \cdot \mathbf{v}_i = -\frac{1}{n_i}\nabla \cdot \mathbf{q}_i,$$

where $\mathbf{q}_i = \frac{5}{2}\left(cn_iT_i/eB_0\right)\hat{z}\times\nabla T_i$ defines the collisionless Righi-Leduc ion heat flux. Substituting the value of $\nabla\cdot\mathbf{v}_i$ from Eq. (2.2) in the above equation one finds

$$n_i\left[\partial_t+\mathbf{v}_i\cdot\nabla\right]T_i-\frac{2}{3}T_i\left[\partial_t+\mathbf{v}_i\cdot\nabla\right]n_i=-\frac{2}{3}\nabla\cdot\mathbf{q}_i. \tag{2.3}$$

To close the system of equations, we need to define the electron density distribution. The three dimensional kappa velocity distribution function $f_\kappa(v)$ for isotropic case can be expressed as [33]

$$f_\kappa(v)=\frac{n_{e0}}{\theta^3}\left(\frac{1}{\pi\kappa}\right)^{3/2}\frac{\Gamma(\kappa+1)}{\Gamma(\kappa-1/2)}\left(1+\frac{v^2-2e\phi/m_e}{\kappa\theta^2}\right)^{-(\kappa+1)}, \tag{2.4}$$

where $\theta=\left[((2\kappa-3)k_BT)/\kappa m\right]^{1/2}$. From the formalization of $\kappa-$ distribution function, it is essential that $\kappa>\frac{3}{2}$ [99]. We can obtain the number density of electrons by integrating the distribution function over velocity space to get

$$n_e=n_{e0}\left[1-\frac{e\phi}{\left(\kappa_e-3/2\right)T_e}\right]^{-(\kappa-1/2)}. \tag{2.5}$$

For non-thermal electron population, the kappa distribution of electrons has the form

$$\delta n_e\simeq\in\left(\frac{\kappa-\frac{1}{2}}{\kappa-\frac{3}{2}}\right)\Phi, \tag{2.6}$$

Here $\Phi\left(=e\phi/T_e\ll 1\right)$ represents the normalized electrostatic potential and n_{e0} is the equilibrium electron number density, and kappa describes the deviation from the Maxwellian

distribution, which can be reproduced by taking the limit $\kappa \to \infty$.

Substituting Eq. (2.1) into continuity equation for ions, and by letting $n_i = n_{i0} + \delta n$ and $T_i = T_{i0} + \delta T$, where δn and δT are, respectively, density and temperature perturbations and are assumed to be much smaller than their equilibrium counterparts, we find

$$\begin{aligned}
&\left(\partial_t + \mathbf{v}_E \cdot \nabla + \mathbf{v}_{Bi} \cdot \nabla\right) N + \mathbf{v}_{Bi} \cdot \nabla T + \tau \left(\mathbf{v}_{Bi} - \mathbf{v}_{ni}\right) \cdot \nabla \Phi \\
&-\rho_s^2 \left[\partial_t + \mathbf{v}_E \cdot \nabla + \mathbf{v}_{D0} \cdot \nabla\right] \nabla_\perp^2 \Phi - \rho_s^2 \nabla \cdot \left[(\mathbf{v}_{D1} \cdot \nabla) \nabla_\perp \Phi\right] = 0 \,,
\end{aligned} \tag{2.7}$$

with $N = \frac{\delta n}{n_{i0}}$ and $T = \frac{\delta T}{T_{i0}}$ denoting the normalized number density and temperature, respectively, $\tau = T_{e0}/T_{i0}$ is the electron to ion temperature ratio, $\rho_s = c_s/\omega_{ci}$ represents ion acoustic Larmor radius, $c_s = \sqrt{T_{e0}/m_i}$ represent the ion-acoustic speed, $\mathbf{v}_{Bi} = -\left(\frac{cT_{i0}}{eB_0}\right) \hat{z} \times \frac{\nabla B_0}{B_0}$ is the ion ∇B_0 drift and $\mathbf{v}_{ni} = -\left(\frac{cT_{i0}}{eB_0}\right) \hat{z} \times \frac{\nabla n_{i0}}{n_{i0}}$ represents the ion ∇n_{i0} drift, $\mathbf{v}_{D0} = (1 + \eta_i)\mathbf{v}_{ni}$ with $\eta_i = \frac{\partial_x \ln T_{i0}}{\partial_x \ln n_{i0}}$ and $\mathbf{v}_{D1} = \left(\frac{cT_{i0}}{eB_0}\right) \hat{z} \times \nabla (N + T)$ is the first order ion diamagnetic drift velocity.

Upon inserting Eq. (2.1) in Eq. (2.3) and using continuity equation to get

$$\begin{aligned}
&\left[\partial_t + \frac{c}{B_0} \hat{z} \times \nabla \phi \cdot \nabla + \frac{5}{3} \mathbf{v}_{Bi} \cdot \nabla\right] T - \frac{2}{3} \left[\partial_t + \frac{c}{B_0} \hat{z} \times \nabla \phi \cdot \nabla\right] N \\
&-\tau \left(\eta_i - \frac{2}{3}\right) \mathbf{v}_{ni} \cdot \nabla \Phi = 0
\end{aligned} \tag{2.8}$$

Equations (2.7) to (2.8), with $N = ((\kappa - \frac{1}{2})/(\kappa - \frac{3}{2}))\Phi = \beta \Phi$ are the required nonlinear mode coupling equations which governs the dynamics of toroidal-ion-temperature-gradient driven mode in the presence of nonthermal electrons. To close set of coupled equations, we define quasineutrality condition i.e., $\delta n_e \simeq \delta n_i$.

2.3 Linear Analysis

In the linear limit, we shall drop the nonlinear terms and retain only the first order linear terms, Eqs. (2.7) and (2.8), in the linear limit, take the form

$$\begin{aligned}(\partial_t + v_{Bi}\partial_y)\, N + \tau\,(v_{Bi} - v_{ni})\,\partial_y\Phi + v_{Bi}\partial_y T - \rho_s^2\partial_t\nabla_\perp^2\Phi \\ - \rho_s^2\left[(1+\eta)\mathbf{v}_{ni}\cdot\nabla\right]\nabla_\perp^2\Phi = 0\end{aligned} \tag{2.9}$$

$$\left[\partial_t + \frac{5}{3}(v_{Bi} - v_{ni})\partial_y\right] T - \frac{2}{3}\left(\partial_t - \frac{5}{2}v_{Ti}\partial_y\right) N - \tau v_{ni}\left(\eta_i - \frac{2}{3}\right)\partial_y\Phi = 0 \tag{2.10}$$

The linear dispersion relation can be derived by using the sinusoidal approximations for the perturbed quantities, i.e., the perturbations are proportional to $\exp[i\,(\mathbf{k}\cdot\mathbf{r} - \omega t)]$, where $\mathbf{k}$ and ω defines, respectively, the wave vector and perturbation frequency. Therefore Eqs. (2.9) and (2.10) in the Fourier space can be written as

$$\begin{aligned}(\omega - \omega_{Bi})\, N - \tau\,(\omega_{Bi} - \omega_{ni})\,\Phi - \omega_{Bi}T + \rho_s^2 k_y^2\omega\Phi \\ - \rho_s^2\left[\omega_{ni}\,(1+\eta_i)\right]k_y^2\Phi = 0\end{aligned} \tag{2.11}$$

$$\left(\omega - \frac{5}{3}\,(\omega_{Bi} - \omega_{ni})\right) T = \frac{2}{3}\left(\omega + \frac{5}{2}\omega_{Ti}\right) N - \tau\omega_{ni}\left(\eta_i - \frac{2}{3}\right)\Phi, \tag{2.12}$$

where $\omega_{Ti} = \mathbf{k}\cdot\mathbf{v}_{Ti}$, $\omega_{ni} = \mathbf{k}\cdot\mathbf{v}_{ni}$ and $\omega_{Bi} = \mathbf{k}\cdot\mathbf{v}_{Bi}$. Eliminating T from Eqs. (2.11) and

(2.12) one finds

$$\left[\omega-\omega_{Bi}-\frac{2}{3}\frac{\omega_{Bi}\left(\omega+\frac{5}{2}\omega_{Ti}\right)}{\left(\omega-\frac{5}{3}\left(\omega_{Bi}-\omega_{ni}\right)\right)}\right]N=-\left[\rho_s^2k_y^2\left\{\omega-\omega_{ni}\left(1+\eta\right)\right\}\right.$$
$$\left.+\frac{\left(\eta_i-\frac{2}{3}\right)\tau\omega_{Bi}\omega_{ni}}{\left(\omega-\frac{5}{3}\left(\omega_{Bi}-\omega_{ni}\right)\right)}\right]\Phi \tag{2.13}$$

The dispersion relation for TITG driven drift mode for kappa distributed electrons can be written as

$$\left[\left(\omega-\omega_{Bi}\right)\left(\omega-\frac{5}{3}\left(\omega_{Bi}-\omega_{ni}\right)\right)-\frac{2}{3}\omega_{Bi}\left(\omega+\frac{5}{2}\omega_{Ti}\right)\right]\beta$$
$$-\tau\left(\omega_{Bi}-\omega_{ni}\right)\left(\omega-\frac{5}{3}\left(\omega_{Bi}-\omega_{ni}\right)\right)+\rho_s^2k_y^2\left\{\omega-\omega_{ni}\left(1+\eta_i\right)\right\} \tag{2.14}$$
$$\left(\omega-\frac{5}{3}\left(\omega_{Bi}-\omega_{ni}\right)\right)+\left(\eta_i-\frac{2}{3}\right)\tau\omega_{Bi}\omega_{ni}=0\ ,$$

which is the desired expression for the toroidal ion-temperature-gradient (TITG) driven drift-waves with nonthermal hot electron population.

To analyze the second order dispersion relation, we plot this dispersion relation by considering some typical tokamak parameters, e.g., $B_0 = 3\times10^5$ G, $T_e = 10$ keV, and assuming $T_i = 0.1T_e$, $\kappa_{ne} = k_y/15$, $\kappa_{Te} = k_y/5$, $\kappa_{Bi} = 0.3\kappa_{ne}$. The real and imaginary part of the frequency is presented as a function of k_y for different values of kappa parameter and the results are depicted in Figs. 2-1 and 2-2. It can be observed in Fig. 2-2 that as kappa increases the growth rate also increases, whereas the real frequency decreases with kappa.

It is worth-mentioning here that the growth rate in this model occurs only if ion to electron temperature proportion is less than unity.. This is because we have neglected the

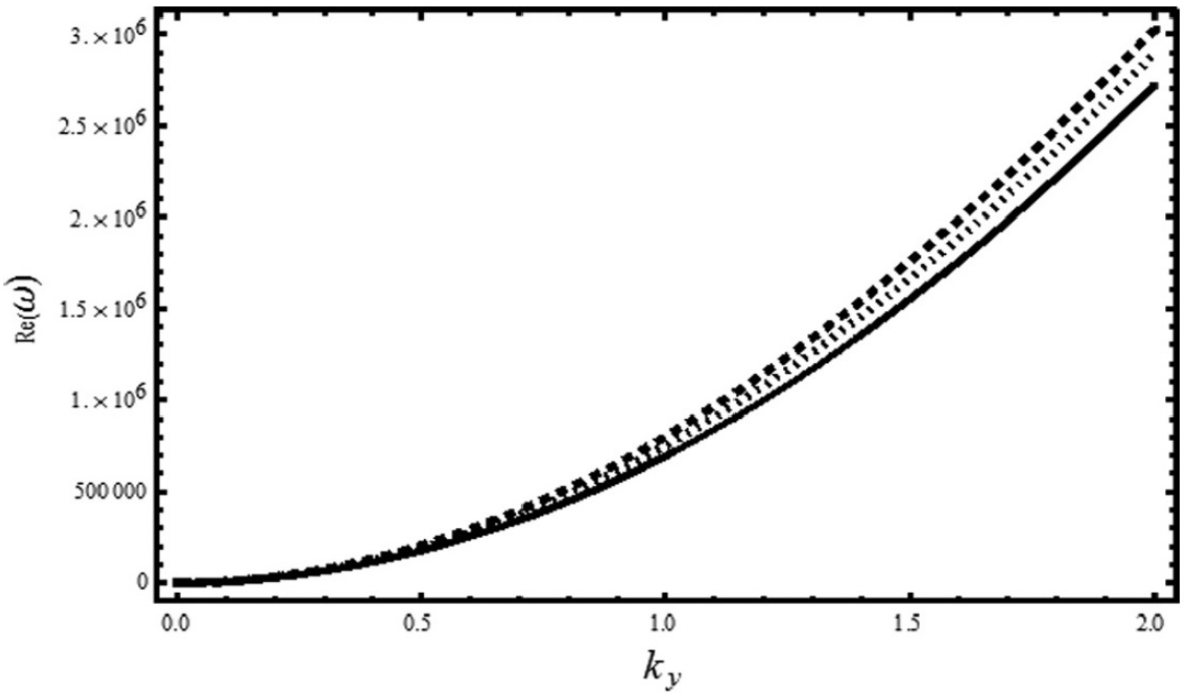

Figure 2-1: Plot of real part of frequency versus k_y, for various values of $\kappa = 3$(solid line), $\kappa = 4$ (dotted line), and $\kappa = 6$ (dashed line).

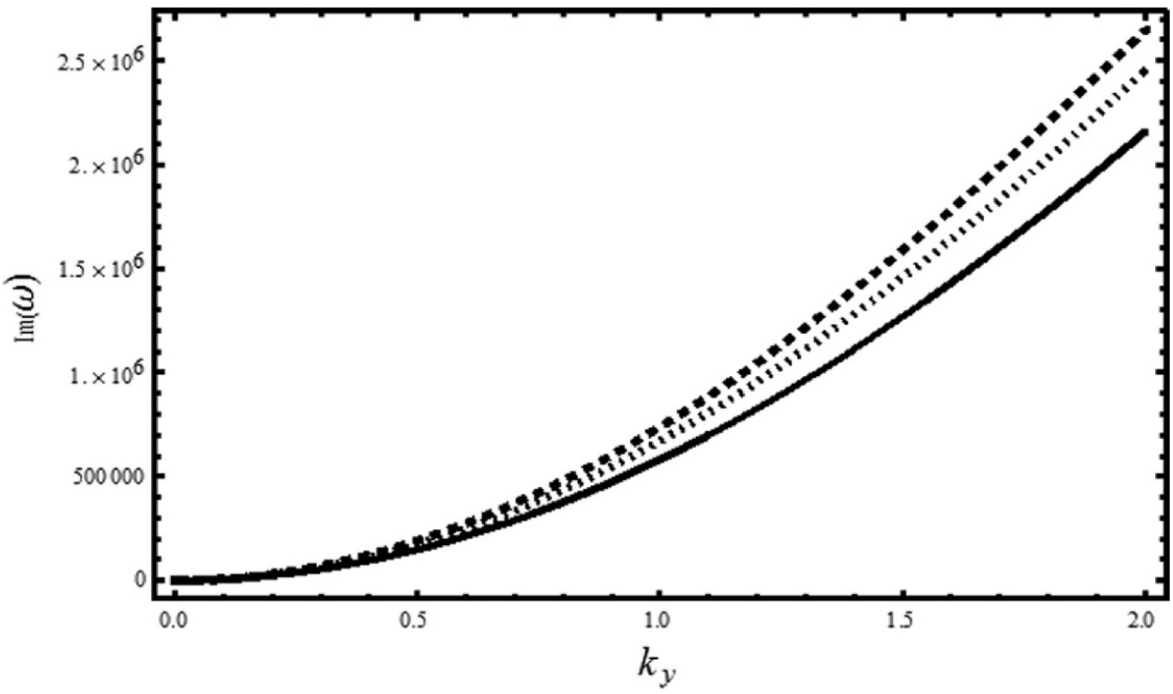

Figure 2-2: Plot of Imaginary part of wave frequency versus k_y, for numerous values of $\kappa = 3$(solid line), $\kappa = 4$ (dotted line), and $\kappa = 6$ (dashed line)

nonlinear finite Larmor radius (FLR) and stress tensor contributions in our calculations. For the detailed calculations including the effect of FLR, we refer the reader to classical paper by Horton, *et al.* [100], where they showed instability and nonlinear transfers to higher k modes from the said complex nonlinear term. However, in our simplified model, we drop out this term for simplicity, which might not be true in numerous hot thermonuclear fusion plasmas such as in Tokamaks. When toroidal-ion-temperature gradient driven mode destabilizes and grows, the amplitude of various modes starts mixing, various type of nonlinear structures can be formed. In the next section, we shall seek the possibility of the formation of various types of coherent nonlinear structure formation, namely the vortex formation.

2.4 Stationary Solutions

In this section, stationary solutions of Eqs. (2.7) and (2.8) are presented by defining a new stationary frame moving with a fixed velocity u in the direction perpendicular to the x-axis. Subsequently, let us define a coordinate $\xi = y - ut$, such that Φ, N and T are functions of ξ and x only. In this newly defined stationary frame Eqs. (2.7) and (2.8) takes the form

$$\left(u - \frac{5}{3}v_B\right)\partial_\xi T - \tau\left(\frac{2}{3} - \eta_i\right)v_n\partial_\xi\Phi - \frac{2}{3}u\partial_\xi N + \rho_s^2\left\{\frac{2}{3}\left[\Phi, N\right] - \left[\Phi, T\right]\right\} = 0, \tag{2.15}$$

where the Poisson's bracket is defined by $[F, G] \equiv \partial_x F\partial_\xi G - \partial_x G\partial_\xi F$. A typical solution of Eq. (2.10) is

$$T = A_0\Phi, \tag{2.16}$$

with

$$A_0 = \frac{\tau\left(\frac{2}{3} - \eta_i\right) v_n + \frac{2}{3} u\beta}{\left(u - \frac{5}{3} v_B\right)}.$$

Substituting for T from Eq. (2.11) in Eq.(2.9) we find

$$\begin{aligned}
&\left[u - \left(1 + \left(A_0 - \tau\right)\beta^{-1}\right) v_B - \tau\beta^{-1} v_n\right] \partial_\xi \Phi - \rho_s^2 \left(u - v_{D0}\right) \partial_\xi \nabla_\perp^2 \Phi \\
&+ \rho_s^4 \omega_{ci} \left(\left\{\beta^{-1} + \tau^{-1}\left(1 + A_0\beta^{-1}\right)\right\}\ \hat{z} \times \nabla\Phi \cdot \nabla\right) \nabla_\perp^2 \Phi = 0. \qquad (2.17)
\end{aligned}$$

To solve Eq. (2.16), we use the following ansätz [26]

$$\nabla_\perp^2 \Phi = C_1 \Phi + C_2 x, \qquad (2.18)$$

where C_1 and C_2 are the constants which satisfy the condition

$$\begin{aligned}
&\left[u - \left(1 + \left(A_0 - \tau\right)\beta^{-1}\right) v_B - \tau\beta^{-1} v_n\right] - \rho_s^2 \left(u - v_{D0}\right) \beta C_1 \\
&- \rho_s^4 \omega_{ci} \beta^2 \left\{\beta^{-1} + \tau^{-1}\left(1 + A_0\beta^{-1}\right)\right\} C_2 = 0 \qquad (2.19)
\end{aligned}$$

Here $\nabla^2 = \frac{\partial^2}{\partial x^2} + \frac{\partial^2}{\partial y^2}$, $\rho_s = \frac{c_s}{\omega_{ci}}$ is the ion sound dispersion radius with ion acoustic speed $c_s = \sqrt{T_{e0}/m_i}$. For localized dipolar vortex solution, define the coordinates $r = \left(x^2 + \xi^2\right)^{\frac{1}{2}}$ and $\theta = \tan^{-1}\left(\frac{\xi}{x}\right)$ which divides (r, θ) plane into the inner $r < R_0$ and outer $r > R_0$ regions of a vortex of radius R_0. First, consider the outer region and cylindrical polar coordinates and by using the standard separation of variables technique, i.e., by

letting $\Phi(r,\theta) = R(r)\cos\theta$, we retrieve the equation for $r > R_0$ region as

$$r^2\frac{\partial^2 R}{\partial r^2} + r\frac{\partial R}{\partial r} - \left(p^2r^2 + 1\right)R = 0, \tag{2.20}$$

where $p^2 = \left[u - \left(1 + (A_0 - \tau)\beta^{-1}\right)v_B - \tau\beta^{-1}v_n\right]/\rho_s^2\beta(u - v_{D0})$. Equation (2.19) is the well known modified Bessel equation having the solution in the form of modified Bessel function of the first kind, K_1. Hence we have

$$\Phi_{out}(r) = \alpha_0 K_1(pr)\cos\theta. \tag{2.21}$$

Similarly, for the inner region, one can write down the solution by letting $q^2 = -\rho_s^2(u\text{-}v_{D0})(p^2+q^2)\,/\,\rho_s^4\omega_{ci}\left\{\beta^{-1} + \tau^{-1}\left(1 + A_0\beta^{-1}\right)\right\}$ to obtain

$$r^2\frac{\partial^2 R}{\partial r^2} + r\frac{\partial R}{\partial r} + \left(q^2r^2 - 1\right)R = -q^2r^3. \tag{2.22}$$

The solution can be written in terms of first order Bessel function J_1, i.e.,

$$\Phi_{in}(r) = [\alpha_1 J_1(qr) - r]\cos\theta, \tag{2.23}$$

The constants α_0 and α_1 can be determined by using the matching conditions at $r = R_0$. The solution of outer and inner regions can be written, respectively, as

$$\Phi_{out}(r) = \frac{UR_0K_1(pr)}{\rho_s^2\beta K_1(pR_0)}\cos\theta, \tag{2.24}$$

and,

$$\Phi_{in}(r) = -\frac{U}{q^2\omega_{ci}\rho_s^2\beta}\left\{\frac{R_0 p^2 J_1(qr)}{J_1(qR_0)} - \left(p^2+q^2\right)r\right\}\cos\theta. \tag{2.25}$$

Using a recurrence relation for the Bessel function $xJ_n^{'}(x) = nJ_n(x) - xJ_{n+1}(x)$, we get the following relation

$$\frac{K_2(pR_0)}{pK_1(pR_0)} = -\frac{J_2(qR_0)}{qJ_1(qR_0)}, \tag{2.26}$$

where J_2 and K_2 are ordinary and modified Bessel functions of second order, respectively. Equations (2.23) and (2.24) admit dipolar vortex solutions. The contour plots for the normalized electrostatic potential Φ in (x,ξ) plane is presented in Fig. (2-1) by using some typical tokamak parameters and for fixed value of nonthermal spectral index $\kappa = 3$.

Furthermore, in the absence of the scalar nonlinearity, we set

$$\left[u - \left(1 + (A_0 - \tau)\beta^{-1}\right)v_B - \tau\beta^{-1}v_n\right] = 0, \tag{2.27}$$

in this case Eq. (2.26) can yield an alternate relation which is satisfied by the vortex chain type solution and can be expressed in terms of well known stationary Navier-Stokes equation, i.e.,

$$\partial_\xi \nabla_\perp^2 \Phi - \frac{\mu c}{uB_0}\left[\Phi, \nabla_\perp^2 \Phi\right] = 0, \tag{2.28}$$

with $\nabla_\perp^2 = \partial^2/\partial x^2 + \partial^2/\partial\xi^2$ and $\mu = T_e\left\{\beta^{-1} + \tau^{-1}\left(1 + A_0\beta^{-1}\right)\right\}/e\,(u - v_{D0})$. For $\mu > 0$ and $v_{D0} \neq u$, Eq. (2.27) is satisfied by

$$\nabla_\perp^2 \Phi = \frac{4\Phi_0 K_0^2}{a_0^2}\exp\left[-\frac{2}{\Phi_0}\left(\Phi - \frac{uB_0}{\mu c}x\right)\right], \tag{2.29}$$

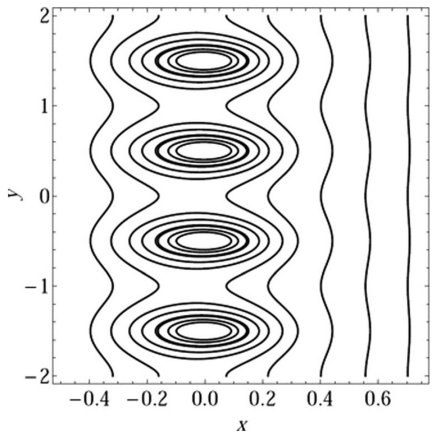

Figure 2-3: Vortex chains profile obtained from Eq. (2.30) for the tokamak parameters.

where Φ_0, K_0, and a_0 are arbitrary constants. The analytical solution of Eq. (2.28) for $a_0 > 1$ admits the vortex chain solution resembling the Kelvin-Stuart cat's eyes and is given by [26]

$$\begin{aligned} \Phi &= \Phi_0 \ln 2 \left[\cosh\left(K_0 x\right) + \left(1 - \frac{1}{a_0^2}\right) \cos\left(K_0 \xi\right)\right] \\ &\quad + \frac{uB_0}{\mu c} x, \end{aligned} \tag{2.30}$$

where Φ_0 describes the vortex amplitude and $2\pi/K_0$ represents the size of the vortex. Figure (2-3) shows a periodic vortex street with periodicity in ξ for the same parameters as described in Fig. (2-1), in our numerical calculations, we have normalized the space coordinates with the ion sound dispersion radius. We note here that the size of vortex profiles are typically of the order of ion sound dispersion radius ρ_s.

2.5 Conclusion

Linear and nonlinear properties of TITG driven drift mode have been studied with nonthermal electron distribution in an inhomogeneous magnetoplasma. We used the drift-approximation for the ion fluid velocity and derived a set of equations for the study of toroidal ITG driven drift mode. In the linear limit, new second order dispersion relation is derived for TITG mode. It is found that the growth rate of TITG mode gets modified with nonthermal electron distribution. While in the nonlinear case, the obtained solution admits stationary solutions in the form of a vortex chain and a dipolar vortices. It turns out that the inclusion of Kappa distributed electrons brings about a decrease in the spatial extent of the nonlinear vortex structures. The present study may be advantageous to realize the origin of drift-waves and associated coherent nonlinear structure formation in toroidal ITG driven drift modes which has applications in space and laboratory plasmas in the presence of nonthermal electrons such as those found in RF heating, ECH experiments, as well as runaway electrons in a tokamak plasmas.

Chapter 3

Tripolar Vortices in ITG Mode in Nonuniform Magnetoplasma

3.1 Introduction

It is a well established fact that the two-dimensional nonlinear partial differential equations with vector-type nonlinearity admits vortex-type solutions. Consider a collisionless magnetized plasma confined in a uniform magnetic field $\mathbf{B} = B_0\hat{\mathbf{z}}$. If the external field is strong enough, the ion-rich plasma column would be confined in a constant axial magnetic field $B_0\hat{\mathbf{z}}$. The ion column causes an electric field $\mathbf{E} = -\boldsymbol{\nabla}\Phi$ along the radial direction of the column. Consequently, $\mathbf{E} \times \mathbf{B}$ drift causes the plasma column to rotate around its axis. The background plasma has a density gradient along the negative-x direction, which causes linear drift waves to propagate along the y direction. The radial electric field and the axial magnetic field cause the ion column to produce an $\mathbf{E} \times \mathbf{B}$ rotation around the axis of the column. The most commonly seen vortex structures are the monopole- and dipole-type vortices. The monopole vortex represents an excess in the

local charge density, whereas, the dipole vortex represents a local charge polarization in the local plasma density. The dipole is seen to be produced in the turbulent wake of a 2-D fluid flowing past an obstacle. It can also be formed through pairing or coupling of two monopolar vortices with opposite rotational directions. The interactions of both the monopole and dipole vortices generate tripolar vortex with closed streamlines.

The tripolar vortices are one of the fundamental vortical structures that are characteristic features of two-dimensional and quasi-three-dimensional flows. Tripolar vortices consist of a core vortex of elliptical shape and two satellite vortices of opposite vorticity. Tripole vortices are excited in rotating fluids, possess angular momentum, but no linear momentum, and rotate steadily around the centre of the core vortex. Studies of the generation and stability of tripoles in homogeneous two-dimensional flows were reported by Carton *et al.* [101], who showed that such structure can appear from the saturated azimuthal instability of a monopolar vortex, as well as from the off-axis collision of two dipolar vortices. The emergence of tripolar structures, together with the fundamental structures of monopoles and dipoles, has also been observed in high-resolution simulations of two-dimensional turbulence [102].

In Chapter 2, we considered low-frequency mode in electron-ion plasma with kappa-distributed electrons and dynamic ions, in the presence of external magnetic field, having equilibrium density, temperature, and magnetic field gradients. Linear as well as nonlinear solution was presented. Specifically, in the nonlinear case, we showed the presence of dipolar and vortex street type solutions. However, in this chapter, we seek the possibility of tripolar vortex, by employing Braginskii's transport equations for the ions and nonthermal-distributed electrons.

3.2 Model Equations

We consider an electron-ion magnetoplasma embedded in applied magnetic field $\mathbf{B}_0 = B_0(x)\hat{z}$, where $\hat{z}$ is a unit vector and $B_0(x)$ is the nonuniform magnetic field. We assume that the equilibrium ion temperature, density and magnetic field gradients are along the x-axis. It is further assumed that the toroidal ITG (TITG) mode frequency is much smaller than the ion-gyrofrequency $\omega_{ci}\,(= eB_0/m_i c)$. Here, the case is purely electrostatic for which $\mathbf{E} = -\nabla\phi$, where ϕ is the electrostatic potential. Using the drift-approximation, the ion fluid velocity can be written as

$$\mathbf{u}_i \simeq \frac{c}{B_0}\mathbf{E}_\perp \times \hat{z} - \frac{c}{eB_0 n_i}\nabla\left(n_i T_i\right)\times\hat{z} + \frac{c}{B_0\omega_{ci}}\left[\partial_t + \left(\mathbf{u}_E + \mathbf{u}_{Di}\right)\cdot\nabla\right]\mathbf{E}_\perp ,$$

$$\mathbf{u}_{i\perp} \simeq \mathbf{u}_E + \mathbf{u}_{Di} + \mathbf{u}_{pi} , \tag{3.1}$$

where $\mathbf{u}_E = \mathbf{E}\times\mathbf{B}$ is the drift velocity of the ion fluid, $\mathbf{u}_{Di}$ is the ion diamagnetic drift velocity, and $\mathbf{u}_{pi}$ is the ion polarization drift velocity. For the TITG mode, we shall ignore the parallel component of the ion fluid velocity. Using Eq. (3.1) the ion continuity equation becomes,

$$\partial_t n_i + \nabla\cdot n_i\left(\mathbf{u}_E + \mathbf{u}_{Di} + \mathbf{u}_{pi} + u_{iz}\,\hat{z}\right) = 0, \tag{3.2}$$

Whereas, the energy balance equation for ion fluid is given by

$$\frac{3}{2}\left(\partial_t + \mathbf{u}_i\cdot\nabla\right)T_i + T_i\nabla\cdot\mathbf{u}_i = -\frac{1}{n_i}\nabla\cdot\mathbf{q}_i,$$

where $\mathbf{q}_i = \frac{5}{2}\left(cn_iT_i/eB_0\right)\hat{z}\times\nabla T_i$ is the collisionless Righi Leduc ion heat flux expression. Substituting the value of $\boldsymbol{\nabla}\cdot\mathbf{u}_i$ from the ion continuity equation (3.2), we get

$$n_i\left[\partial_t + \mathbf{u}_i\cdot\nabla\right]T_i - \frac{2}{3}T_i\left[\partial_t + \mathbf{u}_i\cdot\nabla\right]n_i = -\frac{2}{3}\nabla\cdot\mathbf{q}_i \tag{3.3}$$

To close our system of equations, the electron density is to be defined. The 3D(three dimensional) Kappa distribution function $f_\kappa(u)$ can be written as [103]

$$f_\kappa(u) = \frac{n_{e0}}{\theta^3}\left(\frac{1}{\pi\kappa}\right)^{3/2}\frac{\Gamma(\kappa+1)}{\Gamma(\kappa-1/2)}\left(1+\frac{u^2-2e\phi/m_e}{\kappa\theta^2}\right)^{-(\kappa+1)}, \tag{3.4}$$

where $\theta = \left[((2\kappa-3)k_BT)/\kappa m\right]^{1/2}$. It is required that $\kappa > \frac{3}{2}$ for the validity of Kappa distribution. Integrating this κ distribution over the entire velocity space, we obtain the total electron density.

$$n_e = n_{e0}\left[1-\frac{e\phi}{(\kappa_e-3/2)\,T_e}\right]^{-(\kappa-1/2)}, \tag{3.5}$$

After expansion, the electron number density takes the following form:

$$n_e \simeq n_{e0}\left(1+\frac{\kappa-\frac{1}{2}}{\kappa-\frac{3}{2}}\right)\varphi, \tag{3.6}$$

where φ is the normalized electrostatic potential, defied as $\varphi = e\phi/T_e$, n_{e0} denotes the equilibrium number density of nonthermal electrons, and kappa is the defining factor which describes the deviation from the Maxwellian distribution (which can be retrieved in the limit $\kappa\to\infty$).

Using Eq. (3.1) into the ion continuity equation takes the following form

$$\left(\mathcal{L}_t + \mathbf{u}_{Bi}\cdot\nabla\right)\left(\frac{n_{i1}}{n_{i0}}\right) + \mathbf{u}_{Bi}\cdot\nabla\left(\frac{T_{i1}}{T_{i0}}\right) + \tau\left(\mathbf{u}_{Bi}-\mathbf{u}_{ni}\right)\cdot\nabla\varphi$$
$$-\rho_i^2\left[\mathcal{L}_t + \mathbf{u}_{D0}\cdot\nabla\right]\nabla_\perp^2\varphi - \rho_i^2\nabla\cdot\left[\left(\mathbf{u}_{D1}\cdot\nabla\right)\nabla_\perp\varphi\right] + \partial_z u_{iz} = 0 \tag{3.7}$$

where $\mathcal{L}_t = \partial_t + \mathbf{u}_E\cdot\boldsymbol{\nabla}$, $\tau = T_{e0}/T_{i0}$ is the electron to ion temperature proportion, $\rho_i = c_s/\omega_{ci}$ is the ion gyroradius at constant temperature, $c_s = \sqrt{T_{e0}/m_i}$ is the ion-acoustic speed, $\mathbf{u}_{Bi} = -\left(cT_{i0}/eB_0\right)\hat{z}\times\nabla B_0/B_0$ is the ion grad-B drift,$\mathbf{u}_{ni} = -\left(cT_{i0}/eB_0\right)\hat{z}\times\nabla n_{i0}/n_{i0}$ is the ion ∇n_{i0} drift, $\mathbf{u}_{D0} = (\eta_i+1)\mathbf{u}_{ni}$, with $\eta_i = \left(\partial_x \ln T_{i0}\right)/\left(\partial_x \ln n_{i0}\right)$, $\mathbf{u}_{D1} = \left(cT_{i0}/eB_0\right)\hat{z}\times\nabla(N+T)$, $N = n_{i1}/n_{i0}$ and $T = T_{i1}/T_{i0}$, is the first order ion diamagnetic drift velocity.

Inserting Eq.(3.1) into Eq. (3.3) and using continuity equation yields

$$\left(\mathcal{L}_t + \frac{5}{3}\mathbf{u}_{Bi}\cdot\nabla\right)\left(\frac{T_{i1}}{T_{i0}}\right) - \frac{2}{3}\mathcal{L}_t\left(\frac{n_{i1}}{n_{i0}}\right) - \tau\left(\eta_i - \frac{2}{3}\right)\mathbf{u}_{ni}\cdot\nabla\varphi = 0 \tag{3.8}$$

Equations (3.7) and (3.8), with $N = \left[(\kappa-\frac{1}{2})/(\kappa-\frac{3}{2})\right]\varphi = \beta\varphi$, are the required nonlinear coupling equations to study ITG driven mode in an inhomogeneous magnetoplasma with superthermal population of electrons. It is worth mentioning here that to study the TITG mode, we shall ignore the parallel ion dynamics (i.e., $\partial_z = 0$) for toroidal geometry. Furthermore, to complete our set of nonlinear coupled equations, we use the quasineutrality condition, i.e., $n_{e1} \simeq n_{i1}$.

3.3 Tripolar Vortices

We have re-visited the nonlinear properties of low-frequency non-zero ion temperature gradient mode in a inhomogeneous magnetized plasma in the presence of magnetic field and velocity gradients. We shall show analytically as well as numerically that tripolar vortices. By solving Braginskii's transport equations and for some specific profiles of the equilibrium plasma flow velocity, number density and temperature gradients, new types of solutions in the form of tripolar vortices are found to exist.

Here, we consider a collisionless and non-dissipative electron-ion plasma immersed in an inhomogeneous external magnetic field $B_0(x)\ \hat{z}$, and the equilibrium ion-pressure gradient $\partial p_{i0}/\partial x$, where $p_{i0}(x) = n_0(x)T_{i0}(x)$ is the ion pressure. Thus, the gradients of the unperturbed particle number density (n_0), the temperature (T_{i0}) and the magnetic field (B_0) are assumed to be along x-axis. We further assume that the frequency of the TITG mode is much smaller ($|\ \partial_t\ | \ll \omega_{ci}$) than the ion gyrofrequency. The relevant set of nonlinear equations are already formulated in the previous section, i.e.,

$$\begin{aligned}&\left(\mathcal{L}_t + \mathbf{u}_{Bi}\cdot\nabla\right) N + \tau\left(\mathbf{u}_{Bi} - \mathbf{u}_{ni}\right)\cdot\nabla\left(\varphi + \varphi_0\right) + \mathbf{u}_{Bi}\cdot\nabla T \\ &- \rho_i^2\left\{\left(\mathcal{L}_t + \mathbf{u}_{D0}\cdot\nabla\right)\nabla_\perp^2\varphi + \nabla\cdot\left[\left(\mathbf{u}_{D1}\cdot\nabla\right)\nabla_\perp\varphi\right]\right\} + \partial_z\left[\left(1+N\right)u_{iz}\right] = 0, \qquad (3.9)\end{aligned}$$

$$\left(\mathcal{L}_t + \nu_i + u_{iz}\partial_z\right)u_{iz} = -c_s^2\partial_z\left[\varphi + \tau^{-1}\left(N+T\right)\right], \qquad (3.10)$$

$$\left(\mathcal{L}_t + \frac{5}{3}\mathbf{u}_{Bi}\cdot\nabla + u_{iz}\partial_z\right)T - \frac{2}{3}\left(\mathcal{L}_t + u_{iz}\partial_z\right)N - \tau\left(\eta_i - \frac{2}{3}\right)\mathbf{u}_{ni}\cdot\nabla\varphi = 0 \qquad (3.11)$$

where $\mathcal{L}_t \equiv \partial_t + \mathbf{u}_{EB}\cdot\boldsymbol{\nabla}$ and the contribution $(5/3)\mathbf{u}_{Bi}\cdot\boldsymbol{\nabla}$ arises from the divergence of the Righi-Leduc ion heat flux. The system of Eqs. (3.9) to (3.11) can be closed if we use

the quasi-neutrality condition of the plasma with nonthermal electron distribution for which $\delta n_i \simeq \delta n_e = n_0 \beta \varphi$. Thus Eqs. (3.9)-(3.11) with $N = \beta\varphi$ are the set of nonlinear mode coupling equations to study the TITG driven drift-waves in an inhomogeneous magnetoplasma. The effect of equilibrium perpendicular ion flow velocity, which is due to the radial electric field $-\boldsymbol{\nabla}\varphi_0$, is included in the $\mathbf{E}\times\mathbf{B}$ drift by defining the total electrostatic potential as a sum of equilibrium (φ_0) and perturbed (φ) potentials. Here, we also define the normalized equilibrium potential profile $\varphi_0(x) \approx V_{\perp 0}(x-x_0) + V'_{\perp 0}(x-x_0)^2/2$, such that it describes only the linearly varying perpendicular flows [41].

Here we introduce the normalized parameters $t' = c_s t/L_n$, $x' = x/\rho_i$, $z' = z/L_n$, $\varphi' = e\phi L_n/(\rho_i T_e)$, $T' = \delta T L_n/(\rho_i T_{i0})$, $w = L_n u_{iz}/(\rho_i c_s)$. We shall drop the superscript prime for simplicity of the notations. For nondissipative plasma Eqs. (3.9)-(3.11) takes the following form:

$$\partial_t \left(\beta - \nabla_\perp^2\right)\varphi - \left(1+\beta\tau^{-1}\right)\left[\varphi, \nabla_\perp^2\varphi\right] - \left[1 - (\beta+\tau)\ \epsilon_n\ + K\ \nabla_\perp^2\right]\partial_y\varphi + \epsilon_n\ \partial_y T - \tau^{-1}\nabla\cdot\left[\varphi, \nabla_\perp^2\varphi\right] + \partial_z w_{iz} = 0, \tag{3.12}$$

$$\pounds_t w = -\partial_z\left[\left(1+\tau^{-1}\right)\beta\varphi + T\right]\ , \tag{3.13}$$

$$\left(\pounds_t + \frac{5}{3}\epsilon_n\partial_y\right)T - \frac{2}{3}\beta\pounds_t\varphi + \left(\frac{5}{3} - \tau K\right)\partial_y\varphi = 0, \tag{3.14}$$

where $\pounds_t \equiv \partial_t + (\partial_x\varphi\partial_y - \partial_y\varphi\partial_x)$, $\epsilon_n = L_n/(\tau L_B)$, $K = (1+\eta_i)/\tau$, the Poisson bracket is denoted by $[a,b] \equiv (\partial_x a\partial_y - \partial_y a\partial_x)b$ and $L_n(L_B)$ defines equilibrium density (magnetic field) inhomogeneity scale length. Equations (3.12)-(3.14) are the required set of equations for nonlinear mode coupling to study the TITG modes in a nonuniform magnetoplasma with sheared plasma flows formed due to the nonuniform radial electric field.

In the stationary frame moving with some constant velocity u, in a direction perpendicular to x-axis, so as to obtain a localized type solution of Eqs. (3.12) to (3.14), we shall again define a new frame, as we did in the previous chapter. Since general stationary analytical solution of Eqs. (3.12) to (3.14) cannot be obtained, we shall present here some approximate solutions by ignoring the parallel ion dynamics ($\partial z = 0$). Under this assumption, we assume that $\varphi(x, y - wt)$ and $T(x, y - wt)$, where w represents the phase velocity with which the vortex moves in the y-direction. In order to find the stationary vortex solution in the presence of sheared plasma flows, we assume Gaussian- type density, temperature and magnetic field profiles: [41] so that we may write $\epsilon_n \approx \epsilon_{n0} + \epsilon_n^{'} x$ and $K \approx K_0 + K^{'} x$. With this choice of ϵ_n and K, Eqs. (3.12)-(3.14), take the following form:

$$\begin{aligned}
&\partial_t \ \left(\beta - \boldsymbol{\nabla}_\perp^2\right) \varphi - \left(1 + \beta\tau^{-1}\right) \left[\varphi, \boldsymbol{\nabla}_\perp^2 \varphi\right] \\
&- \left\{1 - (\beta + \tau) \left(\epsilon_{n0} + \epsilon_n^{'} x\right) \ + \left(K_0 + K^{'} x\right) \boldsymbol{\nabla}_\perp^2\right\} \partial_y \varphi \\
&+ \left(\epsilon_{n0} + \epsilon_n^{'} x\right) \partial_y T - \tau^{-1} \boldsymbol{\nabla} \cdot \left[\varphi, \boldsymbol{\nabla}_\perp^2 \varphi\right] = 0,
\end{aligned} \tag{3.15}$$

$$\left\{\left(\pounds_t + \frac{5}{3}\left(\epsilon_{n0} + \epsilon_n^{'} x\right)\right) T - \frac{2}{3}\beta \pounds_t \varphi + \frac{5}{3} - \tau\left(K_0 + K^{'} x\right)\right\} \partial_y \varphi = 0. \tag{3.16}$$

Now energy balance equation reduces to

$$\begin{aligned}
&\partial_t T + [\varphi, T] + \frac{5}{3}\left(\epsilon_{n0} + \epsilon_n^{'} x\right) \partial_y T + v_{\perp 0}^{'} (x - x_0) \partial_y T \\
&+ \left\{\frac{5}{3} - \tau\left(K_0 + K^{'} x\right)\right\} \partial_y \varphi = 0.
\end{aligned} \tag{3.17}$$

For standing wave type vortex solution, we may let $\partial_t = -v\partial_y$. Hence, Eq. (3.17) can

be written as,

$$\left\{-w\partial_y + (\partial_x\varphi\partial_\xi - \partial_\xi\varphi\partial_x) + v_{\perp 0}^{'}(x - x_0)\partial_y + \frac{5}{3}\left(\epsilon_{n0} + \epsilon_n^{'}x\right)\partial_y\right\}T$$
$$+\left\{\frac{5}{3} - \tau\left(K_0 + K^{'}x\right)\right\}\partial_y\varphi = 0,$$

or, more specifically,

$$\left[\partial_x\Phi + \left(v_{\perp 0}^{'} + \frac{5}{3}\epsilon_n^{'}\right)\left\{x - \frac{v + v_{\perp 0}^{'}x_0 - \frac{5}{3}\epsilon_{n0}}{\left(v_{\perp 0}^{'} + \frac{5}{3}\epsilon_n^{'}\right)}\right\}\right]\partial_y T$$
$$-\left\{\partial_x T + \tau K^{'}\left(x + \frac{\tau K_0 - \frac{5}{3}}{\tau K^{'}}\right)\right\}\partial_y\varphi = 0. \tag{3.18}$$

If we choose

$$x_1 = \frac{v + v_{\perp 0}^{'}x_0 - \frac{5}{3}\epsilon_{n0}}{\left(v_{\perp 0}^{'} + \frac{5}{3}\epsilon_n^{'}\right)},$$

and

$$x_2 = -\frac{\tau K_0 - \frac{5}{3}}{\tau K^{'}}.$$

Then Eq. (3.18) reduces to

$$\partial_x\left\{\varphi + \left(v_{\perp 0}^{'} + \frac{5}{3}\epsilon_n^{'}\right)\frac{(x - x_1)^2}{2}\right\}\partial_y T - \partial_x\left\{T + \tau K^{'}\frac{(x - x_2)^2}{2}\right\}\partial_y\varphi = 0. \tag{3.19}$$

In the traveling wave frame, Eq. (3.19) takes the form

$$\left[\varphi + \left(v_{\perp 0}^{'} + \frac{5}{3}\epsilon_n^{'}\right)\frac{(x-x_1)^2}{2},\ T + \tau K^{'}\frac{(x-x_2)^2}{2}\right] = 0. \tag{3.20}$$

We note that it is almost impossible solve Eq. (3.20) analytically to obtain a localized vortex type solution. However, if we set $x_1 = x_2$, which is basically a way to find out the phase velocity of the vortex, we may integrate Eq. (3.20) and get the following expression

$$T + \tau K^{'}\frac{(x-x_1)^2}{2} = f_1\left(\varphi + \left(v_{\perp 0}^{'} + \frac{5}{3}\epsilon_n^{'}\right)\frac{(x-x_1)^2}{2}\right). \tag{3.21}$$

Here f_1 represents an arbitrary function of its argument. For a localized vortex type solution, we have to impose a condition of vanishing of perturbations at infinity, such that

$$T = \frac{K^{'}\tau}{\left(v_{\perp 0}^{'} + \frac{5}{3}\epsilon_n^{'}\right)}\varphi = C_1\varphi. \tag{3.22}$$

Eliminating T from Eq. (3.20), we readily obtain

$$\begin{aligned}
&- w\partial_y(\beta\varphi - \boldsymbol{\nabla}_\perp^2\varphi) + \left(1+\beta\tau^{-1}\right)\left[\left(-\partial_x\varphi\partial_y + \partial_y\varphi\partial_x\right)\boldsymbol{\nabla}_\perp^2\varphi + \left(\partial_x\varphi\partial_y - \partial_y\varphi\partial_x\right)\varphi\right] \\
&- \left\{1 - (\beta+\tau)\left(\epsilon_{n0} + \epsilon_n^{'}x\right) \ + \left(K_0 + K^{'}x\right)\boldsymbol{\nabla}_\perp^2\right\} + \left(\epsilon_{n0} + \epsilon_n^{'}x\right)\partial_y T \\
&+ v_{\perp 0}^{'}(x - x_{\perp 0})\partial_y(\varphi - \boldsymbol{\nabla}_\perp^2\varphi) = 0,
\end{aligned}$$

or

$$\partial_x \left\{ \varphi + \frac{\left(v_{\perp 0}^{'} - K^{'}\right)}{(1+\beta\tau^{-1})} \frac{(x-x_3)^2}{2} \right\} \partial_y (\beta\varphi - \boldsymbol{\nabla}_{\perp}^2 \varphi)$$
$$- \left\{ \partial_x (\beta\varphi - \boldsymbol{\nabla}_{\perp}^2 \varphi) - \frac{(\beta+\tau+C_1)\,\epsilon_n^{'} + K^{'}}{(1+\beta\tau^{-1})} \frac{(x-x_4)^2}{2} \right\} \partial_y \varphi = 0, \tag{3.23}$$

where

$$x_3 = \frac{\left(v_{\perp 0}^{'} x_0 + v + K_0\right)}{\left(v_{\perp 0}^{'} - K^{'}\right)},$$

and

$$x_4 = \frac{(1 - \epsilon_{n0}(\beta+\tau+C_1) - K_0)}{((\beta+\tau+C_1)\,\epsilon_n^{'} + K^{'})}.$$

Equation (3.23) can be rewritten as

$$\left[\varphi + \frac{\left(v_{\perp 0}^{'} - K^{'}\right)}{(1+\beta\tau^{-1})} \frac{(x-x_3)^2}{2}, \beta\varphi - \boldsymbol{\nabla}_{\perp}^2 \varphi - \frac{(\beta+\tau+C_1)\,\epsilon_n^{'} + K^{'}}{(1+\beta\tau^{-1})} \frac{(x-x_4)^2}{2} \right] = 0. \tag{3.24}$$

Setting $x_3 = x_4$, once again, one may write the general solution of (3.24) as

$$\boldsymbol{\nabla}_{\perp}^2 \varphi - \beta\varphi + \frac{(\beta+\tau+C_1)\,\epsilon_n^{'} + K^{'}}{(1+\beta\tau^{-1})} \frac{(x-x_3)^2}{2} = f_2 \left(\varphi + \frac{\left(V_{\perp 0}^{'} - K^{'}\right)}{(1+\beta\tau^{-1})} \frac{(x_3)^2}{2} \right), \tag{3.25}$$

where f_2 is an arbitrary function. Letting $\varphi' = 4\varphi\,(1+\beta\tau^{-1})\,/(v_{\perp 0}^{'} - K^{'})$ and $v_{\perp 0}^{'} \neq K^{'}$,

we get

$$\frac{(v_{\perp 0}^{'}-K^{'})}{4\,(1+\beta\tau^{-1})}\left\{\beta\varphi^{\prime}-\boldsymbol{\nabla}_{\perp}^{2}\varphi^{\prime}\right\}-\frac{(\beta+\tau+C_{1})\,\epsilon_{n}^{'}+K^{'}}{(1+\beta\tau^{-1})}\frac{(x-x_{3})^{2}}{2}$$
$$=f_{2}\left(\varphi^{\prime}+2(x-x_{3})^{2}\right)\frac{\left(v_{\perp 0}^{'}-K^{'}\right)}{4\,(1+\beta\tau^{-1})},$$

$$\left\{\beta\varphi^{\prime}-\boldsymbol{\nabla}_{\perp}^{2}\varphi^{\prime}\right\}-\frac{(\beta+\tau+C_{1})\,\epsilon_{n}^{'}+K^{'}}{(v_{\perp 0}^{'}-K^{'})}2(x-x_{3})^{2}=f_{2}\left(\varphi^{\prime}+2(x-x_{3})^{2}\right).$$

Let $x_3 = x$. Then

$$\frac{b^{2}}{a^{2}}=\left(1+\frac{(\beta+\tau+C_{1})\,\epsilon_{n}^{'}+K^{'}}{(v_{\perp 0}^{'}-K^{'})}\right),$$

and, finally, we obtain

$$\boldsymbol{\nabla}_{\perp}^{2}\varphi=\frac{b^{2}}{a^{2}}\beta\varphi \tag{3.26}$$

A typical tripolar vortex profile for the equipotential contours for the tripolar part of the electrostatic potential is plotted in the two dimensional x-y plane and is shown in Fig. (3-1) by choosing some typical parameters of Tokamak plasma: $T_e = 10$ keV, $n_e = 10^{14}$ cm^{-3}, $\tau = 2$, $B_0 = 3.45\times10^4$ Gauss, $\rho_s = 0.25$ cm, $L_B = 300$ cm, $\epsilon_{n0} = 0.3$, $v_{\perp 0}^{'} = 4.5$, $\eta_i = 3$ and $r_0 = 2$. These values yield $b = 1.03$ and $\lambda_1 = 1.42$, where the normalized parameter K' is approximated with $(1+\eta_i)/\tau$, and $\epsilon_n^{'}$ with $L_n/(\tau L_B)$ such that $L_n = \epsilon_{n0} L_B$. Here, again, we have dropped the superscript prime for simplicity of the notation.

Following the procedure of Ref. [55], we subdivide the space in the form of a circle of some radius r_0 and then solve Eq. (3.26) by employing cylindrical coordinates, taking $r = \sqrt{x^2+y^2}$ and $\theta = \arctan(y/x)$, independently outside and inside that circle and obtain general solution of Eq. (3.26) in the form of Bessel equations. The detailed

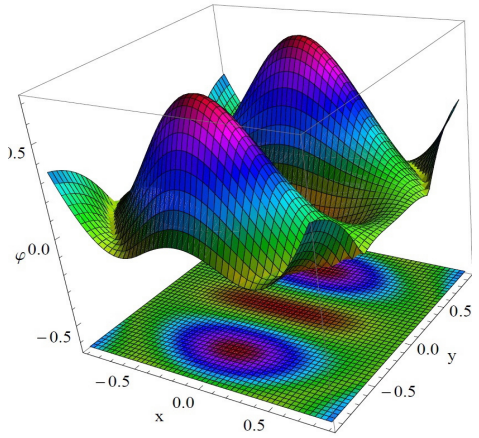

Figure 3-1: Fig.1. (colored online only) A shadowgraph of 3D view of the normalized electrostatic potential for $\kappa = 3$ case for other plasma parameters given in the text.

analysis can be seen from our earlier published work. We numerically solve the Bessel equations for the outer and inner regimes by using the appropriate boundary condition at the boundary of given circle, namely by the continuity of the normalized potential and the continuity of $\partial\varphi/\partial r$ at $r = r_0$. To draw the vortex profile in three-dimensions, we choose the aforementioned typical tokamak parameters and obtained a shadow-graph. The shadow-graph clearly shows tripolar vortex on a scale-length of ion-Larmor radius. The equipotential contours of electrostatic potential resembles with tripolar vortex. The contours show a double vortex between the lobes of a monopolar vortex structure having negative value of the potential. Figure (3-1) shows a shadowgraph of three dimensional (3D) view of the potential for $\kappa = 3$ case Fig. (3-2) in which the nonthermal effect is pronounced and the amplitude of the potential becomes slightly higher than the classical case (kappa$- > \infty$ or simply $\beta - > 1$ case), in which the electrons follow Boltzmann type distribution. It is evident from the shadow plots Fig. (3-1) that the amplitude of the wave potential is small.

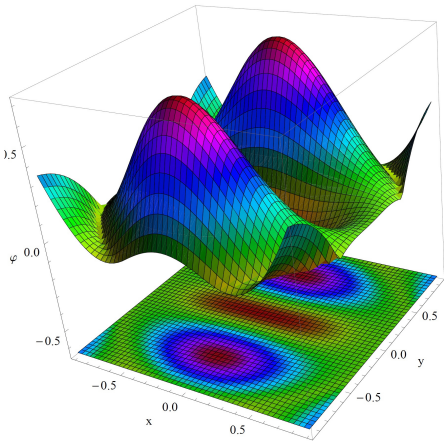

Figure 3-2: Shadow graph of 3D view of the normalized potential for $\kappa - > \infty$ case in which the electrons follow classical Bolzmann type distribution with the same other parameters as taken in Fig.3-1.

3.4 Conclusions

We have studied the nonlinear properties of ITG mode for Maxwellian ions and nonthermal kappa distributed electrons for low frequency inhomogeneous magnetoplasma having equilibrium ion temperature and density gradients. By using drift-approximation, we have formulated the group of nonlinear set of equations that admit stationary solution in the form of a tripolar vortices. For tokamak plasma parameters, we have plotted numerically the tripolar vortices which shows that the inclusion of kappa distributed electrons brings about a decrease in the spatial extent of the nonlinear vortex structures in comparison with Maxwellian distributed counterparts. This work would be useful to gain deep insight the origin of drift-waves and associated coherent nonlinear structure formation in toroidal ITG driven drift modes which has applications in space as well as in laboratory plasmas.

Chapter 4

Sheared Driven Ion Acoustic Vortex Formation in Two-Electron-Temperature Plasma

4.1 Introduction

Linear and nonlinear properties electrostatic waves in multi species plasma has been investigated, whereas the cold electrons are Boltzmannen and the hot component of electrons are Cairn's distributed. The ions are considered dynamic and cold. It is observed that the propagation regime of ion acoustic and drift waves has been changed due to the presence of suprathermal electrons, ion-neutral collisions and ions sheared flow. Hot component of electrons follow Cairn's distribution which significantly changes the growth rate of ions shear flow driven instability. We found that vortex structures get modified in the presence of nothermal electrons.

4.2 Nonlinear Model Equations

The propagation of ion acoustic mode in two electron-temperature and dynamic cold ion collisional magnetoplasma is considered. We assume that cold electrons are Boltzmannen and the hot electrons are Cairn's distributed. The applied magnetic field is constant and pointing in the z-direction such that $\mathbf{B}_0 = B_0\ \hat{\mathbf{z}}$. For electrostatic mode, the perturbed electric field can be related to electrostatic wave potential such that $\mathbf{E} = -\boldsymbol{\nabla}\varphi$. For three component plasma, the charge neutrality condition in equilibrium satisfies the following relation,

$$n_{c0} + n_{h0} = n_{i0}, \tag{4.1}$$

where the index c (h) is used to indicate the cold (and the hot) component of electrons and the index i for the ions. The Cairn's type distributed electrons, the distribution function can be written as follows:[59]

$$f_{h0}(v) = \frac{n_{h0}}{(3\alpha+1)\sqrt{2\pi v_{th}^2}}\left(1+\frac{\alpha v^4}{v_{th}^4}\right)\exp\left(-\frac{v^2}{2v_{th}^2}\right), \tag{4.2}$$

where the equilibrium density of hot electrons is n_{h0} with thermal velocity defined as $v_{th} = \sqrt{T_h/m_e}$. Where T_h is the temperature of hot electrons and α is the nonthermal parameter. The number density of hot electrons can be obtained by integrating over the entire velocity space, such that we have

$$n_h = n_{h0}\left(1-\beta\left(\frac{e\varphi}{T_h}\right)+\beta\left(\frac{e\varphi}{T_h}\right)^2\right)Exp\left(\frac{e\varphi}{T_h}\right), \tag{4.3}$$

Here $\beta = 4\alpha/(1+3\alpha)$. It may be noted here that the above expression reduces to

the well known classical Boltzmann distribution by taking the limit $\alpha = 0$. Whereas, the cold electrons are assumed to be Boltzmannen type, such that

$$n_c = n_{c0} \exp\left[-\frac{e\varphi}{T_c}\right], \tag{4.4}$$

where T_c is the cold electron temperature.

For convenience, we use the notation: the cold electron density proportion is given by $f = n_{c0}/n_{i0}$. Moreover, $\alpha_c = T_{eff}/T_c$, $\alpha_h = T_{eff}/T_h$, and effective temperature $T_{eff} = T_c/(f + (1-f)\tau)$ with $\tau = T_c/T_h$. n_{i0} is the total ion number density, T_i is the temperatures of ions. Expanding Eq.(4.3) $n_h = n_{h0}(1-f)\left(1 - \beta\left(\alpha_h\phi\right) + \beta\left(\alpha_h\phi\right)^2\right) Exp\left(\alpha_h\phi\right)$ by taking $\alpha_h\phi \ll 1$, the hot electrons perturbed part can be written as, $n_{h1} \simeq n_{h0}(1-f)(1-\beta)\left(\alpha_h\phi_1\right)$, whereas the normalized electrostatic potential $\phi = e\varphi/T_{eff}$.

The Poisson's equation (4.4) in the linearized form, and the above expression for the perturbed number density of hot electrons, yield the following result

$$\begin{aligned}\frac{n_{i1}}{n_{h0}} &\simeq \left[f\delta_c + (1-\beta)(1-f)\delta_h\right]\phi - \lambda_D^2\ \nabla^2\phi \\ &= \delta\phi - \lambda_D^2\nabla^2\phi,\end{aligned} \tag{4.5}$$

where $\delta = \left[f\alpha_c + (1-\beta)(1-f)\alpha_h\right]$. n_{c1}, n_{h1} are the perturbed number densities of cold and hot electrons, respectively. Here $\lambda_D = \sqrt{T_{eff}/4\pi n_{i0}e^2}$, $\delta_c = n_{c0}/n_{i0}$, and $\delta_h = n_{h0}/n_{i0}$.

The ion momentum balance equation for the collisional plasma can be written as

$$m_i n_{i0} \left(\partial_t + \mathbf{v}_i \cdot \nabla\right) \mathbf{v}_i = e n_{i0} \left(-\nabla\varphi + \frac{1}{c}\mathbf{v}_i \times \mathbf{B}_0\right) - m_i n_{i0} \nu_{in} \mathbf{v}_i \tag{4.6}$$

where ν_{in} is the collision frequency between the ion-neutrals.

The perpendicular component of cold ion fluid using drift-approximation, for low-frequency waves ($\partial_t \ll \omega_{ci}$, where $\omega_{ci} = eB_0/m_i c$ is the ion gyrofrequency), can be written as

$$\mathbf{v}_{i\perp} \simeq \frac{c}{B_0}\hat{z} \times \nabla\varphi - \frac{c}{B_0\omega_{ci}} \left(\partial_t + \nu_{in} + \mathbf{v}_E \cdot \nabla + (v_{i0}(x) + v_{iz})\partial_z\right) \nabla_\perp \varphi. \tag{4.7}$$

The z-component of ion fluid with ion shear flow is given by

$$\begin{aligned}
\left(\partial_t + \nu_{in} + \mathbf{v}_E.\nabla + (v_{i0}(x) + v_{iz})\partial_z\right) v_{iz} &= -\frac{e}{m_i}\partial_z\varphi + \mathbf{v}_E \cdot \nabla v_{i0}(x) \\
&= -\frac{T_{eff}}{m_i}\left(\partial_z - \frac{\partial_x v_{i0}(x)}{\omega_{ci}}\partial_y\right)\left(\frac{e\varphi}{T_{eff}}\right) \\
&= -c_s^2 \left(\partial_z - S_i\partial_y\right)\phi.
\end{aligned} \tag{4.8}$$

Using drift approximation (4.7), the continuity equation for the ions can be written as

$$\begin{aligned}
&\left(d_t + \nu_{in} + \mathbf{v}_E.\nabla + v_{iz}\partial_z\right)\frac{n_{i1}}{n_{h0}} - \frac{c}{B_0\omega_{ci}}\left(d_t + \nu_{in} + \mathbf{v}_E.\nabla + v_{iz}\partial_z\right)\nabla_\perp^2\varphi \\
&-\nu_{in}\frac{n_{i1}}{n_{h0}} - \frac{c\partial_x \ln n_{i0}}{B_0}\partial_y\varphi + \partial_z v_{iz} = 0,
\end{aligned} \tag{4.9}$$

where $d_t = \partial_t + v_{i0}(x)\partial_z$, and $\mathbf{v}_E = (c/B_0)\hat{z} \times \nabla\varphi$ is the $\mathbf{E} \times \mathbf{B}_0$ drift. Here, we have

assumed that $|\mathbf{v}_E \cdot \nabla| \gg |v_z \partial_z|$. It is worth mentioning here that $\nabla \times \mathbf{v} \neq 0$ can give rise to a vortex type structure in the nonlinear regime. Equations (4.5), (4.8) and (4.9) is the desired set of equations.

4.3 Derivation of Dispersion Relation

To derive a linear dispersion relation, we drop nonlinear terms in Eqs. (4.5)-(4.9), and by using sinusoidal approximation for the perturbed quantities: $\exp\left[-i(\omega t - k_y y - k_z z)\right]$, and finally obtain a quadratic dispersion relation

$$\left(\omega' + i\nu_{in}\right)^2 k_\perp^2 \rho_s^2 + \delta\left(\omega' + i\nu_{in}\right)\left[\omega'\left(1 + \frac{k^2\lambda_D^2}{\delta}\right) - \omega_*\right] - k_z^2 c_s^2\left(1 - \frac{k_y S_i}{k_z}\right) = 0, \quad (4.10)$$

Here Doppler shifted frequency is $\omega' = \omega - k_z v_{i0}(x)$, the Larmor radius of the ions $\rho_i = c_s/\omega_{ci}$, $\omega_* = \left(k_y c T_{eff} \partial_x \ln n_{i0}\right) / \left(\delta e B_0\right)$ is the drift-wave frequency, and $S_i = \partial_x v_{i0}(x)/\omega_{ci}$ is the ion sheared flow parameter.

For collisionless case and for uniform density plasma with $\lambda_D^2 k^2 \ll 1$, Eq. (4.10) reduces to

$$\omega^{'} = k_z c_s \sqrt{\frac{1 - k_y S_i/k_z}{f\alpha_c + (1-f)(1-\beta)\alpha_h + k_\perp^2 \rho_i^2}}, \quad (4.11)$$

It may be noted here that the above dispersion relation shows unstable regime for $k_y S_i > k_z$. In Fig. 4-1, we have plotted a normalized growth rate γ/ω_{ci} vs., $k_z\rho_i$, by taking the same parameters as given in Ref.[68]: i.e., $N_{i0} = 0.1/\text{cm}^3$, $B_0 = 0.2$ G, $T_h = 500eV$, $T_c = 5$ eV, $\tau = 0.04$, $f = 0.1$, $M = u/c_s = 0.98$, $k_y = \sqrt{0.5}/\rho_s$, $S_i = 0.5$, for different values of the nonthermal electron population parameter, $\alpha = 0.22$ (solid black curve) and

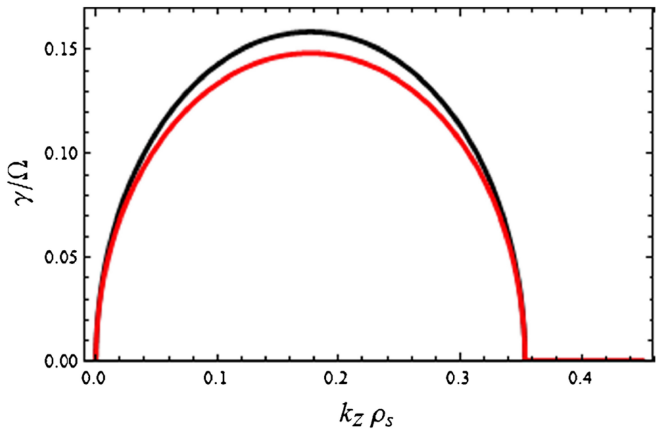

Figure 4-1: Plot of normalized growth rate as a function of $k_z\rho_i$ for the parameters described in the text. The black solid line is for $\alpha = 0.22$ and the red one is for $\alpha = 0.1$.

$\alpha = 0.1$ (red dashed curve). The growth rate of acoustic mode is shown in the graph, in the presence of nonthermal electrons and sheared flow increases.

Whereas, in the presence of ion-neutral collisions, damps the coupled ion-acoustic drift mode with hot electrons for $\omega^{'} << \nu_{in}$. We may let $\omega = \omega_r + i\gamma$, and obtain the following result

$$\gamma = -\frac{\nu_{in}k_{\perp}^2\rho_s^2}{\left(\delta + \lambda_D^2 k^2\right)} - \frac{k_z^2 c_s^2\left(1 - k_y S_i/k_z\right)}{\nu_{in}\left(\delta + \lambda_D^2 k^2\right)}. \tag{4.12}$$

Eq. (4.12) shows a purely damped mode in the absence of parallel ion-sheared flow. Clearly, the ion drift-dissipative mode is found to become unstable for $|S_i|\,k_y > k_z$. Therefore, it is evident from Eq. (4.12) that both the ion acoustic and drift mode get destabilized by the combined effects of ion sheared flow for $|S_i|\,k_y > k_z$ case. The ion sheared flow in a collisional magnetoplasma can drive unstable mode by the coupling of ion-acoustic and drift-mode.

4.4 Nonlinear Analysis

It is well known that when the finite amplitude drift and ion-acoustic waves nonlinearly interact with each other, variety of nonlinear coherent structures can be formed. We use some suitable normalization in order to obtain vortex solution i.e., the time variable is normalized with ω_{ci}^{-1}, the space variables with $\rho_s = c_s/\omega_{ci}$, the fluid velocity of ions with $c_s = \sqrt{T_{eff}/m_i}$ and the number density of ion with its equilibrium number density. The continuity and momentum balance equation for the collisionless ions can be written as:

$$\partial_t n_i + \nabla.(n_i \mathbf{v}_i) = 0, \tag{4.13}$$

$$(\partial_t + \mathbf{v}_i.\nabla)\,\mathbf{v}_i = \text{-}\nabla\phi + \mathbf{v}_i \times \hat{z}, \tag{4.14}$$

Using Eq. (4.7) in the ion continuity equation and by letting $n_i = n_{i0} + n_{i1}$, (where $n_{i1} \ll n_{i0}$), we get

$$D_t(n_{i1} - \nabla_\perp^2\phi) - (\partial_x \ln n_{i0})\,\partial_y\phi + \partial_z v_{iz} = 0,$$

where $D_t = d_t + \hat{z} \times \nabla_\perp\phi \cdot \nabla + v_{iz}\partial_z$. The Poisson's equation(4.5), in the dimensionless form can be expressed as: $n_{i1} = \delta\phi - (\lambda_D^2/\rho_s^2)\nabla^2\phi$, consequently the above equation can be re-written as

$$D_t(\delta\phi - (1 + \lambda_D^2/\rho_s^2)\nabla_\perp^2\phi) - (\partial_x \ln n_{i0})\,\partial_y\phi + \partial_z v_{iz} = 0. \tag{4.15}$$

Here we have used $\nabla_\perp^2 \gg \partial^2/\partial z^2$.

The parallel component of ion equation of motion yields the following result

$$\begin{aligned} D_t v_{iz} &= -\partial_z \phi - \hat{z} \times \nabla_\perp \phi \cdot \nabla v_{i0}(x) \\ &= -\partial_z \phi + S_{i0} \partial_y \phi, \end{aligned} \tag{4.16}$$

where the normalized shear flow parameter is defined as $S_{i0} = \partial_x v_{i0}(x)/\omega_{ci}$.

To obtain stationary solution [104] of Eqs. (4.15) and (4.16), we define a frame (x, ξ), in which we can write $\xi \equiv y + \eta z - u\, t$, where the vortex speed is defined by a parameter u and η is an arbitrary constant. Here we have assumed that $|\hat{z} \times \nabla_\perp \phi \cdot \nabla| >> |v_{iz} \partial_z|$. Equation (4.15) in the transformed frame takes the following form

$$-U \mathcal{L}_\phi v_{iz} = -\left(\eta - S_{i0}\right) \partial_\xi \phi, \tag{4.17}$$

Here we define a differential operator $\mathcal{L}_\phi = \partial_\xi - (1/U)\left(\partial_x \phi \partial_\xi - \partial_\xi \phi \partial_x\right)$ with $U = u - \eta v_{i0}$. It can be shown very easily that the stationary solution of Eq. (4.17) is

$$v_{iz} = \frac{1}{U}(\eta - S_{i0})\phi. \tag{4.18}$$

Inserting v_{iz} from Eq. (4.18) into Eq. (4.15), we get

$$-U \mathcal{L}_\phi (\delta\phi - (1 + \lambda_D^2/\rho_s^2)\nabla_\perp^2 \phi) - \left(\partial_x \ln n_{i0}\right) \partial_\xi \phi + \frac{\eta}{U}(\eta - S_{i0}) \partial_\xi \phi = 0,$$

which on simplification gives

$$\left(\delta - \frac{U_{n*}}{U} - \frac{\alpha(\alpha - S_{i0})}{U^2}\right)\partial_\xi\phi + \left(1 + \frac{\lambda_D^2}{\rho_s^2}\right)\left[\partial_\xi - \frac{1}{U}\hat{z}\times\nabla_\perp\phi\cdot\nabla\right]\nabla_\perp^2\phi = 0, \quad (4.19)$$

where $U_{n*} = (\partial_x \ln n_{i0})$. For $\left(\delta - \frac{U_{n*}}{U} - \frac{\eta(\eta - S_{i0})}{U^2}\right) = 0$, we obtain the following equation

$$\partial_\xi\nabla_\perp^2\phi - \frac{1}{U}[\phi, \nabla_\perp^2\phi] = 0, \quad (4.20)$$

where $\nabla_\perp^2 = \partial_x^2 + \partial_\xi^2$. The above equation is satisfied by

$$\nabla_\perp^2\phi = \frac{4\phi_0}{R^2}\exp\left(-\frac{2}{\phi_0}(\phi - Ux)\right) \quad (4.21)$$

where ϕ_0 and R_0 are some constants. The analytical solution of Eq. (4.21) is

$$\phi = Ux + \phi_0 \ln\left\{2\cosh x + 2\left(1 - \frac{1}{R_0^2}\right)\cos\xi\right\}. \quad (4.22)$$

For $R_0^2 > 1$, Eq. (4.22) gives the well known vortex chain type solution[68, 104]. Here $U = [U_{n*} \pm \sqrt{(U_{n*})^2 + 4\eta(\eta - S_{i0})}]/2$ represents the vortex chain speed. To obtain an analytical solution, we proceed as follows. By retaining the Jacobian nonlinearity, we get

$$\partial_\xi\nabla_\perp^2\phi - \frac{1}{U}[\phi, \nabla_\perp^2\phi] - \psi_1\partial_\xi\phi = 0, \quad (4.23)$$

where $\psi_1 = \left(-\delta + \frac{U_{n*}}{U} + \frac{\eta(\eta - S_{i0})}{U^2}\right)\left(1 + \frac{\lambda_D^2}{\rho_s^2}\right)^{-1}$. The solution of Eq. (4.23) can be written

as

$$\left[\nabla_{\perp}^{2} - \psi_1\right] \phi = f\left(\phi - Ux\right) \tag{4.24}$$

Here we assume the function $f\left(\phi - Ux\right) = F \times \left(\phi - Ux\right)$ i.e., it behaves linearly. Where F is some constant. Thus the Eq.(4.24) gives us

$$\nabla_{\perp}^{2}\phi - \psi_1\phi = F \times \left(\phi - Ux\right). \tag{4.25}$$

Using cylindrical polar coordinates (r, θ) with azimuthal symmetry, Eq.(4.25) can be transformed and the inner region $(r < R_0)$ and the outer region $(r > R_0)$ solutions can be expressed in the following way, where R_0 is the radius of a circle,

$$\phi_{out}(r, \theta) = C_1 K_1(\psi_1 r)\cos\theta. \tag{4.26}$$

and

$$\phi_{in}(r, \theta) = \left[C_2 J_1\left(\psi_2 r\right) + \left(\frac{\psi_1^2 + \psi_2^2}{\psi_2^2}\right) U\ r\right]\cos\theta, \tag{4.27}$$

where $\psi_2^2 = -(\psi_1^2 + F)$, $F = -(\psi_1^2 + \psi_2^2)$, and $K_1(J_1)$ are modified (ordinary) Bessel function of order one, respectively. Here the unknown constants C_1 and C_2 can be calculated by using the continuity of the function ϕ, $\partial_r\phi$, and $\nabla_{\perp}^{2}\phi$ at the boundary of the circle $r = a_0$,

$$C_1 = U\frac{a_0}{K_1(\psi_1 a_0)},\ C_2 = U\left(-\frac{\psi_1^2}{\psi_2^2}\right)\frac{a_0}{J_1(\psi_2 a_0)}, \tag{4.28}$$

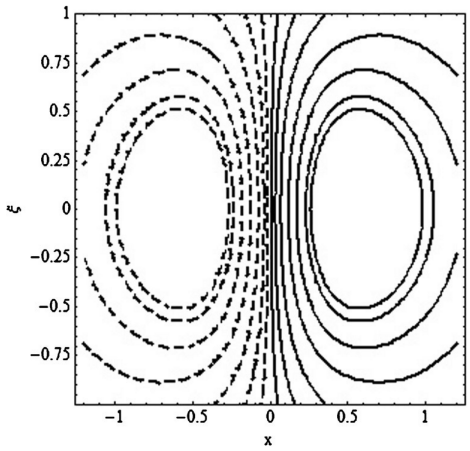

Figure 4-2: The plot of potential ϕ in the contour form in (x, ξ) plane is shown for the mach number $M = u/c_s = 0.98$, with $S_i = 0.1$. The normalization used for the distances is with ρ_i.

and ψ_2 from the following relation

$$\frac{K_2(\psi_1 a_0)}{K_1(\psi_1 a_0)} = -\frac{\psi_1}{\psi_2}\frac{J_2(\psi_2 a_0)}{J_1(\psi_2 a_0)}. \tag{4.29}$$

The above equations (4.26) &(4.27) alongwith the said constants forms dipolar vortices. The contour plot in 2D of the electrostatic potential is plotted in Fig. 4-3 for the same parameters taken in Fig. 4-1. For those parameters, we found $\rho_s = 6196.3$ cm. Notice that like vortex street, the dipolar vortex solution is obtained on the same ρ_s scale size. Equation (4.26) represents a bounded dipolar type solution for $\psi_1 = \left(-\delta + \frac{U_{n*}}{U} + \frac{\eta(\eta - S_{i0})}{U^2}\right) > 0$. For nonthermal plasma, the condition of the boundness gets modified. The Mach number range also gets modified in the presence of hot component of the plasma.

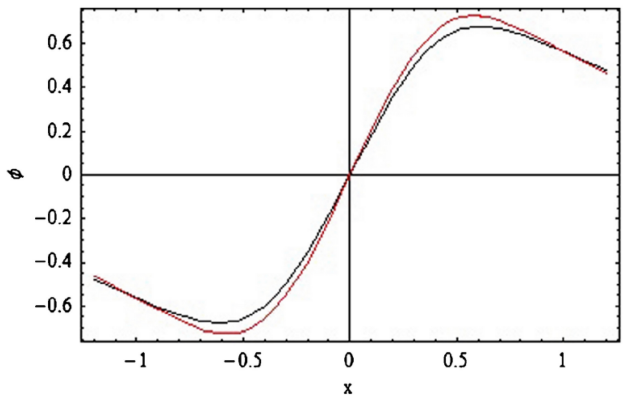

Figure 4-3: The dipolar vortex in 2D is plotted for $\alpha = 0.1$ (in red color) and $\alpha = 0.9$ (black color) for $M = 0.98$.

4.5 Summary

In this chapter, linear/nonlinear properties of coupled ion acoustic and drift waves has been discussed for Cairn's type hot electrons with parallel ion sheared flows. New dispersion relation is derived and instability condition is also discussed. The normalized growth rate is plotted for some space plasma parameters by varying the superthermal electron parameter. The growth rate is found to become higher by increasing the population of hot electrons. On the other hand, for collisionless case, dipolar and vortex street can be formed. It is found that the presence of superthermal electrons changes the vortex structure and its boundedness. The results of our investigation may be beneficial to understand the dynamics of two electron temperature and ion plasma for space applications.

Chapter 5

Electron acoustic soliton in magneto-rotating e-p-i plasma

5.1 Introduction

In this chapter, we focus on electron acoustic soliton formation and its propagation in rotating electron-positron-ion magnetoplasma. We consider cold electrons which are dynamic and follow non-Maxwellian (Cairns type) distribution for the electrons and positrons, and stationary ions, whose mass is very large compared to the electron/positron mass. We first derive a linear dispersion relation and afterwards we investigate how it is affected by magnetic field, the nonthermal parameter, and rotation. For the nonlinear analysis, we derive kdV (Korteweg-de-Vries) equation by employing the usual reductive perturbation method (RPM). The presence of nonthermal positrons, both dip and hump type solitons can be excited, moreover, the inclusion of magneto-rotating drastically affects properties of these solitary waves.

5.2 Derivation of Linear Dispersion Relation

We assume a rotating, magnetized electron-positron-ion plasma with cold electron, nonthermal hot electron-positrons, and static collisionless ions. The nonthermal hot e-p population is taken to be Cairns type distribution (Cairns *et al.* 1995) and the number densities of nonthermal electrons/positrons [84, 105] are taken to be:

$$n_h = n_{oh}\left(1 + \Theta\left[\frac{e\phi}{T_h}\right] + \frac{1}{2}\left[\frac{e\phi}{T_h}\right]^2 + \cdots\right) \tag{5.1}$$

$$n_p = n_{op}\left(1 - \Theta\left[\frac{e\phi}{T_p}\right] + \frac{1}{2}\left[\frac{e\phi}{T_p}\right]^2 + \cdots\right), \tag{5.2}$$

where $\Theta \equiv (1-\beta)$. For $\beta \longrightarrow 0$, one gets the Boltzmannen distributions, i.e., $n_h \longrightarrow n_{oh}\exp(\frac{e\phi}{T_h})$, $n_p \longrightarrow n_{op}\exp(-\frac{e\phi}{Tp})$.

For a collisionless, rotating magnetized plasma, the set of fluid equations are

$$\frac{\partial n_c}{\partial t} + \boldsymbol{\nabla}.(n_c\mathbf{u}_c) = 0, \tag{5.3}$$

and,

$$m_e n_c\left(\frac{\partial \mathbf{u}_c}{\partial t} + (\mathbf{u}_c.\boldsymbol{\nabla})\mathbf{u}_c\right) = -en_c\mathbf{E} - en_c(\frac{\mathbf{u}_c \times \mathbf{B}}{c}) + 2m_e n_c(\mathbf{u}_c \times \boldsymbol{\Omega}), \tag{5.4}$$

where e is the charge of electron, n_c is the cold species of electron number density, and $\mathbf{u}_c$ is the fluid velocity of the cold electrons, $\mathbf{E} = -\boldsymbol{\nabla}\phi$ is the electric field and $\mathbf{B} = B_0\mathbf{z}$ is the applied magnetic field, $\boldsymbol{\Omega}$ is the angular frequency of rotating frame [70]) i.e.,

$\mathbf{\Omega} = \Omega_x \hat{x} + \Omega_z \hat{z}$. To close the set of modeled equations, we use Gauss's law to write

$$\boldsymbol{\nabla} \cdot \mathbf{E} = 4\pi e \ \left(n_o + n_p - n_h - n_c\right), \tag{5.5}$$

where n_0 is the equilibrium number density of fixed positive ions. In the equilibrium state, one can write $n_0 + n_{0p} = n_{0c} + n_{0h}$, where n_{0s} $(s = p, c, h)$ are the equilibrium number densities. Eqs. (5.1) and (5.2) in the normalized form are

$$n_h = \left(1 - \beta\varphi + \beta\varphi^2\right) \exp(\varphi) = 1 + \Theta\varphi + \frac{\varphi^2}{2} + \cdots$$

$$n_p = \left(1 + \beta\rho\varphi + \beta\rho^2\varphi^2\right) \exp(-\rho\varphi) = 1 - \rho\Theta\varphi + \frac{\rho^2\varphi^2}{2} + \cdots$$

Similarly, The normalized form of Gauss's law is

$$\partial_x^2\varphi + \partial_z^2\varphi = 1 + n_c\sigma - \delta - \alpha + \Theta\left(1 + \alpha\rho\right)\varphi + (1 - \alpha\rho^2)\frac{\varphi^2}{2} + \cdots \tag{5.6}$$

The normalized version of Eqs. (5.3) and (5.4) is

$$\frac{\partial n_c}{\partial t} + \boldsymbol{\nabla}.(n_c\mathbf{u}_c) = 0 \tag{5.7}$$

$$\frac{\partial \mathbf{u}_c}{\partial t} + (\mathbf{u}_c.\boldsymbol{\nabla})\mathbf{u}_c = \boldsymbol{\nabla}\varphi - R(\mathbf{u}_c \times \mathbf{z}) + 2(\mathbf{u}_c \times \mathbf{\Gamma}), \tag{5.8}$$

or, rewriting in the component form as

$$\partial_t n_c + \partial_x(n_c u_{cx}) + \partial_z(n_c u_{cz}) = 0, \tag{5.9}$$

$$\partial_t u_{cx} + u_{cx}\partial_x u_{cx} + u_{cz}\partial_z u_{cx} = \partial_x \varphi - \Gamma_{eff}\ u_{cy}\ , \tag{5.10}$$

$$\partial_t u_{cy} + u_{cx}\partial_x u_{cy} + u_{cz}\partial_z u_{cy} = 2u_{cz}\Gamma_x + \Gamma_{eff}\ u_{cx}\ , \tag{5.11}$$

$$\partial_t u_{cz} + u_{cx}\partial_x u_{cz} + u_{cz}\partial_z u_{cz} = \partial_z \varphi - 2u_{cy}\Gamma_x. \tag{5.12}$$

Here $\alpha = n_{op}/n_{oh}$, $\sigma = n_{oc}/n_{oh}$, $\delta = n_o/n_{oh}$, $\rho = T_h/T_p$. Furthermore, $R = \Omega_{ce}/\ \omega_{ph}$ and $\Gamma = \Omega/\ \omega_{ph}$ are, respectively, the normalized cold electron gyrofrequency and the plasma rotational frequency, $\Gamma_{eff} = R - 2\ \Gamma_z$, with $\Gamma_x = \Gamma_0 \sin\theta$ and $\Gamma_z = \Gamma_0 \cos\theta$ are various components of plasma rotational frequency and $\Gamma_0 = \Omega_0/\ \omega_{ph}$ represents the magnitude of dimensionless rotational frequency. The cold electron fluid velocity u_{cj} $(j = x, y, z)$ is normalized with $u_{th} = \sqrt{T_h/m_e}$, the number densities are normalized with equilibrium densities, the electrostatic potential φ is normalized by T_h/e. Moreover, the space variables with $\lambda_{Dh} = \sqrt{T_h/4\pi n_{oh} e^2}$ and the time variable is normalized with $\omega_{ph}^{-1} = \sqrt{m_e/4\pi n_{oh} e^2}$ [84].

The model equations, namely (5.6, 5.9-5.12), after linearization and use of the plane wave approximation for all perturbed quantities ($f_1 \sim e^{i(k_x x + k_y y - \omega t)}$) lead to the fol-

lowing linear dispersion relation

$$\omega^4(k^2+(1+\alpha\rho)\,\Theta)-\omega^2((\Gamma_{eff}^2+4\Gamma_x^2)(k^2+(1+\alpha\rho)\,\Theta)+\sigma k^2)+(2k_x\Gamma_x-k_z\Gamma_{eff})^2\sigma=0, \tag{5.13}$$

If we consider long perturbation wavelength, then Eq. (5.13) takes the following form

$$\omega^4-\omega^2((\Gamma_{eff}^2+4\Gamma_x^2)+c_{sep}^2k^2)+(2k_x\Gamma_x-k_z\Gamma_{eff})^2c_{sep}^2=0. \tag{5.14}$$

Here $c_{sep}=\omega_{pc}\lambda_{Deff}=\sqrt{(n_{oc}T_hT_p)\,/\,(n_{op}T_h+n_{oh}T_p)\,(1-\beta)m_e}$ represents the phase speed of modified EAW, $\lambda_{Deff}=(\lambda_{Dp}\lambda_{Dh})\,/\sqrt{(1-\beta)}\sqrt{(\lambda_{Dh}^2+\lambda_{Dp}^2)}$ is modified Debye length in the presence of hot electrons and positrons. Where, $\lambda_{Dp}=\sqrt{T_p/4\pi n_{op}e^2}$ and $\lambda_{Dh}=\sqrt{T_h/4\pi n_{oh}e^2}$ are the Debye lengths of electrons and positrons, respectively. The plasma frequency of the cold species of electrons is given by $\omega_{pc}=\sqrt{4\pi n_{oc}e^2/m_e}$ [84]. Equation (5.13) in the absence of rotation and magnetic effects ($\Gamma_x=\Gamma_{eff}=0$) has the form $\omega/k=\sqrt{(n_{oc}T_hT_p)\,/\,(n_{op}T_h+n_{oh}T_p)\,(1-\beta)m_e}$ as reported earlier in Ref. [84]. In the presence of external magnetic field (i.e., $\Gamma_x=\Gamma_z=0$, $\Gamma_{eff}=R$) and in the limit $\omega\ll R$, $k_x\ll k_z$, Eq. (5.13) leads to the dispersion relation $\omega^2=c_{sep}^2k_z^2/(1+c_{sep}^2k^2/R^2)$ describing an electron acoustic mode in a magnetized e-p-i-plasma, and which for much longer wavelength becomes $\omega^2=c_{sep}^2k_z^2$, a result similar to the case when both rotation and magnetic field were absent. However, in the limits $\omega\sim R$, $k_z\ll k_x$, $\Gamma_x=\Gamma_z=0$, $\Gamma_{eff}=R$, one finds $\omega^2=R^2+c_{sep}^2k_z^2$, i.e., an electron-cyclotron wave. Furthermore, in the presence of slow rotation only (i.e., $R=0$, $\Gamma_{eff}=-2\Gamma_z$, $\Gamma_x\neq\Gamma_z\neq0$, $\omega\sim\Gamma_0$), Eq. (5.13) gives $\omega^2=4\Gamma_0^2+c_{sep}^2k^2$, which is also an electron-cyclotron like mode but this time rotational effect plays the role of a magnetic-field-like effect.

It is evident from the above mentioned linear dispersion relation of EAW that electron acoustic mode significantly gets modified in a rotating magnetized e-p-i-plasma (in addition to the nonthermal effects of electrons and positrons that we have already explored in Ref. [84]). It is well known that soliton is formed when the dispersion and steepening effects are balanced, thus, its structural properties would also be modified in a rotating magnetized e-p-i-plasma as we shall discuss in the next sections.

5.3 Derivation of kdV Equation

In this section, we shall derive the nonlinear kdV equation from Eqs. (5.5),(5.8) and(5.9), we employ the well known reductive perturbation technique, in this regard let us define the stretched variables as [70, 106]

$$\xi = \epsilon^{1/2}\left(l_x x + l_z z - \lambda t\right),\ \tau = \epsilon^{3/2} t, \tag{5.15}$$

where $\epsilon \ll 1$ is an expansion parameter and is proportional to the perturbation amplitude, λ is the normalized speed of the wave, $u_{th} = \sqrt{T_h/m}$ denoting the thermal speed, l_x and l_z are the direction cosines of the wave vector k, thus $l_x^2 + l_z^2 = 1$. Using reductive perturbation method (RPM), expanding the quantities n_c, u_{cj} $(j = x, y, z)$, and φ in the

power series form, we get

$$\begin{aligned} n_c &= 1 + \epsilon n_c^{(1)} + \epsilon^2 n_c^{(2)} + \epsilon^3 n_c^{(3)} + \cdots , \\ u_{cx} &= \epsilon^{3/2} u_{cx}^{(1)} + \epsilon^{5/2} u_{cx}^{(2)} + \epsilon^{7/2} u_{cx}^{(3)} + \cdots , \\ u_{cy} &= \epsilon^{3/2} u_{cy}^{(1)} + \epsilon^{5/2} u_{cy}^{(2)} + \epsilon^{7/2} u_{cy}^{(3)} + \cdots , \\ u_{cz} &= \epsilon u_{cz}^{(1)} + \epsilon^2 u_{cz}^{(2)} + \epsilon^3 u_{cz}^{(3)} + \cdots , \\ \varphi &= \epsilon \varphi^{(1)} + \epsilon^2 \varphi^{(2)} + \epsilon^3 \varphi^{(3)} + \cdots . \end{aligned} \tag{5.16}$$

Using Eqs. (5.15) and (5.16) in Eqs. (5.6, 5.9-5.12), and collecting different powers of ϵ. The zeroth order in ϵ, gives $1 + \sigma = \delta + \alpha$.

The next higher order terms gives,

$$\begin{aligned} n_c^{(1)} &= -\frac{\Theta\,(1+\alpha\rho)}{\sigma}\varphi^{(1)},\; u_{cy}^{(1)} = \frac{l_x}{\Gamma_{eff}}\partial_\xi \varphi^{(1)},\; u_{cz}^{(1)} = -\frac{1}{\lambda}(l_z - 2l_x\frac{\Gamma_x}{\Gamma_{eff}})\varphi^{(1)}, \\ n_c^{(1)} &= -\frac{1}{\lambda^2}(l_z^2 - 2l_x l_z \frac{\Gamma_x}{\Gamma_{eff}})\varphi^{(1)} \end{aligned} \tag{5.17}$$

Using these expression in Eq. (5.16) leads to the following linear dispersion relation,

$$\lambda = \sqrt{\frac{\sigma}{(1+\alpha\rho)\,\Theta}}\left(l_z^2 - 2l_x l_z \frac{\Gamma_x}{\Gamma_{eff}}\right)^{1/2} \tag{5.18}$$

Equation (5.18) gives the normalized modified EAW phase speed in the presence of nonthermal electrons and positrons, as well as due to the presence of external magnetic

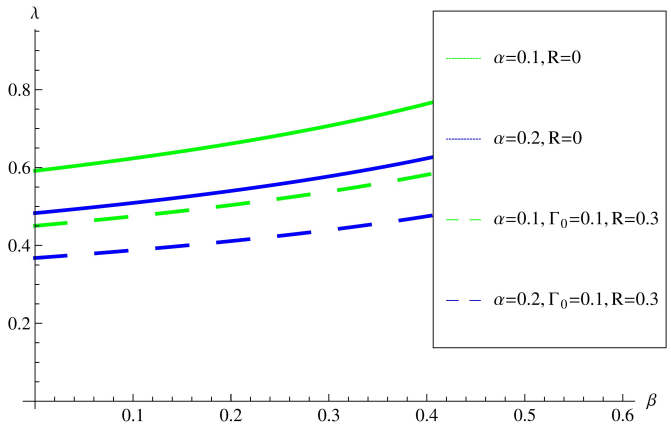

Figure 5-1: Plot of normalized EAW phase speed λ with β in the presence (dashed curves) and in the absence (solid curves) of magneto-rotating effects at different positron concentrations. The other parameters are $\sigma = 0.7$, $\rho = 10$, $\theta = 10°$, $l_x = 0.3$, $\Gamma_0 = 0.1$.

field and rotational effects. For parallel wave propagation, one can take $l_z = 1$, $l_x = 0$, and as a result Eq. (5.18) reduces to $\omega/k = \omega_{pc}\lambda_{Deff} = \sqrt{(n_{oc}T_hT_p)\,/\,(n_{op}T_h + n_{oh}T_p)\,(1-\beta)m_e}$ (Jilani et al. 2013b). Figure (5-1), shows that the phase speed of EAW increases with the increase of β, and this is true even in the presence (dotted curves) of magnetic field. However, the magneto-rotating effects and with the rise of positron concentration reduces the wave phase speed. We note that in the absence of magnetic field (R), Eq. (5.18) gives $\lambda = \sqrt{\frac{\sigma}{(1+\alpha\rho)\Theta}}\,(l_z^2 + l_x l_z \tan\theta)^{1/2}$, here if we ignore magnetic field also eliminates the Coriolis force effect, and there remains what only is the angle (θ) of rotation axis and the obliqueness of wave propagation with the magnetic field axis (z-axis) that encounter the linear dispersion relation. Figure (5-2) displays the variations of the EAW phase speed (Eq. (5.18)), the left most plot shows that the phase speed decreases with the increase of α and the angle of wave propagation with respect to external magnetic field. The middle plot shows that phase speed enhances with σ parameter and degrades with increasing rotation. The right most plot shows that the phase speed decreases with ρ and increases with the magnetic field strength. It is evident from all these plots that dispersion prop-

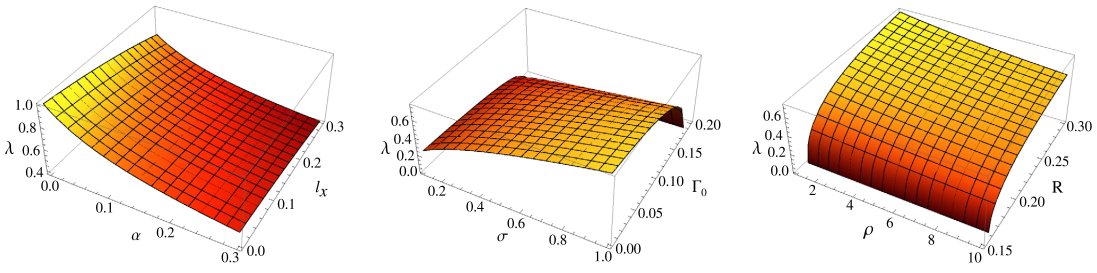

Figure 5-2: Variation of normalized EAW phase speed λ with various parameters. Left most plot, ($\sigma = 0.7$, $\rho = 10$, $\theta = 10^\circ, R = 0.3, \beta = 0.3$, $\Gamma_0 = 0.1$) middle plot,($\alpha = 0.1$, $\sigma = 0.1, \rho = 10$, $\theta = 10^\circ, R = 0.3, \beta = 0.3$, $l_x = 0.3$), Right most plot, ($\alpha = 0.1$, $\sigma = 0.1$, $\theta = 10^\circ, R = 0.3, \beta = 0.3$, $l_x = 0.3, \Gamma_0 = 0.1$).

erties are significantly gets modified with the presence of magneto-rotating effects and consequently the solitary wave structure would also gets modified.

Next, we collect the next higher order terms, that is of the order of ϵ^2, the Poisson's equation (5.6), the continuity (5.9), and momentum (5.10-5.12) equations gives us the following results,

$$\partial_\xi^2 \varphi^{(1)} - \sigma n_c^{(2)} - \Theta\,(1+\alpha\rho)\,\varphi^{(2)} - (1-\alpha\rho^2)\frac{\left[\varphi^{(1)}\right]^2}{2} = 0,$$

$$u_{cy}^{(2)} = \frac{l_x}{\Gamma_{eff}}\partial_\xi \varphi^{(2)},\; u_{cz}^{(2)} = -\frac{\lambda}{\Gamma_x}\partial_\xi u_{cy}^{(1)},$$

$$\partial_\tau u_{cz}^{(1)} - \lambda\partial_\xi u_{cz}^{(2)} + + l_z u_{cz}^{(1)}\partial_\xi u_{cz}^{(1)} + 2\Gamma_x u_{cy}^{(2)} - l_z\partial_\xi\varphi^{(2)} = 0,$$

$$\partial_\tau n_c^{(1)} - \lambda\partial_\xi n_c^{(2)} + l_z\partial_\xi(n_c^{(1)}u_{cz}^{(1)}) + l_z\partial_\xi u_{cz}^{(2)} = 0,$$

Finally, eliminating $n_c^{(2)}$, $u_{c(y,\,z)}^{(2)}$, $\varphi^{(2)}$ and using Eq. (5.16), we obtain the standard KdV equation,

$$\partial_\tau \Phi + A\;\Phi\partial_\xi\Phi + B\;\partial_\xi^3\Phi = 0, \tag{5.19}$$

where $\Phi = \varphi^{(1)}$

$$\begin{aligned} A &= \frac{\lambda^4(\alpha\rho^2 - 1) - 3\sigma P^2}{2\sigma P\lambda}, \; B = \frac{\lambda^3}{2P\sigma} \text{ with} \\ P &= l_z^2 - 2l_x l_z \frac{\Gamma_x}{\Gamma_{eff}} \end{aligned}$$

Clearly, these coefficients become similar to the coefficients of Ref. (Jilani et al. 2013b) for the wave propagation parallel to the magnetic field (i.e., for $l_z = 1$, $l_x = 0$). Thus, dispersion and steepening of wave with coefficients are vividly affected by rotation and magnetic field when the wave propagates at some oblique angle ($0 < l_z < 1$) to the magnetic field.

5.3.1 Solution of KdV Equation

To find a localized solution of Eq. (5.19), we choose a new coordinate ζ defined as $\zeta = \xi - u\tau$, where u is the normalized (by $\sqrt{T_h/m}$) speed of nonlinear soliton. The soliton solution has the form [78]

$$\Phi = \varphi_0 \sec h^2 \left(\frac{\xi}{\triangle} \right), \tag{5.20}$$

where $\varphi_0 = 3u/A$ is the amplitude, and $\triangle = \sqrt{4B/u}$ is the width of the soliton. From Eq. (5.20), it is evident that ($\xi \longrightarrow \infty$, $\Phi \longrightarrow 0$), i.e., it is a localized solitary structure.

5.4 Discussion of Results

We have investigate the effects of magnetic field, rotation parameters and obliqueness of the wave propagation along-with other normalized physical parameters of interest including $\alpha = n_{op}/n_{oh}$, $\sigma = n_{oc}/n_{oh}$, and $\rho_0 = T_h/T_p$, on the EA soliton structures. To preserve the charge neutrality condition of e-p-i plasma, we choose a slow rotation of plasma frame (i.e., $\Gamma_0 \ll 1$). Also, to make the background electric field (generated due to rotational effect) negligible, we assumed the angle θ to be small and $R \ll 1$ (Hussain et al., 2013). We have selected the appropriate range of parameters ($n_{oc} \sim (0.1 - 0.4)\text{cm}^{-3}$, $n_{op} \sim (1.5 - 3)$ cm^{-3}, $n_{oh} \sim (1.5 - 3)$ cm^{-3}, $T_h \sim (200 - 1000)$ eV, $T_p \sim (200 - 1000)$ eV, $\beta \sim (0.25 - 0.6)$) to cover a wide variety of system of plasma ranging from laboratory to astrophysical and space plasmas [89, 106]. As EAW dynamics is linked up with the dynamics of cold electrons and is relatively low-frequency electrostatic mode with phase speed v_{ph} lying in the range $u_{tc} \ll v_{ph} \ll u_{tp}$,$u_{th}$, to avoid Landau damping and, therefore, allowing the nonlinear soliton structure formation[78].

Figures 5-3(a, b) show how nonlinearity (A) and dispersion (B) coefficients varies with superthermal population parameter. The dashed curves are in the presence of magneto-rotating effects and the solid curves are in the absence of magneto-rotating effects (caused by the elimination of magnetic field effect) wherein the wave propagates at some oblique angle to the z-axis. In Fig. (5-3a) we demonstrate that both in the absence (solid curves) and presence (dashed curves) of magneto-rotating effects, there is a transition in the sign of nonlinearity coefficient from negative ($A < 0$) to positive ($A > 0$) at a common critical value of nonthermal parameter ($\beta \approx 0.3$) in the presence of positrons, thereby leading to the existence of both dip ($A < 0$) and hump ($A > 0$) type solitons. However, in the absence of positrons ($\alpha = 0$) we will always find $A < 0$, therefore, in this case only dunk type solitons exist both in the absence and presence of magneto-rotating effects (see Fig.

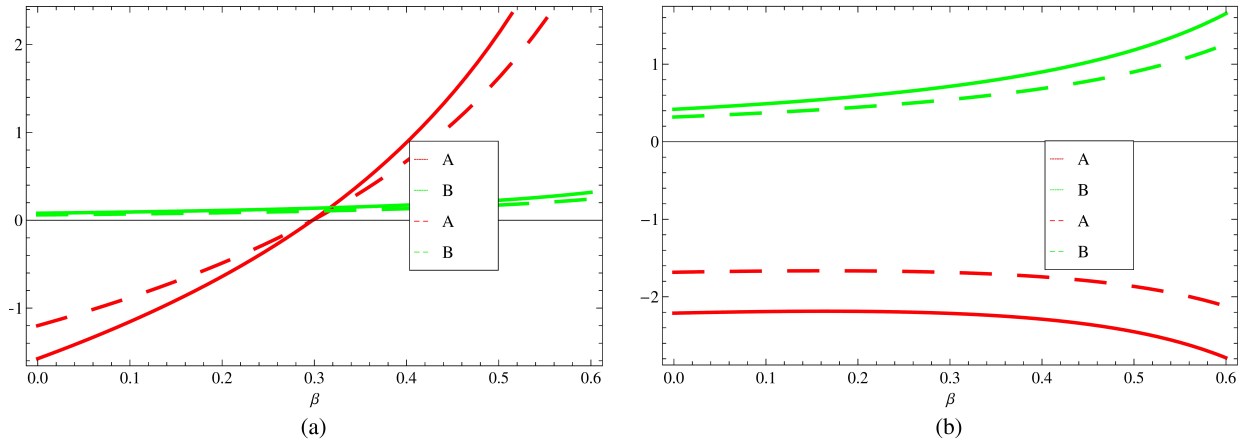

Figure 5-3: (a) Variation of coefficients A, B with β parameter in the presence of positrons (dashed curves $R = 0.3$, $\Gamma_0 = 0.1$) and (solid curves $R = 0$). The other parameters are $\alpha = 0.2$, $\sigma = 0.7$, $\rho = 10$, $\theta = 10^\circ$, $l_x = 0.3$. (b) Variation of coefficients A, B with β parameter in the presence of positrons (dashed curves $R = 0.3$, $\Gamma_0 = 0.1$) and (solid curves $R = 0$). The other parameters are $\alpha = 0$, $\sigma = 0.7$, $\rho = 10$, $\theta = 10^\circ$, $l_x = 0.3$.

(5-3b)).Figures 5-4(a, b) illustrate the variation of bump and dunk type soliton structures

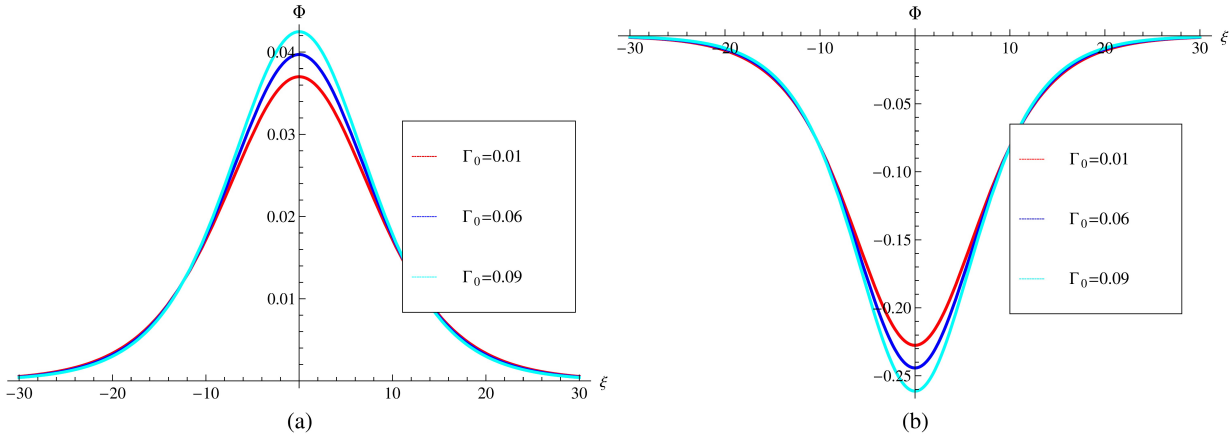

Figure 5-4: (a) Variation of hump type EA soliton structure with Γ_0(rotation frequency). The other parameters are $\alpha = 0.1$, $\sigma = 0.7$, $\rho = 10$, $\theta = 10^\circ$, $R = 0.3$, $\beta = 0.4$, $l_x = 0.3$, $u = 0.01$. (b) Variation of dip type EA soliton structure with Γ_0(rotation frequency). The other parameters are $\alpha = 0.1$, $\sigma = 0.7$, $\rho = 10$, $\theta = 10^\circ$, $R = 0.3$, $\beta = 0.25$, $l_x = 0.3$, $u = 0.01$.

with rotation effect (Γ_0) due to the Coriolis force in the presence of constant magnetic field. Clearly, increase in normalized rotation frequency increases the amplitudes of both bump and dunk type structures and there is a degradation in width of these structures.

In Fig. 5-5(a) and Fig. 5-5(b) we demonstrate that the amplitudes of both positive and negative potential solitary structures depreciate while the widths of these structures enhance with the increase of normalized electron-cyclotron frequency (R). In Figs. 5-6(a, b) the obliqueness of the wave propagation along the direction of magnetic field is studied. It is shown that the amplitudes of both opposite polarity structures amplify with the increasing values of angle of propagation with the magnetic field. Now in the remaining discussions we have compared the results of different parameters on the solitary waves both in the absence (solid wave profiles) and presence (dashed wave profiles) of magneto-rotating effects. In all these discussions the EASWs are assumed to propagate at an oblique angle with z-axis.

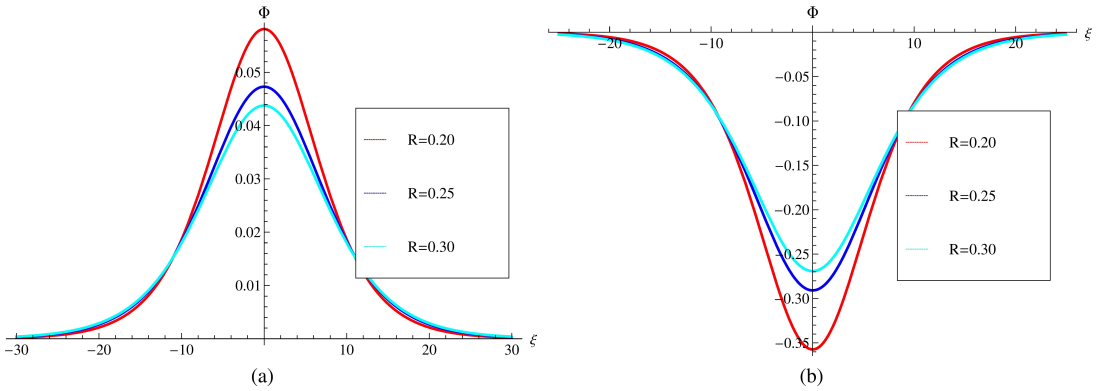

Figure 5-5: (a) Variation of hump type EA soliton structure with R(electron rotation frequency). The other parameters are $\alpha = 0.1$, $\sigma = 0.7$, $\rho = 10$, $\theta = 10^{\circ}$, $\Gamma_0 = 0.1$, $\beta = 0.4$, $l_x = 0.3$, $u = 0.01$. (b) Variation of dip type EA soliton structure with Γ_0(rotation frequency). The other parameters are $\alpha = 0.1$, $\sigma = 0.7$, $\rho = 10$, $\theta = 10^{\circ}$, $\Gamma_0 = 0.1$, $\beta = 0.25$, $l_x = 0.3$, $u = 0.01$.

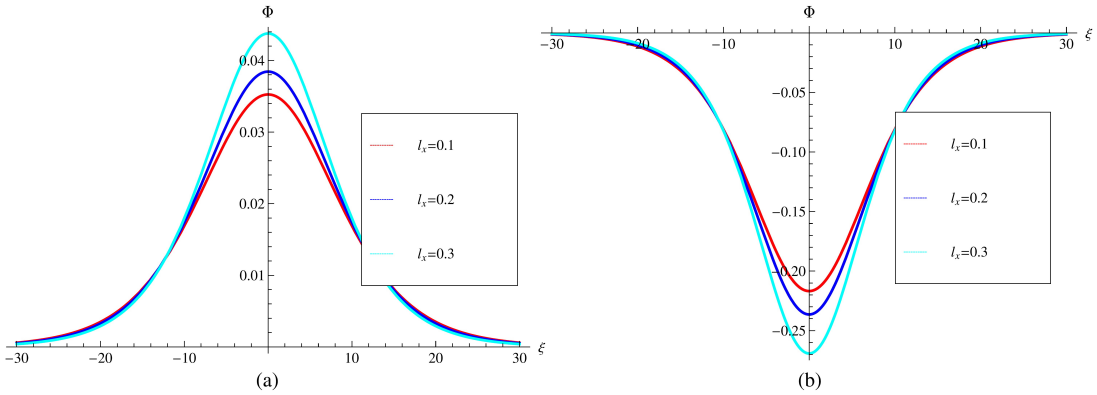

Figure 5-6: (a) Variation of hump type EA soliton structure with l_x(obliqueness of wave propagation along magnetic field). The other parameters are $\alpha = 0.1$, $\sigma = 0.7$, $\rho = 10$, $\theta = 10^{\circ}$, $\Gamma_0 = 0.1$, $\beta = 0.4$, $R = 0.3$, $u = 0.01$. (b) Variation of dip type EA soliton structure with l_x(obliqueness of wave propagation along magnetic field). The other parameters are $\alpha = 0.1$, $\sigma = 0.7$, $\rho = 10$, $\theta = 10^{\circ}$, $\Gamma_0 = 0.1$, $\beta = 0.25$, $R = 0.3$, $u = 0.01$.

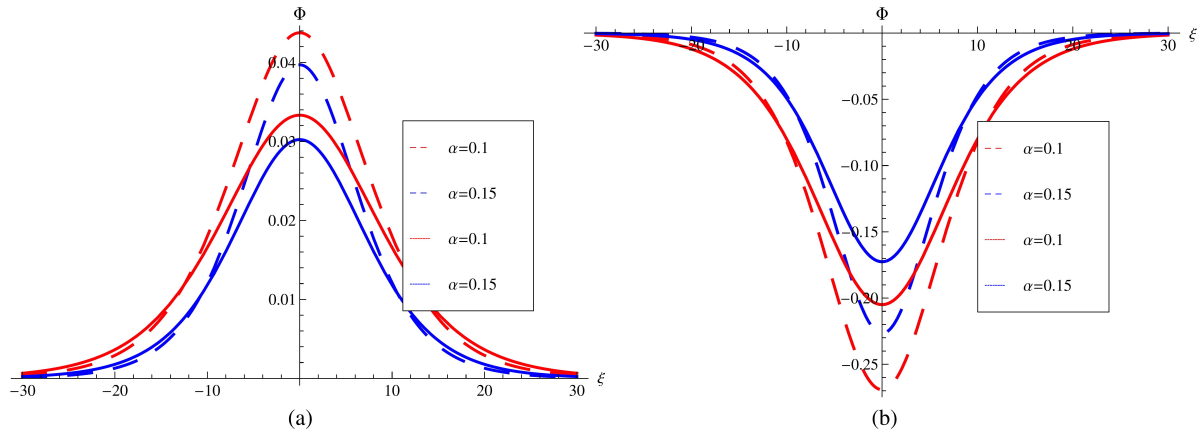

Figure 5-7: (a) Variation of hump type EA soliton structure with α parameter in the presence (dashed curves $R = 0.3$, $\Gamma_0 = 0.1$) and in the absence (solid curves $R = 0$) of magneto-rotating effects. The other parameters are $\sigma = 0.7$, $\beta = 0.4$, $\rho = 10$, $u = 0.01$, $\theta = 10^\circ$, $l_x = 0.3$. (b) Variation of dip type EA soliton structure with α parameter in the presence (dashed curves $R = 0.3$, $\Gamma_0 = 0.1$) and in the absence (solid curves $R = 0$) of magneto-rotating effects. The other parameters are $\sigma = 0.7$, $\beta = 0.25$, $\rho = 10$, $u = 0.01$, $\theta = 10^\circ$, $l_x = 0.3$.

Figures 5-7(a, b) narrate the effects of increasing hot positron concentration relative to hot electrons both in the absence (solid wave profiles) and presence (dashed wave profiles) of magneto-rotating effects. It is observed that an increase in positron concentration decreases the amplitude of both bump and dunk type solitons. However, the amplitudes of these structures are enhanced in the presence (dashed profiles) of magneto-rotating effects. Physically, an increase in hot positrons concentration depletes hot electrons, and as a result, the charge neutrality is maintained by the gain of cold inertial electrons within the localized nonlinear structure which leads to a decrease of amplitude. Similarly, the variations in the wave profiles of Figs. 5-8(a, b) can be described. Here, the increase in cold electrons concentration relative to that of hot electrons decreases the amplitude of bump soliton whereas the negative potential solitary profile amplifies the same. However, magneto-rotating effects make the structures more spiky.

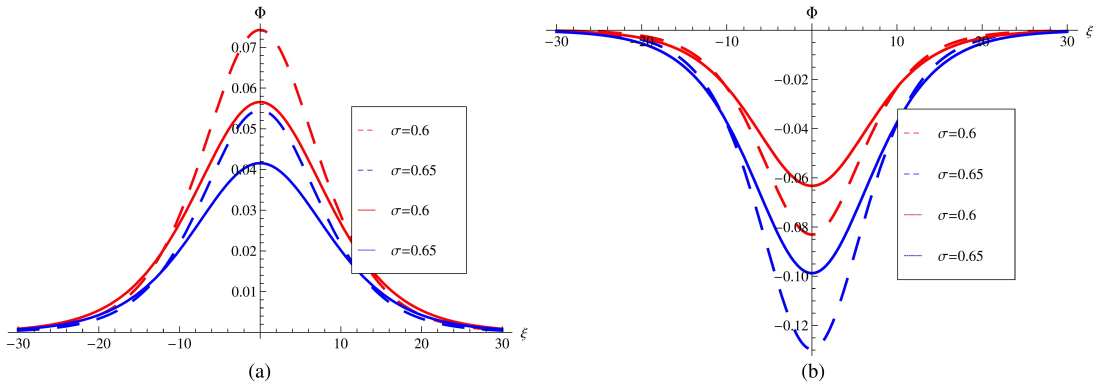

Figure 5-8: (a) Variation of hump type EA soliton structure with σ parameter in the presence (dashed curves $R = 0.3$, $\Gamma_0 = 0.1$) and in the absence (solid curves $R = 0$) of magneto-rotating effects. The other parameters are $\alpha = 0.1$, $\beta = 0.4$, $\rho = 10$, $u = 0.01$, $\theta = 10^\circ$, $l_x = 0.3$. (b) Variation of dip type EA soliton structure with α parameter in the presence (dashed curves $R = 0.3$, $\Gamma_0 = 0.1$) and in the absence (solid curves $R = 0$) of magneto-rotating effects. The other parameters are $\alpha = 0.1$, $\beta = 0.25$, $\rho = 10$, $u = 0.01$, $\theta = 10^\circ$, $l_x = 0.3$.

Figures 5-9(a, b) show the effect of increase in hot electron temperature relative to that of hot positrons on the EASWs. The bump type soliton decreases whereas dunk type soliton enhances in amplitude. Whereas, in both cases magneto-rotating effects amplify the solitary wave profiles (dashed profiles) in terms of amplitude. Physically, the decrease in hot positron temperature (or increase in hot electron temperature) causes the effective Debye length to reduce. Under such conditions there is an increase in the leakage of hot electrons from Debye sphere and causes the hot positron concentration to enhance and, hence, an attractive potential is developed among cold dynamical electrons and hot positrons, resulting into a negative potential solitary wave profile which amplifies with hot electrons temperature. Likewise, the bump soliton diminishes because of reduction in repulsive potential among hot and cold electrons in the localized solitary wave.

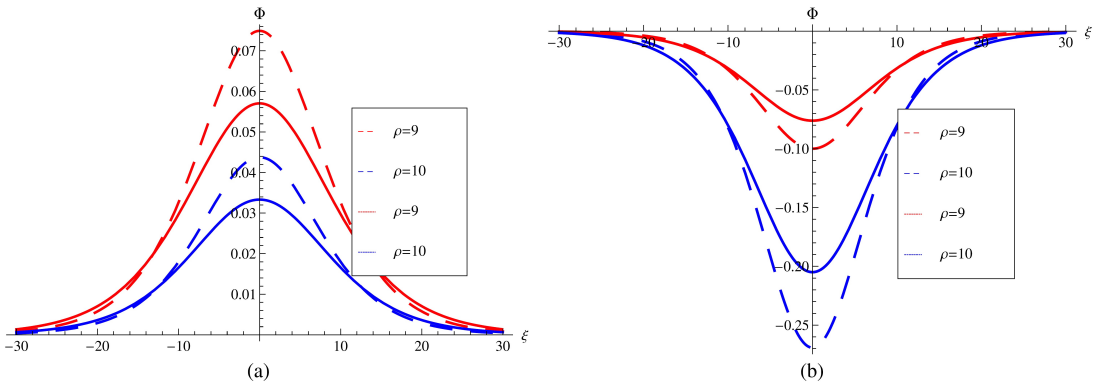

Figure 5-9: (a) Variation of hump type EA soliton structure with ρ parameter in the presence (dashed curves $R = 0.3$, $\Gamma_0 = 0.1$) and in the absence (solid curves $R = 0$) of magneto-rotating effects. The other parameters are $\alpha = 0.1$, $\beta = 0.4$, $\sigma = 0.7$, $u = 0.01$, $\theta = 10^\circ$, $l_x = 0.3$. (b) Variation of dip type EA soliton structure with ρ parameter in the presence (dashed curves $R = 0.3$, $\Gamma_0 = 0.1$) and in the absence (solid curves $R = 0$) of magneto-rotating effects. The other parameters are $\alpha = 0.1$, $\beta = 0.25$, $\sigma = 0.7$, $u = 0.01$, $\theta = 10^\circ$, $l_x = 0.3$.

5.5 Conclusion

In the present study, we have extensively investigated the properties of electrostatic EA solitary waves in a collisionless e-p-i nonthermal magnetoplasma in a rotating frame under the Coriolis force. We have derived a LDR for the EAWs and rederived various electrostatic modes under various limiting cases from LDR. Regarding the nonlinear analysis of EAWs, we have derived the KdV equation by using a standard reductive perturbation method. It is found that in the presence of positrons both bump and dip type solitary structures exist. The variations in the structures of these solitary wave profiles have been studied under various physical parameters of interest and it is found that (a) coupled magneto-rotating effects seem to amplify the nonlinear structures, (b) the omission of magnetic field also cancels the rotating frequency, however, there remains the angle of rotation axis that affects the nonlinear structures, (c) the increase in rotation frequency due to Coriolis force in the presence of constant magnetic field increases the amplitudes of both solitary structures, (d) the increase in electron cyclotron frequency at

constant rotational frequency depreciates these structures, and (e) the increasing value of angle of the wave propagation with the magnetic field amplifies the amplitudes of both opposite polarity structures. In addition, the variations in the soliton profiles with various parameters ($\sigma = n_{oc}/n_{oh}$, $\alpha = n_{op}/n_{oh}$, $\rho_0 = T_h/T_p$) of interest are discussed.

5.6 Future Work

In most of the laboratory and space plasmas, the plasma beta could exceed the electron to ion mass ratio, necessitating the incorporation of electromagnetic effects on the ITG modes. In future, one should study electromagnetic ITG modes. Furthermore, ITG mode is important in most of the magnetically confined thermonuclear fusion plasmas. In magnetically confined fusion plasmas, anomalous transport and particle fluxes are generally calculated by using mixing length hypothesis. In ITG modes with nonthermal electrons, new expressions for anomalous particle fluxes must be calculated. In future one should estimate anomalous heat transport and particles fluxes. In this thesis our main focus of attention in ITG mode was under various situations, when the amplitude of ITG driven waves grow can form various types of nonlinear structures such as dipolar, tripolar vortices etc. To the best of our knowledge, no one has attempted to see the possibility of solitons and shock formation in ITG driven modes in the presence of nonthermal Kappa and Cairns distributed electrons using more sophisticated homotopoy perturbation method. Furthermore, in magnetosphere and even in tokamak plasma, multi-ions are always present. This work can be extended for multi-ion case in the presence of nonthermal electrons. The above mentioned two problems should be investigated in future work.

Turnitin Originality Report

Linear and nonlinar study of drift waves in nonthermal distributed electrons Iqbal by Javed

From IRs (Institutional Repository)

- Processed on 2018年02月15日 14:19 PKT
- ID: 916378638
- Word Count: 16257

Similarity Index
8%
Similarity by Source

Internet Sources:
1%
Publications:
7%
Student Papers:
1%

sources:

1 3% match (publications)
Jilani, K., Arshad M. Mirza, and Tufail A. Khan. "Electrostatic electron acoustic solitons in electron-positron-ion plasma with superthermal electrons and positrons", Astrophysics and Space Science, 2014.

2 2% match (publications)
Nazia Batool, W. Masood, Arshad M. Mirza. "The effects of nonthermal electron distributions on ion-temperature-gradient driven drift-wave instabilities in electron-ion plasma", Physics of Plasmas, 2012

3 < 1% match (publications)
Arshad M. Mirza, Anisa Qamar, M. Yaqub Khan, M. Ayub. "Formation of tripolar vortices in toroidal ion-temperature-gradient driven modes in the presence of dust contamination", Physics of Plasmas, 2007

4 < 1% match (student papers from 19-Jan-2012)
Submitted to Higher Education Commission Pakistan on 2012-01-19

5 < 1% match (publications)
Ahmad, Ali, and W. Masood. "Modified Zakharov–Kuznetsov equation for a non-uniform electron–positron–ion magnetoplasma with kappa-distributed electrons", Journal of Plasma Physics, 2015.

6 < 1% match (publications)
Nazia Batool. "Ion-temperature-gradient-driven modes in bi-ion magnetoplasma", Physica Scripta, 12/2008

15/2/2018
DR. AMIR WASEEM
Associate Professor
Department of Chemistry
Quaid-i-Azam University
Islamabad-45320

15/2/18
KHALID BASHIR
Assistant Professor
DRSM UBSAS
Quaid-i-Azam University
ISLAMABAD

Turnitin Originality Report

Linear and nonlinar study of drift waves in nonthermal distributed electrons by Javed Iqbal

From IRs (Institutional Repository)

- Processed on 2018年02月15日 14:19 PKT
- ID: 916378638
- Word Count: 16257

Similarity Index
8%
Similarity by Source

Internet Sources:
1%
Publications:
7%
Student Papers:
1%

sources:

1 3% match (publications)
Jilani, K., Arshad M. Mirza, and Tufail A. Khan. "Electrostatic electron acoustic solitons in electron-positron-ion plasma with superthermal electrons and positrons", Astrophysics and Space Science, 2014.

2 2% match (publications)
Nazia Batool, W. Masood, Arshad M. Mirza. "The effects of nonthermal electron distributions on ion-temperature-gradient driven drift-wave instabilities in electron-ion plasma", Physics of Plasmas, 2012

3 < 1% match (publications)
Arshad M. Mirza, Anisa Qamar, M. Yaqub Khan, M. Ayub. "Formation of tripolar vortices in toroidal ion-temperature-gradient driven modes in the presence of dust contamination", Physics of Plasmas, 2007

4 < 1% match (student papers from 19-Jan-2012)
Submitted to Higher Education Commission Pakistan on 2012-01-19

5 < 1% match (publications)
Ahmad, Ali, and W. Masood. "Modified Zakharov–Kuznetsov equation for a non-uniform electron–positron–ion magnetoplasma with kappa-distributed electrons", Journal of Plasma Physics, 2015.

6 < 1% match (publications)
Nazia Batool. "Ion-temperature-gradient-driven modes in bi-ion magnetoplasma", Physica Scripta, 12/2008

7 < 1% match (publications)
NAZIA BATOOL. "Formation of dipolar vortices and vortex streets due to nonlinearly interacting ion-temperature-gradient-driven modes in dense magnetoplasmas", Journal of Plasma Physics, 04/2011

8 < 1% match (student papers from 24-Oct-2014)
Submitted to Gauhati University on 2014-10-24

9 < 1% match (publications)
W. Masood. "Obliquely propagating nonlinear structures in dense dissipative electron positron ion magnetoplasmas", Astrophysics and Space Science, 02/2012

10 < 1% match (Internet from 06-Sep-2017)
http://paduaresearch.cab.unipd.it/5816/1/Tesi_scaggion_30012013.pdf

11 < 1% match (publications)
Mirza, Arshad M., W. Masood, and Tufail A. Khan. "Vortex formation in nonlinearly coupled modes in a magnetized quantum plasma", Astrophysics and Space Science, 2013.

12 < 1% match (publications)
SKANARUL ISLAM. "Ion-acoustic solitary waves in a multi-species magnetized plasma consisting of non-thermal and isothermal electrons", Journal of Plasma Physics, 04/24/2008

13 < 1% match (publications)
Allahyari, Elaheh, Shahrooz Saviz, and Mahmood Ghoranneviss. "Plasma Effect on the Fast- and Mixed-Wave Modes of Gyrotron Devices", IEEE Transactions on Plasma Science, 2015.

14 < 1% match (student papers from 25-Mar-2016)
Submitted to Higher Education Commission Pakistan on 2016-03-25

15 < 1% match (publications)
S. K. El-Labany. "Dust acoustic solitary waves and double layers in a dusty plasma with trapped electrons", Physics of Plasmas, 2003

16 < 1% match (student papers from 18-Nov-2016)
Submitted to Higher Education Commission Pakistan on 2016-11-18

17 < 1% match (student papers from 11-Mar-2014)
Submitted to Higher Education Commission Pakistan on 2014-03-11

18 < 1% match (student papers from 30-Jun-2015)
Submitted to Higher Education Commission Pakistan on 2015-06-30

19 < 1% match (Internet from 29-Jan-2013)
http://www.nifs.ac.jp/report/annrep11/pdf/370.pdf

20 < 1% match (publications)
Bernhard Mollay, Harald F. Kauffmann. " Direct electronic energy transfer in the presence of static site-energy disorder–dipolar coupling ", The Journal of Chemical Physics, 1992

21 < 1% match (student papers from 20-Mar-2017)
Submitted to Higher Education Commission Pakistan on 2017-03-20

22 < 1% match (Internet from 30-Jun-2017)
http://www.nonlin-processes-geophys.net/11/215/2004/npg-11-215-2004-metrics.html

23 < 1% match (publications)
Elwakil, S.A., A.M. El-hanbaly, A. Elgarayh, E.K. El-Shewy, and A.I. Kassem. "Nonlinear electron-acoustic rogue waves in electron-beam plasma system with non-thermal hot electrons", Advances in Space Research, 2014.

24 < 1% match (publications)
Victo S. Filho. "Effect of anharmonicities in the critical number of trapped condensed atoms with an attractive two-body interaction", Physical Review A, 10/2002

25 < 1% match (student papers from 24-Sep-2014)
Submitted to Higher Education Commission Pakistan on 2014-09-24

26 < 1% match (Internet from 18-Jan-2018)
https://www.nonlin-processes-geophys.net/11/275/2004/npg-11-275-2004-metrics.html

27 < 1% match (Internet from 25-Jul-2016)
https://docs.com/dharmendra-kumar-singh/3287/mcgraw-hill-principles-and-applications-of

28 < 1% match (Internet from 21-Dec-2017)
https://d-nb.info/1009626175/34

29 < 1% match (publications)
International Journal of Numerical Methods for Heat & Fluid Flow, Volume 22, Issue 6 (2012-09-15)

30 < 1% match (publications)
"One time repair/restoration of e.T.P. 1 & e.T.P 2.", Mena Report, May 16 2015 Issue

31 < 1% match (publications)
Lamperti, Marco, Alessia Allevi, Maria Bondani, Radek Machulka, Václav Michálek, Ondřej Haderka, and Jan Peřina. "Optimal sub-Poissonian light generation from twin beams by photon-number resolving detectors", Journal of the Optical Society of America B, 2014.

32 < 1% match (publications)
S S Ghosh. "Fully Nonlinear Compressive Ion Acoustic Solitary Waves in a two Electron Temperature Plasma with Warm Ions", Physica Scripta, 03/01/2000

paper text:

Contents 1 Introduction 7 2 Toroidal ITG Driven Vortices in Nonuniform Magnetoplasma 18 2.1 Preamble . . . . . 18 2.2 Mathematical Formulation . . . . . . 19 2.3 Linear Analysis . . . . . 23 2.4 Stationary Solutions . . . . . 27 2.5 Conclusion . . . . . 32 3 Tripolar Vortices in ITG Mode in Nonuniform Magnetoplasma 33 3.1 Introduction . . . . . 33 3.2 Model Equations . . . . . 35 3.3 Tripolar Vortices . . . . . 38 3.4 Conclusions . . . . . 46 4 Sheared Driven Ion Acoustic Vortex Formation in Two-Electron-Temperature Plasma 47 4.1 Introduction . . . . . 47 4.2 Nonlinear Model Equations 48 4.3

Derivation of Dispersion Relation . . . . . 4.4 Nonlinear Analysis . . . . 4.5 Summary . . . . . 5 Electron acoustic soliton in magneto-rotating e-p-i plasma 5.1 Introduction . . . . . 5.2 Derivation of Linear Dispersion Relation . . . . . 5.3 Derivation of kdV Equation . . . . . 5.3.1 Solution of KdV Equation . . . . . 5.4 Discussion of Results . . . . . 5.5 Conclusion . . . . . 5.6 FutureWork..... 51 53 58 59 59 60 64 68 69 75 76 List of Figures 2-1 Plot of real part of frequency versus ky , for various values of = 3(solid line), = 4 (dotted line), and = 6 (dashed line). . . . . 25 2-2 Plot of Imaginary part of wave frequency versus ky , for numerous values of = 3(solid line), = 4 (dotted line), and = 6 (dashed line) . . . . . 26 2-3 Vortex chains pro…le obtained from Eq. (2.30) for the tokamak parameters. 31 3-1 Fig.1. (colored online only) A shadowgraph of 3D view of the normalized electrostatic potential for = 3 case for other plasma parameters given in the text. . . . . 3-2 Shadow graph of 3D view of the normalized potential for > 1 case in which the electrons follow classical Bolzmann type distribution with the same other parameters as taken in Fig.3-1. . . . . 4-1 Plot of normalized

13**growth rate as a function of** kz i for **the** parameters described **in**

the text. The black solid line is for = 0:22 and the red one is for = 0:1: . . . . . 4-2 The plot of potential in the contour form in (x;) plane is shown for the mach number M = u=cs = 0:98, with Si = 0:1. The normalization used for the distances is with i: . . . . . 45 46 52 57 4-3 The dipolar vortex in 2D is plotted for = 0:1 (in red color) and = 0:9 (black color) for M = 0:98: . . . . . 5-1 Plot of normalized EAW phase speed with in the presence (dashed curves) and in the absence (solid curves) of magneto-rotating e¤ects at di¤erent positron concentrations. The other parameters are = 0:7; = 10; = 10 ; lx = 0:3, 0 = 0:1. . . . . 5-2 Variation of normalized EAW phase speed with various parameters. Left most plot, (= 0:7; = 10; = 10 ; R = 0:3; = 0:3; 0 = 0:1) middle plot,(= 0:1; = 0:1; = 10; = 10 ; R = 0:3; = 0:3; lx = 0:3), Right most plot, (= 0:1; = 0:1; = 10 ; R = 0:3; = 0:3; lx = 0:3; 0 = 0:1). 5-3 (a) Variation of coe¢ cients

1**A; B with parameter in the** presence **of positrons**

(dashed curves R = 0:3; 0 = 0:1) and (solid curves R = 0). The other parameters are = 0:2; = 0:7; = 10; = 10 ; lx = 0:3: (b) Variation of coe¢ cients

1**A; B with parameter in the** presence **of positrons**

(dashed curves R = 0:3; 0 = 0:1) and (solid curves R = 0). The other parameters are = 0; = 0:7; = 10; = 10 ; lx = 0:3: . . . . . 5-4 (a)

1**Variation of hump type EA soliton structure with**

0(rotation fre- quency). The other parameters are = 0:1; = 0:7, = 10, = 10 , R = 0:3, = 0:4, lx = 0:3,

1**u = 0:01.** (b) **Variation of dip type EA soliton structure with** 0(rotation frequency). **The other parameters are**

= 0:1; = 0:7, = 10, = 10 , R = 0:3, = 0:25, lx = 0:3, u = 0:01. . . . . 58 66 67 70 71 5-5 (a)

1**Variation of hump type EA soliton structure with**

R(electron rotation frequency). The other parameters are = 0:1; = 0:7, = 10, = 10 , 0 = 0:1, = 0:4, lx = 0:3,

1**u = 0:01.** (b) **Variation of dip type EA soliton structure with** 0(rotation frequency). **The other parameters are**

= 0:1; = 0:7, = 10, = 10 , 0 = 0:1, = 0:25, lx = 0:3, u = 0:01. . . . . 5-6 (a)

1**Variation of hump type EA soliton structure with**

lx(obliqueness of wave propagation along magnetic …eld). The other parameters are = 0:1; = 0:7, = 10, = 10 , 0 = 0:1, = 0:4, R = 0:3,

1**u = 0:01.** (b) **Variation of dip type EA soliton structure with**

lx(obliqueness of wave propagation along magnetic …eld). The other parameters are = 0:1; = 0:7, = 10, = 10 , 0 = 0:1, = 0:25, R = 0:3, u = 0:01. . . . . 5-7 (a)

1**Variation of hump type EA soliton structure with parameter** in **the**

presence (dashed curves R = 0:3, 0 = 0:1) and in the absence (solid curves R = 0) of magneto-rotating e¤ects. The other parameters are = 0:7, = 0:4, = 10, u = 0:01, = 10 , lx = 0:3. (b)

1**Variation of dip type EA soliton structure with parameter** in **the**

presence (dashed curves R = 0:3, 0 = 0:1) and in the absence (solid curves R = 0) of magneto-rotating e¤ects. The other parameters are = 0:7, = 0:25, = 10, u = 0:01, = 10 , lx = 0:3. . . . . 72 72 73 5-8 (a)

1**Variation of hump type EA soliton structure with parameter** in **the**

presence (dashed curves R = 0:3, 0 = 0:1) and in the absence (solid curves R = 0) of magneto-rotating e¤ects. The other parameters are = 0:1, = 0:4, = 10, u = 0:01, = 10 , lx = 0:3. (b)

1**Variation of dip type EA soliton structure with parameter** in **the**

presence (dashed curves R = 0:3, 0 = 0:1) and in the absence (solid curves R = 0) of magneto-rotating e¤ects. The other parameters are = 0:1, = 0:25, = 10, u = 0:01, = 10 , lx = 0:3. . . . . 5-9 (a)

1**Variation of hump type EA soliton structure with parameter** in **the**

presence (dashed curves R = 0:3, 0 = 0:1) and in the absence (solid curves R = 0) of magneto-rotating e¤ects. The other parameters are = 0:1, = 0:4, = 0:7, u = 0:01, = 10 , lx = 0:3. (b)

1**Variation of dip type EA soliton structure with parameter** in **the**

presence (dashed curves R = 0:3, 0 = 0:1) and in the absence (solid curves R = 0) of magneto-rotating e¤ects. The other parameters are = 0:1, = 0:25, = 0:7, u = 0:01, = 10 , lx = 0:3. . . . . . 74 75 Chapter 1 Intro duction The rapid urbanization and growing population has resulted in a still increasing need for energy, considering the rising energy demand and the constrained availability of energy resources, one needs more e¢ cient utilization of energy and to develop new technologies as a long term solution. Taking into account the environmental requirements and the need to invest in a sustainable energy economy, new viable energy sources must be exploited. The power reactors based on the process of nuclear fusion may provide an almost unlimited supply of energy in the future. It has been over …ve decades that the scientists and engineers are trying to achieve controlled nuclear fusion reactions on earth for the future energy needs of the man kind. In this regard fusion physicists are involved extensively in designing fusion devices which can con…ne hot thermonuclear plasma. It is a well established fact that nuclear fusion reactions are occurring in stars, e.g., sun is a massive fusion reactor. The fundamental principle of this process is quite simple: If two light nuclei fuse together under speci…c reaction conditions, this

10**results in** the **reduction of the total mass and a consequent release of energy in the form of kinetic energy of the reaction products.** However, **because the**

nuclei are positively charged, there is strong Coulomb repulsion between them. To achieve nuclear fusion reactions, we have to bring the two nuclei at a distance in which strong nuclear force overcomes the repulsive barrier. Various types of schemes have been devised among which, perhaps the most suitable scheme is the magnetic con…nement fusion (MCF). In the said scheme suitable ions, e.g., Hydrogen isotopes, are heated up to thermonuclear fusion temperatures of the order of 108 K, and are con…ned by the use of di¤erent magnetic …eld con…gurations. There are two major issues associated with controlled fusion reactions on earth, namely, heating of fusion fuel to very high temperatures, and the con…nement of such hot fuel long enough to achieve considerable fusion reactions. These requirements can be presented mathematically by the well known Lawson criterion which states, in its simplest form, that the product of number density (n) and con…nement time ( ) must satisfy the condition: n > 1014 sec/cm3 for a deuteron (D) and triton (T) plasma at 10 keV temperatures [1]. One of the primary objective in all MCF schemes is to con…ne very hot plasma for su¢ ciently long time so as to satisfy the Lawson criterion. However, in most of fusion devices, the observed con…nement time, due to various plasma instabilities, is much smaller than that demanded by the said criterion and, hence, both the particle and energy loss have been detected. Moreover, the experimentally measured losses have been much larger than theoretical predictions which points toward some additional (anomalous) losses that have not been properly taken into account. For correct interpretation and predictions for the behavior of present and future fusion devices like ITER, it is important to examine and understand the associated anomalous transport in the con…ning magnetic …eld. It is generally believed that in MCF plasma devices, e.g., tokamaks or stellarators, the

19**ion-temperature-gradient (ITG) driven drift-wave instability** is **the** source **of** anomalous transport. **The**

ITG mode is also known as i-mode, where i = dx(ln Ti)=dx(ln ni) with Ti and ni denoting, respectively, the ion temperature and density. Physically, the unstable i-mode

18**arises due to free energy stored in the form of ion temperature**

(density) gradient. It has been found, as in Ref. [2], that i = 2=3 represents a threshold value 8 of instability, moreover, for a short wavelength case i > 0:902 is required for instability, whereas i = 2 corresponds to a hard threshold condition for anomalous transport. In 1957, Tserkovnikov [3] discovered the ITG mode of instability and, later on, Rudakov and Sagdeev [4] performed a local analysis and derived instability criterion in the presence of ITGs. The later investigation was then further extended by Pogutse [5] by considering inhomogeneous magnetoplasma with sheared-ion ‡ows and accounting for kinetic ion e¤ects. Coppi et al., [6] on the other hand, assumed that both the electrons and ions are adiabatic and, using the slab geometry, obtained a Weber type equation with eigenvalue condition for unstable i mode. By considering kinetic-ion e¤ects, Kadomtsev and Pogutse [7] obtained a critical value of i 1 for marginal stability that was later con…rmed numerically by Waltz et al. [8]. Hinton and Horton [9] accomplished nonlinear analysis of collisional drift mode by using the two-‡uid model, these results were found to be in agreement with some laboratory experiments. Coppi and Spight [10] modelled the ITG driven drift wave instability di¤erently and is termed as ion mixing mode (IM) mode. When a neutral gas is injected in tokamak plasmas through a stable discharge and the rate of density rises, this phenomenon can only be explained through this IM mode [10], Antonsen et al. [11]. Horton et al., [12] and Coppi and Pegoraro [13], showed that this instability is usually caused by the magnetic …eld curvature. For toroidal geometry, the numerical simulations of the ITG driven mode by Guzdar et al. [14] has indicated a threshold ic value by including the Landau resonance. The properties of the ITG mode with the magnetic shear e¤ect have been investigated by Hahm and Tang [15]. We can divide ITG driven mode in two main types, namely, slab type and interchange mode. The slab type is the result of coupling of drift and ion acoustic wave that is determined by the local ion temperature gradients. Whereas, the interchange mode, also called toroidal branch, is determined in the presence of bad curvature of magnetic …eld 9 lines in the …nite ion temperature gradient [16]. It has been reported that the anomalous thermal transport observed in stellarators and tokamaks are caused by the turbulence of the said branches of the ITG driven mode. When the magnetic …eld curvature is weaker than magnetic shear, the slab type ITG-driven instability is dominated which is the major source for the anomalous thermal transport [17, 18]. The investigations of the ITG mode is an important topic in the studies of fusion plasmas [19]. The e¤ect of i on toroidal modes have also been investigated by Kadomtsev [20], moreover, ballooning mode formalism [6] is also employed for the description of these modes. The presence of a toroidal mode determined by toroidal i e¤ects alone was …rst mentioned by Horton et al. [9], and was subsequently studied extensively by Horton and Braginskii in [21, 22]. Several studies have been carried out to understand the

3**toroidal- ion-temperature-gradient (TITG) driven**

mode and it has been shown that an instability arises in inhomogeneous applied magnetic …eld. Shukla and Weiland [23] and Shukla [24] derived the group of equations for the nonlinear coupled TITG and showed that these coupled modes were self organized and give rise to dipolar type of vortices [26]. The existence of such type of vortices has been realized in experiments [27] as well as in numerical simulations [28, 29]. The satellite

2**observations of space plasmas,** during **the last two decades, have**

shown a universal existence of

2**ion and electron** extent that **are far away** form **their**

equilibrium site [30, 31]. These particles with suprathermal behavior can adequately be represented by the so called

2**kappa distributions, which** comprises **the core** as Maxwellian **and**

power law for the high-energy tail, e.g., Vasyliunas [32], way back in 1968, …tted OGO1 and OGO2 solar wind data using kappa distributions. The distribution was an empirical …t for the detected particles. From that point forward, suprathermal distributions for linear as well as nonlinear structures was extensively embraced by various researchers [33, 34] for the regimes of ion and dust-acoustic. 10 Non-Maxwellian distribution of electrons have also been found to exist in toroidal fusion devices, e.g., the electron cyclotron heating (ECH) experiments on stellarators and tokamaks illustrate the existence of a superthermal tail in the electron distribution function. These experiments also show a disagreement between the linear theory of microwave absorption and the experimental observations [35]. Although the distribution function of electrons is Maxwellian in the Q-machine, it is non-Maxwellian in the case of radio frequency

5**(RF) discharge.** Consequently, **the generalized Lorentzian** (kappa) **distribution function is** required **to simulate the electron distribution function**

in these devices. The Maxwellian distribution is a special case of more general kappa distribution, i.e., ! 1 [36]. In tokamak fusion devices, under the in‡uence of the toroidal electric …eld, elec- trons will experience a driving force, and due to the decrease of the Coulomb collision frequency there is an increase in their kinetic energy. Electric …eld will continuously accelerate those electrons having energy higher than some critical value (vcr) [37], such accelerated electrons are named as runaway electrons. As runaway electrons are contin- uously accelerated in the parallel direction of the toroidal magnetic …eld, the formerly Maxwellian electron distribution function start to form a runaway particle tail. This results in a strong anisotropic velocity distribution [38]. The free energy due to the non-Maxwellian component can be exchanged via resonant interaction between electrons and plasma oscillations. Above a certain threshold, the Parail–Pogutes instability can be excited and limit either the runaway energy or the runaway con… nement [39, 40]. In toroidal fusion devices the nonlinear vortex structures can play signi…cant role in particle transport, for instance, the vortices may provide the transportation of heat ‡ux along the magnetic …eld. The existence of coherent vortical structures, which are believed to be the building blocks in turbulent physical situations, is a characteristic feature of two-dimensional or 11 quasi-two dimensional ‡ows, such as planetary atmospheres and oceans, laboratory ex- periments with rotating and/or strati…ed ‡uids and strongly magnetized plasmas. These structures have a life time much longer than their period of rotation [41]. Monopoles are not steadily propagating since they couple to linear waves and, hence, are consid- ered to be long-lived and have importance for ‡ow dynamics [42]. The interaction of monopole and dipole generates a tripole. Tripole includes a core of central vortex which is rotating clockwise and two opposite polarity satellite vortices, are easily excited in rotating ‡uids [43, 44]. Such structures carry angular momentum but no linear momen- tum. Experimental evidences with explicit solution have been put forward by Kinzner and Khvoles [45], whereas the same are studied in the presence of magnetic and velocity (and background) shear ‡ow by Chakrabarti et al. [47]. Strong monopolar structures, quasi-stationary solutions, are developed into tripolar-like structures when propagating essentially perpendicular to the density gradient [48]. Double immersed dipolar type shapes, called quadrupolar vortices, are a result of shear in magnetic …eld or in the ‡ows [47]. The vortices discussed above play a vital role in transport of particles and energy in astrophysical objects as well as in laboratory plasmas. As discussed earlier, the ITG mode was studied a long time ago by Rudakov and Sagdeev in 1961. Additional e¤ects, for example, magnetic curvature, parallel compress- ibility have been investigated by Rudakov, Jerman etc. [19, 49]. In slab geometry, the ITG modes couple with ion acoustic modes and, hence, destabilize the local temperature gradient. In toroidal geometry the i-mode becomes unstable by magnetic curvature e¤ect, and, is e¤ective even in the limit kk ! 0 [50]. Experimental observations on the Alcator C tokamak suggested that i instability can be correlated to anomalous transport [49]. In electrostatic limit, the i mode

propagation is along the ion diamagnetic drift. In the ion ‡uid limit, i = 0, while for instability threshold ITG mode in sheared slab geometry, Ln=LT = i 1 [8]. In toroidal geometry, the ITG mode is driven by ion 12 curvature drift rather than its parallel motion and the threshold could be in the range of 1 i 2 [14]. The particle distributions, modeled as kappa distributions, having high energy tails are numerously detected in astronomical plasmas. The presence of non-Maxwellian dis- tribution have insightful e¤ects on transport phenomena and propagation of waves. Such distributions …t to the data obtained in satellite-based experiments [32, 51]. Space plas- mas, e.g., solar wind, terrestrial magnetospheres and interstellar medium comprehend a signi…cant degree of non-thermal particles [52]. The ITG mode has been investigated for di¤erent non-Maxwellian distributions in the linear regime, and the study concludes that the phase velocity modi…es

> 2**in the presence of nonthermal electrons** [53]. **The**

study has been further extended by including dust contaminated plasma with charge ‡uctuating e¤ect in Ref. [54]. More recently, Mirza et al.[55] considered ITG driven vortices in inhomogeneous magnetoplasma with nonthermal electrons. The present investigation is an extension of [55] to tripolar vortices in non-Maxwellian plasmas. In di¤erent plasma systems such as in the magneto-tail, in auroral ionosphere, in the Earth's bow shock region, magnetosphere and in the laboratory produced plasmas, hot and cold population of electrons have been observed ([57, 56] and the references therein). Hence this topic has got lot of attention among researchers around the globe [58]. Based upon the space data and theoretical models , di¤erent non-thermal distributions have been proposed, e.g., distribution [32], Cairn's distribution [59] etc. A lot of research has been devoted to investigate the superthermality e¤ects on the linear and nonlinear wave propagation [60, 61]. The e¤ect of nonthermal electrons on acoustic solitary wave formation has been discussed by several authors: namely, Gill et al. [62], has discussed the ion-acoustic type solitary wave propagation in the presence of suprathermal electrons and the formation of double layer using reductive perturbation method (RPM). Saini et al. [64]. The authors, El-Tantawy et al., [65] discussed the solitary wave propagation in non-extensive electron positron and ion plasma. Shan et al., [66] studied vortex formation by the

> 5**ion acoustic** and **drift** wave **in the presence of** nonthermal **electrons.**

This work was further extended by Adnan et al. [67]. The role of nonthermal hot electrons on the linear/nonlinear (ITG mode driven vortices) behavior of ITG driven mode has been explored, respectively, by Batool et al. [53] and Zakir et al. [54]. Recently, Rufai et al.[68] studied ion-acoustic and super soliton formation in the pres- ence of two types of electrons, i.e., the Cairn's type for energetic electrons and Maxwellian type for the inertialess electrons in the presence of dynamic cold

> 23**ions. It was** shown **that the presence of** hot **electrons** extends **the**

limit of Mach number supersonic level. In this regard,

> 11**we have extended the work of** Rufai **et al.,**

by including ions shear ‡ow in the parallel direction, and investigated the e¤ect of hot electrons on formation of dipolar and street type vortices. We have also found the modi…ed behavior of the shear ‡ow instability in the presence of highly energetic electrons. Coriolis force plays a dominant role in cosmic phenomena, rotating plasma in lab- oratory devices as well as in space plasmas [69, 70]. Most of the astrophysical plasma environments (for instance, neutron stars, pulsars, quasars, black-hole

magnetospheres, etc.) and in toroidal devices, the magnetized plasma rotates quite rapidly and, hence, the Coriolis e¤ect plays a signi…cant role in plasma dynamics. The physics of such plasma system can be coined in terms of noninertial (rotating) frames. Under such observations, the e¤ect of Coriolis force on the linear wave propagation in an ideal lower ionosphere has been studied, which is of great importance in the structure of rotating magnetic stars, the star cycle, and sunspot development [71, 72]. In nature, the formation of a star into a neutron star under the conservation laws of angular momentum and magnetic ‡ux decreases with the rotational inertia and causes the presence of frozen-in force lines leading to a rapidly rotating and highly magnetized plasma. Such plasma environments 14 are enriched in electrons, positrons and ions. One of the aim of the present work is to model such a plasma system to study nonlinear wave propagation in a magneto-rotating plasma. Many authors have investigated the e¤ect of Coriolis force on wave evolution in both unmagnetized and magnetized plasmas [71, 73] and it has been established that the Coriolis force has an e¤ective magnetic-…eld-like in‡uence in a rotating plasma [74]. The Coriolis force e¤ects on the pulsar radiation have been investigated in Ref. [75] where it is observed that an increase in rotation causes the soliton radiation known as pulsar radiation. The study of astrophysical plasma has shown that the formation of nebulons is governed by the rotation of the body. In the Refs. [76, 77] the authors have explored the magneto-rotating e-p-i plasma and have shown that the rotation and magnetic …eld make the solitary waves more spiky. It has been further shown that the rotational e¤ects bifurcate the region of

> 15**compressive and rarefactive solitary waves** [71, 74]. **In**

most of these studies the

> 15**propagation of ion-** and dust **-acoustic** solitary **waves in**

magneto-rotating plasmas have been analyzed. Quite recently, we have studied the e¤ects of magnetic … eld on the

> 26**electron acoustic solitary waves** (EASW's) **in a** rotating **electron–** positron ions **with**

dynamic electrons with …nite temperature and mass, nonthermal electron-positrons and stationary massive positive ions and have obtained interesting new results. The EASW's formation is due to the temperature anisotropy of electrons, and depends on the di¤erence of temperature, the cold electrons provide the inertia and the hot electrons develop the required pressure for the restoring force to excite EAW. Similarly, for the ion acoustic

> 1**waves (IAW) in** pure **electron-ion plasma, the inertia is provided by the massive ions and inertialess** electrons which gives **the restoring force** [78]. Furthermore, **in the** dynamics **of** EASW's **the**

ions form a stationary background because of its large mass. In most of the astrophysical plasma positrons are frequently observed, resulting in electron-positron-ion plasmas. The origin of these energetic particles in space plasmas 15 is the cosmic rays and solar wind. The introduction of positrons leads to signi…cant modi…cation in restoring force [79, 80]. Even in the tokamak plasma systems, a small percentage of positrons also exists, which are generated, due to the collisions of run- away electrons with plasma species [81]. Their presence has also been reported in the UK based tokamak, namely, the joint European Torus (JET) [82]. Mostly, the elec- trons and positrons in astrophysical plasma environments are highly energetic

[83] and are often described with the high energy tail distribution functions. The interaction of high energy cosmic protons as well as collisions of heavy nuclei molecules of the upper atmosphere which produces nonthermal electrons/positrons which are collisionless [84]). Moreover, such particles also exist in the magneto-tail of the earth's sheath boundary layer region, this nonthermal population of plasma particles is formed when the out- ‡ows of

> 1**hot electron-positron plasma from pulsars enter into an interstellar cold, low density electron-ion plasma**

[78]. In neutron stars, pulsars, black-hole magnetospheres, earth's magnetosphere, etc., the EAWs, when nonlinearly coupled forms various

> 5**types of nonlinear structures such as solitons, shocks,**

double layers, electron holes, etc. [85]. Electron-positron-ion plasma also exists in the early universe, pulsars magnetosphere, in the active galactic nuclei, solar atmosphere, quasars, in the rapidly rotating and highly magnetized plasmas [86]. In recent years, a lot of interesting work has been reported in which various proper- ties of linear and nonlinear electrostatic EAWs have been studied, such as EASWs

> 22**and shock waves in a dissipative, nonplanar space plasma**

in the presence of nonthermal hot electrons, and negative potential solitary waves [87] etc. Further, spherical EASWs in plasma with superthermal electrons have been investigated by Borhanian et al : [88] and

> 2**it is** shown **that** with **an increase in the nonthermal population** parameter **the** amplitude **of the**

solitary waves also increases. Mamun et al. [89], have considered the obliquely propagating EA solitary waves in magnetized nonthermal hot electrons, obeying vor- 16 tex type distribution in the presence of stationary ions as a background in electron-ion plasma. On the other hand, Singh and Lakhina [90] have investigated the problem of excitation of EAWs in the magnetosphere and found that the frequency and the growth rate of EAW gets reduced in the presence of hot background electrons. Lakhina et al. [63, 91] proposed

> 1**a general model to study ion(electron) acoustic solitons/double** layers **in multi-component space plasmas.** Dike **et al.**

[72]., have investigated nonlinear EA solitary waves in plasmas having non-Maxwellian kappa-distributed hot electrons. However, in all of these analysis the in‡uence of nonthermal positron component and magneto-rotating e¤ects have not been considered. In our recent work [84] we have included the nonthermal electrons and positrons components in our study on the EASWs and we found that in the presence of positrons the polarity of these solitary waves can switch. As in nature, most of the astrophysical plasmas are magnetized in rotating frames, therefore, its natural to extend the investigations of EASWs under magneto-rotating e¤ects to have a more realistic picture. Thus,

28in order to model the magneto-rotating e¤ects and that of the

presence of hot positron and electrons

1on the linear/nonlinear electrostatic EAWs in the laboratory and in astrophysical space plasmas,

we have incorporated a magneto-rotating electron-positron-ion plasma. The plasma considered here consists of nonthermal elec- trons and positrons which are nonthermal alongwith cold dynamic electrons and heavy

1ions to provide a stationary background for the EAWs to exist.

Chapter 2 Toroidal ITG Driven Vortices in Nonuniform Magnetoplasma 2.1 Preamble In MCF devices, among other instabilities, the

3ion-temperature-gradient (ITG) driven drift wave instability is believed to be one of the

major candidates responsible for anom- alous transport of particles. This instability is also known as ITG mode or, simply the i mode of instability, where i LLTn = ddxx llnn nTii00

2is the ratio of density and temperature gradient scale lengths. The source of available free energy for ITG instability is the ion- temperature gradients. The importance of

ion temperature gradient modes in burning fusion plasmas is well known, to the best of our knowledge the ITG mode was …rst dis- covered by Tserkovnikov [3]. It was then investigated in detail by Rudakov and Sagdeev [4] using local analysis for a ‡at density pro…le

2to explain the origin of ‡uctuations and associated cross …eld anomalous transport in tokamak plasmas.

In toroidal geometry, i mode has been been considered by Coppi et al., [92]. The existence of a toroidal i mode was …rst pointed out by Horton et al. [12], and subsequently several others studies were made [93, 94], where it was shown that an instability arises in the presence of inhomo- geneous applied magnetic …eld for i > 1.4. Shukla and Weiland [24, 95]

2derived the nonlinear set of equations for the coupled ITG and toroidal-ion-temperature-gradient (TITG) modes, and it was shown that nonlinearly interacting ITG and TITG modes self- organizes in the form of dipolar vortices

[25, 26]. In this Chapter, we shall

6**examine the** nonlinear **properties of the low-frequency** elec- trostatic toroidal **ITG-driven mode for**

inhomogeneous magnetized plasma in the presence of nonthermal electron population and obtain the dipolar and vortex chains type vortices. We derive here a set of

7**nonlinear equations** that **govern the dynamics of low-frequency** (i.e., ! **!ci,**

where

7**!ci is the ion gyro-frequency)** TITG **driven** mode **in the presence of equilibrium density, temperature, and magnetic** …eld **gradients.**

7**In the nonlinear case, solutions in the form of dipolar vortices and vortex streets are**

presented for a plasma comprising of Maxwellian ions and nonthermal electrons in the presence of external mag- netic …eld. By

6**using Braginskii's transport equations for the ions and** kappa **distributed electrons,** new set of **mode coupling equations are derived.**

The results have been applied for tokamak plasmas and the scale lengths, over which the nonlinear vortex structures gets modi…ed, have been derived

2**in the presence of kappa distributed electrons.**

2.2 Mathematical Formulation Consider an

2**electron-ion plasma in an inhomogeneous** externally applied **magnetic** …eld **B0 (B0(x)z^; where z^** de…nes **a unit vector** in **the z-** direction) **and B0 is the strength of magnetic** …eld. **The**

equilibrium ion-temperature gradient rTi0 (x) ; ion-density gradient rni0 (x) and magnetic …eld gradients rB0

3**(x) are** along **the x-** axis. **For low-frequency**

of TITG mode, we assume that

9the wave frequency ! !ci(= eB0=mic; where, !ci is the ion- gyrofrequency, e is the magnitude of electronic charge, mi is the mass of ion, and c is the speed of light). Here we

2consider electrostatic case for which E = r , where E denotes the

electric …eld and represents the

2electrostatic potential. Using the drift-approximation (valid for low-frequency modes, i.e., ! !ci), the

perpendicular

2component of ion-‡ uid velocity can be expressed as vi?

B0 z^ r + eB0ni ^z r (niTi) ' c c c [@t + (vE + vDi) r] r? ; B0!ci vi = vE + vDi + vpi ; (2

2.1) where vE is the well known E B drift velocity of the ionic ‡uid, vDi is the ion- diamagnetic drift velocity and vpi is the ion-polarization drift velocity.

For toroidal ITG (TITG) mode, we ignore the parallel to B0

2ion dynamics, i.e., viz = 0, which means that the dynamics of

nonlinear TITG mode is considered by ignoring the coupling of ion-sound waves. The

16perturbed ion number density can be calculated with the help of ion continuity

equation in drift-approximation as follows

2@ni @t + r ni (vE + vDi + vpi)

= 0: (2.2) The

2ion temperature perturbation can be estimated

using ion energy balance equation 3 1 2

2[@t + vi r] Ti + Tir vi = r qi; ni where qi = 52 (cniTi=eB0) z^

rTi de…nes the collisionless Righi-Leduc

2ion heat ‡ux. Substituting the value of r vi

from Eq. (2.2) in the above equation one …nds

17ni [@t + vi r] Ti Ti [@t + vi r] ni = r qi:

2 2 3 3 (2.3)

2To close the system of equations, we need to de…ne the electron density

distribution. The

8three dimensional kappa velocity distribution function f (v) for isotropic case can be expressed as

[33] ne0 1 3=2 f (v) = (+ 1) v2 2e =me (+1) 3 (1

8=2) 1+ 2 ; (2.4) where = [((2 3)kBT)= m]1=2. From the formalization of distribution function, it is essential that > 32

[99]. We can obtain the

21number density of electrons by integrating the distribution function over velocity space

to get (

251=2) ne = ne0 1 e (e 3=2)

Te : (2.5)

2For non-thermal electron population, the kappa distribution of electrons has the form

1 ne '2 23 ; (2.6) 2 Here (= e =Te 1) represents the normalized electrostatic potential and ne0 is the equilibrium electron number density, and kappa describes the deviation from the Maxwellian distribution, which can be reproduced by taking the limit ! 1. Substituting Eq. (2.1) into continuity equation for ions, and by

2letting ni = ni0 + n and Ti = Ti0 + T , where n and T are,

respectively, density and temperature perturbations and are assumed to be much smaller than their equilibrium counterparts; we …nd (@t + vE r + vBi r) N + vBi rT + (vBi vni) r 2s [@t+vE r + vD0 r] r2? 2sr [(vD1 r)r?] = 0 ; (2.7) with N = ni0 and T = Ti0 denoting the normalized number density and tempera- n T ture, respectively, = Te0=Ti0 is the electron to ion temperature ratio, s = cs=!ci represents ion acoustic Larmor radius, cs = Te0=mi represent the ion-acoustic speed, vBi = ceTBi00 z^ rBB00 is the ion rB0 drift anpdvni ceTBi00 z^ rnni0i0 represents the ion = rni0 drift, vD0 = (1 + i)vni with i = @@xx llnn nTii00 and vD1 = ceTBi00 z^ r(N + T) is the …rst order ion diamagnetic drift velocity. Upon inserting Eq. (2.1) in Eq. (2.3) and using continuity equation to get @t + z^ c B0 2 i 3 r r + vBi 5 3 r T 2 3 vni r =0 @t + z^ c r r N B0 (2.8) Equations (2.7) to (2.8), with N = ((12)=(32)) = are the required nonlin- ear mode coupling equations which

3governs the dynamics of toroidal-ion-temperature- gradient driven mode in the presence of

nonthermal electrons. To close set of

2coupled equations, we de…ne quasineutrality condition i.e.,

ne ' ni. 2.3 Linear Analysis In the linear limit, we shall drop the nonlinear terms and retain only the …rst order linear terms, Eqs. (2.7) and (2.8), in the linear limit, take the form (@t + vBi@y) N + (vBi vni) @y + vBi@yT 2s@tr2? (2.9) s2 [(1 +)vni r] r2? = 0 @t + (vBi vni)@y 5 2 5 2 3 T 3 @t vT i@y 2 N vni i 3 @y = 0 (2.10) The linear dispersion relation can be derived by using the sinusoidal approximations for the perturbed quantities, i.e., the perturbations

3are proportional to exp[i (k r !t)], where k and ! de…nes, respectively, the wave vector and perturbation frequency. There- fore Eqs. (2. 9) and

(2.10)

2in the Fourier space can be written as

(! !Bi) N (!Bi !ni) !BiT + 2sky2! 2s [!ni (1 + i)] ky2 = 0 (2.11) ! 5 2 5 3 (!Bi !ni) T = ! + !T i 3 2 N !ni 2 i 3 ; (2.12) where !T i = k vT i, !ni = k vni and !Bi = k vBi. Eliminating T from Eqs. (2.11) and (2.12) one …nds " ! !Bi 2 !Bi ! + 52 !T i 3 ! 53 (!Bi !ni) # N= s2ky2 f! !ni (1 +)g + ! i 2 3 !Bi!ni 53 (!Bi !ni) # (2.13) The dispersion relation for TITG driven drift mode for kappa distributed electrons can be written as (! !Bi) ! (!Bi !ni) 5 2 !Bi ! + !Ti 5 3 3 2 (!Bi !ni) ! (!Bi !ni) + 2sk2y f! !ni (1 + i)g 5 3 (2.14) ! 5 3 (!Bi !ni) + 2 i 3 !Bi!ni = 0 ; which is the desired expression for the toroidal ion-temperature-gradient (TITG) driven drift-waves with nonthermal hot electron population. To analyze the second order dispersion relation, we plot this dispersion relation by considering some typical tokamak parameters, e.g., B0 = 3 105 G, Te = 10 keV, and assuming Ti = 0:1Te, ne = ky=15; Te = ky=5, Bi = 0:3 ne: The real and imaginary part of the frequency is presented as a function of ky for di¤erent values of kappa parameter and the results are depicted in Figs. 2-1 and 2-2: It can be observed in Fig. 2-2 that as kappa increases the growth rate also increases, whereas the real frequency decreases with kappa. It is worth-mentioning here that the growth rate in this model occurs only if ion to electron temperature proportion is less than unity.. This is because we have

neglected the Figure 2-1: Plot of real part of frequency versus ky, for various values of = 3(solid line), = 4 (dotted line), and = 6 (dashed line). Figure 2-2: Plot of Imaginary part of wave frequency versus ky, for numerous values of = 3(solid line), = 4 (dotted line), and = 6 (dashed line) nonlinear …nite Larmor radius (FLR) and stress tensor contributions in our calculations. For the detailed calculations including the e¤ect of FLR, we refer the reader to classi- cal paper by Horton, et al. [100], where they showed instability and nonlinear transfers to higher k modes from the said complex nonlinear term. However, in our simpli…ed model, we drop out this term for simplicity, which might not be true in numerous hot thermonuclear fusion plasmas such as in Tokamaks. When toroidal-ion-temperature gra- dient driven mode destabilizes and grows, the amplitude of various modes starts mixing, various type of nonlinear structures can be formed. In the next section, we shall seek the possibility of the formation of various types of coherent nonlinear structure formation, namely the vortex formation. 2.4 Stationary Solutions In this section, stationary solutions of Eqs. (2.7) and (2.8) are presented by de…ning a new stationary frame moving with a …xed velocity u in the direction perpendicular to the x-axis. Subsequently, let us de…ne a coordinate = y ut; such that , N and T are functions of and x only. In this newly de…ned stationary frame Eqs. (2.7) and (2.8) takes the form u 5 2 2 3 vB @ T 3 i vn @ 3 u@ N + s2 [; N] [; T] = 0; 2 3 (2.15) where the Poisson's bracket is de…ned by [F; G] @xF @ G @xG@ F . A typical solution of Eq. (2.10) is T = A0 ; (2.16) with 2 A0 = 3 i vn + 23 u u 53 vB : Substituting for T from Eq. (2.11) in Eq.(2.9) we …nd u 1 + (A0 + s4!ci 1 +) 1 vB 1vn @ 2s (u vD0) @ r2? 1 1 + A0 1 z^ r r r2? = 0: (2.17) To solve Eq. (2.16), we use the following ansätz [26] r2? = C1 + C2x; (2.18) where C1 and C2 are the constants which satisfy the condition u 1 + (A0) vB 1 1vn 2s (u vD0) C1 4s!ci 2 1+ 1 1 + A0 1 C2 = 0 (2.19) Here r2 = @@x22 + @@y22 , s = !ccsi is the ion sound dispersion radius with ion acoustic speed cs = Te0=mi. For localized dipolar vortex solution, de…ne the coordinates r = x2 + 2 2 apnd = tan 1 which divides (r;) plane into the inner r < R0 and outer 1 x r > R0 regions of a vortex of radius R0. First, consider the outer region and cylindrical polar coordinates and by using the standard separation of variables technique, i.e., by letting (r;) = R (r) cos , we retrieve the equation for r > R0 region as r2 @r2 + r @r @2R @R p2r2 + 1 R = 0; (2.20) where p2 = u 1 + (A0) 1 vB 1vn = 2s (u vD0). Equation (2.19) is the well known modi…ed Bessel equation having the solution in the form of modi…ed Bessel function of the …rst kind, K1: Hence we have out (r) = 0K1 (pr) cos : (2.21) Similarly, for the inner region, one can write down the solution by letting q2 = 2s(u- vD0)(p2 + q2) = 4s!ci 1 + 1 1 + A0 1 to obtain r2 @r2 + r @r + q2r2 1 R = q2r3: @2R @R (2.22) The solution can be written in terms of …rst order Bessel function J1, i.e., in (r) = [1J1 (qr) r] cos ; (2.23) The constants 0 and 1 can be determined by using the matching conditions at r = R0. The solution of outer and inner regions can be written, respectively, as out (r) = U R0K1 (pr) 2 s K1 (pR0) cos ; (2.24) and, in (r) = U q2!ci 2s R0p2J1 (qr) p2 + q2 r cos : (2.25) J1 (qR0) Using a recurrence relation for the Bessel function xJn0 (x) = nJn (x) xJn+1 (x), we get the following relation K2 (pR0) J2 (qR0) pK1 (pR0) = qJ1 (qR0) ; (2.26) where J2 and K2 are ordinary and modi…ed Bessel functions of second order, respectively. Equations (2.23) and (2.24) admit dipolar vortex solutions. The contour plots for the normalized electrostatic potential in (x;) plane is presented in Fig. (2-1) by using some typical tokamak parameters and for …xed value of nonthermal spectral index = 3. Furthermore, in the absence of the scalar nonlinearity, we set u 1 + (A0) 1 vB 1vn = 0; (2.27) in this case Eq. (2.26) can yield an alternate relation which is satis…ed by the vortex chain type solution and can be expressed in terms of well known stationary Navier-Stokes equation, i.e., @ r2? uB0 ; r2? c with r2? = @2=@x2+ @2=@ 2 and = Te 1 + > 0 and vD06 = u, Eq. (2.27) is satis…ed by = 0; (2.28) 1 1 + A0 1 =e (u vD0). For r2? 4 a002K02 exp = 2 uB0 0 c x ; (2.29) Figure 2-3: Vortex chains pro…le obtained from Eq. (2.30) for the tokamak parameters. where 0, K0, and a0 are arbitrary constants. The analytical solution of Eq. (2.28) for a0 > 1 admits the vortex chain solution resembling the Kelvin-Stuart cat's eyes and is given by [26] = 0 ln 2 cosh (K0x) + 1 + uB0 c x; 1 a02 cos (K0) (2.30) where 0 describes the vortex amplitude and 2 =K0 represents the size of the vortex. Figure (2-3) shows a periodic vortex street with periodicity in for the same parameters as described in Fig. (2-1), in our numerical calculations, we have normalized the space coordinates with the ion sound dispersion radius. We note here that the size of vortex pro…les are typically of the order of ion sound dispersion radius s. 2.5 Conclusion Linear and nonlinear properties of TITG driven drift mode have been studied with non- thermal electron distribution in an inhomogeneous magnetoplasma. We used the drift- approximation for the ion ‡uid velocity and derived a set of equations for the study of toroidal ITG driven drift mode. In the linear limit, new second order dispersion relation is derived for TITG mode. It is found that the growth rate of TITG mode gets modi…ed

with nonthermal electron distribution. While in the nonlinear case, the obtained solution admits stationary solutions in the form of a vortex chain and a dipolar vortices. It turns out that the inclusion of Kappa distributed electrons brings about a decrease in the spa- tial extent of the nonlinear vortex structures. The present study may be advantageous to realize the origin of drift-waves and associated coherent nonlinear structure formation in toroidal ITG driven drift modes which has applications in space and laboratory plas- mas in the presence of nonthermal electrons such as those found in RF heating, ECH experiments, as well as runaway electrons in a tokamak plasmas. Chapter 3 Tripolar Vortices in ITG Mode in Nonuniform Magnetoplasma 3.1 Introduction It is a well established fact that the two-dimensional nonlinear partial di¤erential equa- tions with vector-type nonlinearity admits vortex-type solutions. Consider a collisionless magnetized plasma con…ned in a uniform magnetic …eld B = B0^z. If the external …eld is strong enough, the ion-rich plasma column would be con…ned in a constant axial magnetic …eld B0z^. The ion column causes an electric …eld E = r along the radial direction of the column. Consequently, E B drift causes the plasma column to rotate around its axis. The background plasma has a density gradient along the negative-x direction, which causes linear drift waves to propagate along the y direction. The radial electric …eld and the axial magnetic …eld cause the ion column to produce an E B rotation around the axis of the column. The most commonly seen vortex structures are the monopole- and dipole-type vortices. The monopole vortex represents an excess in the local charge density, whereas, the dipole vortex represents a local charge polarization in the local plasma density. The dipole is seen to be produced in the turbulent wake of a 2-D ‡uid ‡owing past an obstacle. It can also be formed through pairing or coupling of two monopolar vortices with opposite rotational directions. The interactions of both the monopole and dipole vortices generate tripolar vortex with closed streamlines. The tripolar vortices are one of the fundamental vortical structures that are charac- teristic features of two-dimensional and quasi-three-dimensional ‡ows. Tripolar vortices consist of a core vortex of elliptical shape and two satellite vortices of opposite vorticity. Tripole vortices are excited in rotating ‡uids, possess angular momentum, but no linear momentum, and rotate steadily around the centre of the core vortex. Studies of the generation and stability of tripoles in homogeneous two-dimensional ‡ows were reported by Carton et al. [101], who showed that such structure can appear from the saturated azimuthal instability of a monopolar vortex, as well as from the o¤-axis collision of two dipolar vortices. The emergence of tripolar structures, together with the fundamental structures of monopoles and dipoles, has also been observed in high-resolution simulations of two-dimensional turbulence [102]. In Chapter 2, we considered low-frequency mode in electron-ion plasma with kappa- distributed electrons and dynamic ions, in the presence of external magnetic …eld, having equilibrium density, temperature, and magnetic …eld gradients. Linear as well as nonlin- ear solution was presented. Speci…cally, in the nonlinear case, we showed the presence of dipolar and vortex street type solutions. However, in this chapter, we seek the possi- bility of tripolar vortex, by employing Braginskii's transport equations for the ions and nonthermal-distributed electrons. 3.2 Model Equations We consider an electron-ion magnetoplasma embedded in applied magnetic …eld B0 = B0(x)z^ , where z^ is a unit vector and B0(x) is the nonuniform magnetic …eld. We assume that the equilibrium ion temperature, density and magnetic …eld gradients are along the x-axis. It is further assumed that the toroidal ITG (TITG) mode frequency is much smaller than the ion-gyrofrequency !ci (= eB0=mic). Here, the case is purely electrostatic for which E = r , where is the electrostatic potential. Using the drift-approximation, the ion ‡uid velocity can be written as ' c ui B0 E? z^ eB0ni r (niTi) z^ c + c B0!ci [@t + (uE + uDi) r] E? ; ui? ' uE + uDi + upi ; (3.1) where uE = E B is the drift velocity of the ion ‡uid, uDi is the ion diamagnetic drift velocity, and upi is the ion polarization drift velocity. For the TITG mode, we shall ignore the parallel component of the ion ‡uid velocity. Using Eq. (3.1) the ion continuity equation becomes, @tni + r ni (uE + uDi + upi + uiz z^) = 0; (3.2) Whereas, the energy balance equation for ion ‡uid is given by 3 2 (@t + ui r) Ti + Tir ui = 1 r qi; ni where qi = 52 (cniTi=eB0) z^ rTi is the collisionless Righi Leduc ion heat ‡ux expression. Substituting the value of r ui from the ion continuity equation (3.2), we get ni [@t + ui r] Ti Ti [@t + ui r] ni = r qi 2 2 3 3 (3.3) To close our system of equations, the electron density is to be de…ned. The 3D(three dimensional) Kappa distribution function f (u) can be written as [103] ne0 1 3=2 f (u) = (+ 1) u2 2e =me (+1) 3 (1+ 2 ; (3.4) 1=2) where = [((2 3)kBT)= m]1=2. It is required that > 32 for the validity of Kappa distribution. Integrating this distribution over the entire velocity space, we obtain the total electron density. 1 e (1=2) ne = ne0 (e 3=2) Te ; (3.5) After expansion, the electron number density takes the following form: 1 ne ' ne0 1 + 2 3 '; (3.6) 2 where ' is the normalized electrostatic potential, de…ned as ' = e

=Te, ne0 denotes the equilibrium number density of nonthermal electrons, and kappa is the de…ning factor which describes the deviation from the Maxwellian distribution (which can be retrieved in the limit ! 1). Using Eq. (3.1) into the ion continuity equation takes the following form (Lt + uBi r) ni1 ni0 + uBi Ti0 + (uBi uni) r' r Ti1 i2 [Lt + uD0 r] r2?' i2r [(uD1 r)r?'] + @zuiz = 0 (3.7) where Lt = @t + uE r, = Te0=Ti0 is the electron to ion temperature propor- tion, i = cs=!ci is the ion gyroradius at constant temperature, cs = Te0=mi is the ion-acoustic speed, uBi = (cTi0=eB0) z^ rB0=B0 is the ion grad-B pdrift,uni = (cTi0=eB0) z^ rni0=ni0 is the ion rni0 drift, uD0 = (i+1)uni, with i = (@x ln Ti0) = (@x ln ni0), uD1 = (cTi0=eB0) z^ r(N + T), N = ni1=ni0 and T = Ti1=Ti0, is the …rst order ion dia- magnetic drift velocity. Inserting Eq.(3.1) into Eq. (3.3) and using continuity equation yields Lt + uBi 5 Ti1 3 r Ti0 2 2 3 Lt ni1 ni0 i 3 uni r' = 0 (3.8) Equations (3.7) and (3.8), with N = (12)=(32) ' = ', are the required nonlin- ear coupling equations to study ITG driven mode in an inhomogeneous magnetoplasma with superthermal population of electrons. It is worth mentioning here that to study the TITG mode, we shall ignore the parallel ion dynamics (i.e., @z = 0) for toroidal geometry. Furthermore, to complete our set of nonlinear coupled equations, we use the quasineutrality condition, i.e., ne1 ' ni1. 3.3 Tripolar Vortices We have re-visited the nonlinear properties of low-frequency non-zero ion temperature gradient mode in a inhomogeneous magnetized plasma in the presence of magnetic …eld and velocity gradients. We shall show analytically as well as numerically that tripolar vortices. By solving Braginskii's transport equations and for some speci…c pro…les of the equilibrium plasma ‡ow velocity, number density and temperature gradients, new types of solutions in the form of tripolar vortices are found to exist. Here, we consider a collisionless and non-dissipative electron-ion plasma immersed in an inhomogeneous external magnetic …eld B0(x) z^, and the equilibrium ion-pressure gradient @pi0=@x, where pi0(x) = n0(x)Ti0(x) is the ion pressure. Thus, the gradients of the unperturbed particle number density (n0), the temperature (Ti0) and the magnetic …eld (B0) are assumed to be along x-axis. We further assume that the frequency of the TITG mode is much smaller (j @t j !ci) than the ion gyrofrequency. The relevant set of nonlinear equations are already formulated in the previous section, i.e., (Lt + uBi r) N + (uBi uni) r (' + '0) + uBi rT 2 i (Lt + uD0 r) r2?' + r [(uD1 r) r?'] + @z [(1 + N) uiz] = 0; (3.9) (Lt + i + uiz@z) uiz = c2s@z ' + 1 (N + T) ; (3.10) Lt + uBi r+uiz@z 5 2 2 3 T 3 (Lt + uiz@z) N i 3 uni r' = 0 (3.11) where Lt @t + uEB r and the contribution (5=3)uBi r arises from the divergence of the Righi-Leduc ion heat ‡ux. The system of Eqs. (3.9) to (3.11) can be closed if we use the quasi-neutrality condition of the plasma with nonthermal electron distribution for which ni ' ne = n0 '. Thus Eqs. (3.9)-(3.11) with N = ' are the set of nonlinear mode coupling equations to study the TITG driven drift-waves in an inhomogeneous magnetoplasma. The e¤ect of equilibrium perpendicular ion ‡ow velocity, which is due to the radial electric …eld r'0, is included in the E B drift by de…ning the total electrostatic potential as a sum of equilibrium ('0) and perturbed (') potentials. Here, we also de…ne the normalized equilibrium potential pro…le '0(x) V?0(x x0)+V?00(x x0)2=2, such that it describes only the linearly varying perpendicular ‡ows [41]. Here we introduce the normalized parameters t0 = cst=Ln, x0 = x= i, z0 = z=Ln, '0 = e Ln=(iTe), T0 = TLn=(iTi0), w = Lnuiz=(ics). We shall drop the superscript prime for simplicity of the notations. For nondissipative plasma Eqs. (3.9)-(3.11) takes the following form: @t r2? ' 1+ 1 '; r2?' 1 (+) n + K r2? @y ' + n @y T 1r '; r2?' + @zwiz = 0; (3.12) $tw = @z 1 + 1 '+T $t + n@y 5 T 2 5 3 3 $t' + 3 K ; (3.13) @y ' = 0; (3.14) where $t @t + (@x'@y @y'@x), n = Ln=(LB), K = (1 + i)= , the Poisson bracket is denoted by [a; b] (@xa@y @ya@x)b and Ln(LB) de…nes equilibrium density (mag- netic …eld) inhomogeneity scale length. Equations (3.12)-(3.14) are the required set of equations for nonlinear mode coupling to study the TITG modes in a nonuniform mag- netoplasma with sheared plasma ‡ows formed due to the nonuniform radial electric …eld. In the stationary frame moving with some constant velocity u, in a direction perpen- dicular to x-axis, so as to obtain a localized type solution of Eqs. (3.12) to (3.14), we shall again de…ne a new frame, as we did in the previous chapter. Since general station- ary analytical solution of Eqs. (3.12) to (3.14) cannot be obtained, we shall present here some approximate solutions by ignoring the parallel ion dynamics (@ z = 0). Under this assumption, we assume that '(x; y wt) and T (x; y wt), where w represents the phase velocity with which the vortex moves in the y-direction. In order to …nd the stationary vortex solution in the presence of sheared plasma ‡ows, we assume Gaussian- type den- sity, temperature and magnetic …eld pro…les: [41] so that we may write n n0 + 0nx and K K0 + K 0 x. With this choice of n and K , Eqs. (3.12)-(3.14), take the following form: @t r2? ' 1+ 1 '; r2?' 1 (+) n0 + 0nx + K0 + K0x r2? @y' + n n0 + 0nx @yT 1r '; r2?' = 0; o (3.15) $t + 5 n0 + 0nx T 2 3 3 $t' + 5 3 K0 + K 0 x @y ' = 0: (3.16) Now energy balance equation reduces to @tT + ['; T] + n0 + 0nx @yT + v0?0(x x0)@yT 5 3 + 5 3 K0 + K 0 x @y ' = 0:

(3.17) For standing wave type vortex solution, we may let @t = v@y. Hence, Eq. (3.17) can be written as, w@y + (@x'@ @ '@x) + v?00(x x0)@y + n0 + 0nx @y 5 3 T + 5 3 K0 + K 0 x @y ' = 0; or, more speci… cally, " @x + v0?0 + 0n 5 3 (x v +vv?0?000x+0 53 0n53 n0)# @y T @xT + K0 x + K0 5 3 K 0 @y ' = 0: (3.18) If we choose x1 = v +vv?00?00x+0 53 0n53 n0 ; and 5 x2 = K0 K 0 3: Then Eq. (3.18) reduces to @x ' + v?00 + 0n (x 5 x1

29)2 3 2 @y T @x T + K0 (x x2)2

2 @y ' = 0: (3.19) In the

3traveling wave frame, Eq. (3.19) takes the form

" ' + v?00 + 0n (x x1)2 ; T + K0 (x x2)2 5 3 2 2 # = 0: (3.20) We note that it is almost impossible solve Eq. (3.20) analytically to obtain a localized vortex type solution. However, if we set x1 = x2, which is basically a way to …nd out the phase velocity of the vortex, we may integrate Eq. (3.20) and get the following expression T + K0 (x x1)2 = f1 ' + v?00 + 0n (x x1)2 5 2 3 2 ! : (3.21) Here f1 represents an arbitrary function of its argument. For a localized vortex type solution, we have to impose a condition of vanishing of perturbations at in…nity, such that T = v?00 + 53 0n K0 ' = C1': (3.22) Eliminating T from Eq. (3.20), we readily obtain w@y(' r2?') + 1 + 1 (@x'@y + @y'@x) r2?' + (@x'@y @y'@x) ' 1 (+) n0 + 0nx + K0 + K0x r2? + n0 + 0nx @yT +v?0(x x?0)@y(' r2?') = 0; n0 o or @x ' + v?00 K0 (x x3)2 @y(' r2?') ((1 + 1) 2) @x(' r2?') (+ (1++C1) 1n0)+ K0 (x x4)2 2 @y ' = 0; (3.23) where x3 = v0?0x00 + v + K0 ; v?0 K 0 and x4 = (1((n+0(++C1+) C0n1+) K0K)0): Equation (3.23) can be rewritten as " '+ 1) 2 ;' r2?' (+ (1++C1) 0n + K0 (x x4)2 v?00 K 0 (x x3)2 (1 + 1) 2 # = 0: (3.24)

3Setting x3 = x4, once again, one may write the general solution of

(3.24) as r?2' ' + (+ (1++C1) 10n)+ K0 (x x3)2 = f2 ' + (V1?+00 1) K 0 (x3)2 2 2 ! ; (3.25) where f2 is an arbitrary function. Letting '0 = 4' (1 + 1) =(v?00 K0) and v?006 = K0, we get (v?00 K0) 4 (1 + 1) ' 0 r2?'0 (+ (1++C1) 10n)+ K0 (x x3)2 2 = f2 '0 + 2(x x3)2 v0?0 K0 4 (1 + 1) ; '0 r2?'0 Let x3 = x. Then and, …nally, we obtain (+ (v+?00C1)K0n0)+ K0 2(x x3)2 = f2 '0 + 2(x x3)2 : b2 a2 = 1+ (+ + C1) 0n + K0 (v?00 K 0) ; r2?' = ab22 ' (3.26) A typical tripolar vortex pro…le for the equipotential contours for the tripolar part of the electrostatic potential is plotted in the two dimensional x-y plane and is shown in Fig. (3-1)

6by choosing some typical parameters of Tokamak plasma:

Te = 10 keV, ne = 1014 cm 3, = 2, B0 = 3:45 104 Gauss, s = 0:25 cm, LB = 300 cm; n0 = 0:3, v?00 = 4:5, i = 3 and r0 = 2. These values yield b = 1:03 and 1 = 1:42, where the normalized parameter K0 is approximated with (1 + i)= , and 0n with Ln=(LB) such that Ln = n0LB. Here, again, we have dropped the superscript prime for simplicity of the notation. Following the procedure of Ref. [55], we subdivide the space in the form of a circle of some radius r0 and then solve Eq. (3.26) by employing

24cylindrical coordinates, taking r = x2 + y2 and = arctan(y=x),

independently outside and inside that circle and obtaipngeneral solution of Eq. (3.26) in the form of Bessel equations. The detailed Figure 3-1: Fig.1. (colored online only) A shadowgraph of 3D view of the normalized electrostatic potential for = 3 case for other plasma parameters given in the text. analysis can be seen from our earlier published work. We numerically solve the Bessel equations for the outer and

inner regimes by using the appropriate boundary condition at the boundary of given circle, namely by the continuity of the normalized potential and the continuity of @'=@r at r = r0. To draw the vortex pro…le in three-dimensions, we choose the aforementioned typical tokamak parameters and obtained a shadow-graph. The shadow-graph clearly shows tripolar vortex on a scale-length of ion-Larmor radius. The equipotential contours of electrostatic potential resembles with tripolar vortex. The contours show a double vortex between the lobes of a monopolar vortex structure having negative value of the potential. Figure (3-1) shows a shadowgraph of three dimensional (3D) view of the potential for = 3 case Fig. (3-2) in which the nonthermal e¤ect is pronounced and the amplitude of the potential becomes slightly higher than the classical case (kappa > 1 or simply > 1 case), in which the electrons follow Boltzmann type distribution. It is evident from the shadow plots Fig. (3-1) that the amplitude of the wave potential is small. Figure 3-2: Shadow graph of 3D view of the normalized potential for > 1 case in which the electrons follow classical Bolzmann type distribution with the same other parameters as taken in Fig.3-1. 3.4 Conclusions We have studied the nonlinear properties of ITG mode for Maxwellian ions and nonther- mal kappa distributed electrons for low frequency inhomogeneous magnetoplasma having equilibrium ion temperature and density gradients. By using drift-approximation, we have formulated the group of nonlinear set of equations that

3**admit stationary** solution **in the form of a tripolar**

vortices. For tokamak plasma parameters, we have plotted numerically the tripolar vortices which shows that the inclusion of kappa distributed electrons brings about a decrease in the spatial extent of the nonlinear vortex structures in comparison with Maxwellian distributed counterparts. This work would be useful to gain deep insight the origin of drift-waves and associated coherent nonlinear structure formation in toroidal ITG driven drift modes which has applications in space as well as in laboratory plasmas. Chapter 4 Sheared Driven Ion Acoustic Vortex Formation in Two-Electron-Temperature Plasma 4.1 Introduction Linear and nonlinear properties electrostatic waves in multi species plasma has been investigated, whereas the cold electrons are Boltzmannen and the hot component of elec- trons are Cairn's distributed. The ions are considered dynamic and cold. It is observed that the propagation regime of ion acoustic and drift waves has been changed due to the presence of suprathermal electrons, ion-neutral collisions and ions sheared ‡ow. Hot component of electrons follow Cairn's distribution which signi…cantly changes the growth rate of ions shear ‡ow driven instability. We found that vortex structures get modi…ed in the presence of nothermal electrons. 4.2 Nonlinear Model Equations The propagation of ion acoustic mode in two electron-temperature and dynamic cold ion collisional magnetoplasma is considered. We assume that cold electrons are Boltzmannen and the hot electrons are Cairn's distributed. The applied magnetic …eld is constant and pointing in the z-direction such that B0 = B0 ^z. For electrostatic mode, the perturbed electric …eld can be related to electrostatic wave potential such that E = r'. For three component plasma, the charge neutrality condition in equilibrium satis…es the following relation, nc0 + nh0 = ni0; (4.1) where the index c (h) is used to indicate the cold (and the hot) component of electrons and the index i for the ions. The Cairn's type distributed electrons, the distribution function can be written as follows:[59] fh0(v) = nh0 (3 + 1) 2 vt2h p v4 v2 1 + vt4h exp 2v2th ; (4.2) where the equilibrium density of hot electrons is nh0 with thermal velocity de…ned as vth = Th=me. Where Th is the temperature of hot electrons and is the nonthermal parampeter. The number density of hot electrons can be obtained by integrating over the entire velocity space, such that we have nh = nh0 1 e' + e' 2 e' T h T h ! Exp T ; (4.3) h Here = 4 =(1 + 3). It may be noted here that the above expression reduces to the well known classical Boltzmann distribution by taking the limit = 0. Whereas, the cold electrons are assumed to be Boltzmannen type, such that nc = nc0 exp e' Tc ; (4.4) where Tc is the cold electron temperature. For convenience, we use the notation: the cold electron density proportion is given by f = nc0=ni0. Moreover, c = Teff =Tc, h = Teff =Th, and e¤ective temperature Teff = Tc=(f + (1 f)) with = Tc=Th. ni0

5**is the** total **ion number density,** Ti **is the** temper- atures **of**

ions. Expanding Eq.(4.3) nh = nh0(1 f) 1 (h) + (h)2 Exp (h) by taking h 1, the hot electrons perturbed part can be written as, nh1 ' nh0(1 f)(1)(h 1), whereas the normalized electrostatic potential = e'=Teff. The Poisson's equation (4.4) in the linearized form, and the above expression for the perturbed number density of hot electrons, yield the following result nh0 '[f c+(1)(1 f) h] ni1 D 2 r 2 = D2r2 ; (4.5) where =[f c+(1)(1 f) h]:nc1;nh1aretheperturbednumberdensitiesofcold and hot electrons, respectively. Here D = Teff=4 ni0e2, c = nc0=ni0, and h = nh0=ni0. p The ion momentum balance

27**equation for the** collisional plasma **can be written as** mini0 **(@t**

+ vi r) vi = eni0 r' + vi B0 mini0 invi 1 c (4.6) where in is the collision frequency between the ion-neutrals. The perpendicular component of cold ion ‡uid using drift-approximation, for low- frequency waves (@t !ci, where !ci = eB0=mic is the ion gyrofrequency), can be written as vi? B0 z^ r' B0!ci (@t + in + vE r + (vi0(x) + viz)@z) r?': ' c c (4.7) The z-component of ion ‡uid with ion shear ‡ow is given by (@t+ in+vE:r+ (vi0(x)+viz)@z)viz = = = e @z' + vE rvi0(x) mi Tef f mi @z @xvi0(x) e' !ci @y Teff c2s (@z Si@y) : (4.8) Using drift approximation (4.7), the continuity equation for the ions can be written as (dt + in + vE:r + viz@z) nnhi10 B0!ci (dt + in + vE:r + viz@z) r2?' c ni1 c@x ln ni0 in nh0 B0 @y ' + @z viz = 0; (4.9) where dt = @t+ vi0(x)@z, and vE = (c=B0)z^ r' is the E B0 drift. Here, we have assumed that jvE rj jvz@zj. It is worth mentioning here that r v6 = 0 can give rise to a vortex type structure in the nonlinear regime. Equations (4.5), (4.8) and (4.9) is the desired set of equations. 4.3 Derivation of

6**Dispersion Relation To derive a linear dispersion relation, we**

drop nonlinear terms in Eqs. (4.5)-(4.9), and by using sinusoidal approximation for the perturbed quantities: exp [i(!t kyy kzz)], and …nally obtain a quadratic dispersion relation (!0 + i in)2 k?2 2s + (!0 + i in) !0 1 + k2 2D ! kz2 c2s 1 ky Si kz = 0; (4.10) HereDopplershiftedfrequencyis!0=! kzvi0(x),theLarmorradiusoftheions i= cs=!ci,! =(kycTeff@xlnni0)=(eB0)isthedrift-wavefrequency,andSi=@xvi0(x)=!ci istheionsheared‡owparameter. For collisionless case and for uniform density plasma with 2Dk2 1, Eq. (4.10) reducesto !0 = kzcs 1 kySi=kz sf c + (1 f)(1) h + k?2 i2 ; (4.11) It may be noted here that the above dispersion relation shows unstable regime for kySi > kz. In Fig. 4-1, we have plotted a normalized growth rate =!ci vs., kz i, by taking the same parameters as given in Ref.[68]: i.e., Ni0 = 0:1/cm3, B0 = 0:2 G, Th = 500eV , Tc = 5 eV, = 0:04, f = 0:1, M = u=cs = 0:98, ky = 0:5= s, Si = 0:5, for di¤erent p values of the nonthermal electron population parameter, = 0:22 (solid black curve) and Figure 4-1: Plot of normalized

13**growth rate as a function of** kz i for **the** parameters described **in**

the text. The black solid line is for = 0:22 and the red one is for = 0:1: = 0:1 (red dashed curve). The growth rate of acoustic mode is shown in the graph, in the presence of nonthermal electrons and sheared ‡ow increases. Whereas, in the presence of ion-neutral collisions, damps the coupled ion-acoustic drift mode with hot electrons for !0 << in. We may let ! = !r + i , and obtain the following result = +in k?22D ks2 2 kz2c2s (1 kySi=kz) in + D2 k2 : (4.12) Eq. (4.12) shows a purely damped mode in the absence of parallel ion-sheared ‡ow. Clearly, the ion drift-dissipative mode is found to become unstable for jSij ky > kz. Therefore, it is evident from Eq. (4.12) that both the ion acoustic and drift mode get destabilized by the combined e¤ects of ion sheared ‡ow for jSij ky > kz case. The ion sheared ‡ow in a collisional magnetoplasma can drive unstable mode by the coupling of ion-acoustic and drift-mode. 4.4 Nonlinear Analysis It is well known that when the …nite amplitude drift and ion-acoustic waves nonlinearly interact with each other, variety of nonlinear coherent structures can be formed. We use some suitable normalization in order to obtain vortex solution i.e., the time variable is normalized with !ci1, the space variables with s = cs=!ci, the ‡uid velocity of ions with cs = Teff=mi and the number density of ion with its equilibrium number density. The contipnuity and momentum balance equation for the collisionless ions

14**can be written as:** @tni + **r:(nivi) = 0; (4.** 13) (@t + **vi:** r) **vi = -r + vi** z^; **(4.**

14) Using Eq. (4.7) in the ion continuity equation and by letting ni = ni0 + ni1, (where ni1 ni0), we get Dt(ni1 r2?) (@x ln ni0) @y + @zviz = 0; where Dt = dt + z^ r? r + viz @z . The Poisson's equation(4.5), in the dimensionless form can be expressed as: ni1 = (2D= 2s)r2 , consequently the above equation can be re-written as Dt ((1 + 2D= 2s)r2?) (@x ln ni0) @y + @zviz = 0: (4.15) Here we have used r2? @2=@z2. The

12**parallel component of** ion **equation of motion** yields **the following**

result Dtviz = @z z^ r? rvi0(x) = @z + Si0@y ; (4.16) where the normalized shear ‡ow parameter is de…ned as Si0 = @xvi0(x)=!ci: To obtain stationary solution [104] of Eqs. (4.15) and (4.16), we de…ne a frame (x;); in which we can write y + z u t, where the vortex speed is de…ned by a parameter u and is an arbitrary constant. Here we have assumed that jz^ r? rj >> jviz @z j. Equation (4.15) in the transformed frame takes the following form U L viz = (Si0) @ ; (4.17) Here we de…ne a di¤erential operator L = @ (1=U) (@x @ @ @x) with U = u vi0. It can be shown very easily that the stationary solution of Eq. (4.17) is viz = 1 U (Si0) : (4.18) Inserting viz from Eq. (4.18) into Eq. (4.15), we get UL ((1 + 2D= 2s)r2?) (@x ln ni0) @ + U (Si0)@ = 0; which on simpli…cation gives Un (Si0) U U2 @ + 1+ 2D @ 1 2s U z^ r? r r 2 ? = 0; (4.19) where Un = (@x ln ni0). For Un U (U2Si0) = 0, we obtain the following equation @ r2? U1 [; r2?] = 0; (4.20) where r2? = @x2 + @2. The above equation is satis…ed by r2? = 4 0 exp R2 2 (U x) (4.21) 0 where 0 and R0

11**are some constants. The analytical solution of Eq.** (4.21) **is**

= U x +

11**0 ln 2 cosh x + 2 1** R02 1 **cos**

: (4.22) For R20 > 1, Eq. (4.22) gives the well known vortex chain type solution[68, 104]. Here U = [Un (Un)2 + 4 (Si0)]=2 represents the vortex chain speed. To obtain an q analytical solution, we proceed as follows. By retaining the Jacobian nonlinearity, we get @ r2? U1 [; r2?] 1@ = 0; (4.23) where 1 = + UUn + (U2Si0) 1 + D2 . The solution of Eq. (4.23) can be written 2 1 s as r?2 1 =f(U x) (4.24) Here we assume the function f (U x) = F (F is some constant. Thus the Eq.(4.24) gives us U x) i.e., it behaves linearly. Where r2? 1 =F (U x) : (4.25) Using cylindrical polar coordinates (r;) with azimuthal symmetry, Eq.(4.25) can be transformed and the inner region (r < R0) and the outer region (r > R0) solutions can be expressed in the following way, where R0 is the radius of a circle, out(r;) = C1K1(1r) cos : (4.26) and 2 in(r;) = C2J1 (2r) + 1 + 2 2 2 2 Ur cos ; (4.27) where 22 = (21 + F), F = (21 + 22), and K1(J1) are

4**modi…ed (ordinary) Bessel** function **of order one,** respectively. **Here**

the unknown constants C1 and C2

4**can be calculated by using the continuity of** the function , **@r , and** r2? **at the boundary of the** circle **r**

= a0, a0 21 a0 C1 = U K1(1a0); C2 = U 22 J1(2a0) ; (4.28) Figure 4-2: The plot of potential in the contour form in (x;) plane is shown for the mach number M = u=cs = 0:98, with Si = 0:1. The normalization used for

the distances is with i: and 2 from the following relation K2(1a0) K1(1a0) = 1 J2(2a0): (4.29) 2 J1(2a0) The above equations (4.26) &(4.27) alongwith the said constants forms dipolar vor- tices. The contour plot in 2D of the electrostatic potential is plotted in Fig. 4-3 for the same parameters taken in Fig. 4-1. For those parameters, we found s = 6196:3 cm. Notice that like vortex street, the dipolar vortex solution is obtained on the same s scale size. Equation (4.26) represents a bounded dipolar type solution for 1 = + UUn (U2Si0) > 0: For nonthermal plasma, the condition of the boundness gets + modi…ed: The Mach number range also gets modi…ed in the presence of hot component of the plasma. Figure 4-3: The dipolar vortex in 2D is plotted for =

310:1 (in red color) and = 0: 9 (black color) for M = 0:

98: 4.5

4Summary In this chapter, linear/nonlinear properties of coupled ion acoustic and drift waves has been

discussed for Cairn's type hot electrons with parallel ion sheared ‡ows. New dis- persion relation is derived and instability condition is also discussed. The normalized growth rate is plotted for some space plasma parameters by varying the superthermal electron parameter. The growth rate is found to become higher by increasing the pop- ulation of hot electrons. On the other hand, for collisionless case, dipolar and vortex street can be formed.

1It is found that the presence of superthermal electrons

changes the vortex structure and its boundedness. The results of our investigation may be bene- …cial to understand the dynamics of two electron temperature and ion plasma for space applications. Chapter 5 Electron acoustic soliton in magneto-rotating e-p-i plasma 5.1 Introduction In this chapter, we focus on electron acoustic soliton formation and its propagation in rotating electron-positron-ion magnetoplasma. We consider cold electrons which are dynamic and follow non-Maxwellian (Cairns type) distribution for the electrons and positrons, and stationary ions, whose mass is very large compared to the electron/positron mass. We …rst derive a linear dispersion relation and afterwards we investigate how it is a¤ected by magnetic …eld, the nonthermal parameter, and rotation. For the nonlinear analysis, we derive kdV (Korteweg-de-Vries) equation by employing the usual reductive perturbation method (RPM). The presence of nonthermal positrons, both dip and hump type solitons can be excited, moreover, the inclusion of magneto-rotating drastically a¤ects properties of these solitary waves. 5.2 Derivation of Linear Dispersion Relation We assume a rotating, magnetized electron-positron-ion plasma with cold electron, non- thermal hot electron-positrons, and static collisionless ions. The nonthermal hot e-p population is taken to be Cairns type distribution (Cairns et al. 1995) and the number densities of nonthermal electrons/positrons [84, 105] are taken to be: nh = noh 1 + e + 1 Th 2 e 2 Th + ! (5.1) np = nop 1

30e T p 1 + 2 e T p 2

+ ! ; (5.2) where (1). For ! 0, one gets the Boltzmannen distributions, i.e., nh ! noh exp(Teh), np ! nop exp(Te p). For a collisionless, rotating magnetized plasma, the set of ‡uid equations are @nc @t + r: (ncuc) = 0; (5.3) and, @u = B me nc @tc +(uc:r)uc encE enc(uc c) + 2menc(uc); (5.4) where e

4**is the** charge **of electron,** nc **is the** cold species of **electron number density, and** uc **is the ‡uid velocity** of **the**

cold electrons,

4**E = r is the** electric …eld **and B** = B0z **is the** applied **magnetic …eld,** is **the** angular frequency **of**

rotating frame [70]) i.e., = xx^+ zz^. To close the set of modeled equations, we use Gauss's law to write r E = 4 e (no + np nh nc) ; (5.5) where n0 is the equilibrium number density of …xed positive ions. In the equilibrium state, one can write n0 + n0p = n0c + n0h, where n0s (s = p; c; h) are the equilibrium number densities. Eqs. (5.1) and (5.2) in the normalized form are nh = 1 ' + '2 exp(') = 1 + ' + '2 2 + np = 1 + ' + 2'2 exp(') = 1 '+ Similarly, The normalized form of Gauss's law is 2 '2 2 + @x2' + @z2' = 1 + nc + (1 +) ' + (1 2) '2 2 + (5.6) The normalized version of Eqs. (5.3) and (5.4) is @nc @t + r:(ncuc) = 0 (5.7) @uc @t + (uc:r)uc = r' R(uc z) + 2(uc); (5.8) or, rewriting in the component form as @tnc + @x(ncucx) + @z(ncucz) = 0, (5.9) @tucx + ucx@xucx + ucz@zucx = @x' eff ucy ; (5.10) @tucy + ucx@xucy + ucz@zucy = 2ucz x + eff ucx ; (5.11) @tucz + ucx@xucz + ucz@zucz = @z' 2ucy x: (5.12) Here = nop=noh, = noc=noh, = no=noh, = Th=Tp. Furthermore, R = ce= !ph and = = !ph are, respectively, the normalized cold electron gyrofrequency and the plasma rotational frequency, eff = R 2 z, with x = 0sin and z = 0cos are various components of plasma rotational frequency and 0 = 0= !ph represents the magnitude of dimensionless rotational frequency. The cold electron ‡uid velocity ucj (j = x; y; z) is normalized with uth = Th=me, the number densities are normalized with equilibrium densities, the electrostatipcpotential ' is normalized by Th=e. Moreover, the space variables with Dh = Th=4 nohe2 and the time variable is normalized with !ph1 = me=4 nohe2 [84]. p Thepmodel equations, namely (5.6, 5.9-5.12), after linearization and use of the plane wave approximation for all perturbed quantities (f1 ei(kxx + kyy !t)) lead to the fol- lowing linear dispersion relation !4(k2 + (1 +)) !2((2eff + 4 2x)(k2 + (1 +)) + k2) + (2kx kz eff)2 = 0; x (5.13) If we consider long perturbation wavelength, then Eq. (5.13) takes the following form !4 !2((2eff + 4 2x) + c2sepk2) + (2kx kz eff)2c2sep = 0: x (5.14) Here csep = !pc Deff = (nocThTp) = (nopTh + nohTp) (1)me represents the phase speed of modi…ed EAW, pDeff = (Dp Dh) = (1) (D2h + 2Dp) is modi…ed

1**Debye length in the presence of** hot electrons **and** ppositrons. qWhere, **Dp**

= Tp=4 nope2 and Dh = Th=4 nohe2 are the Debye lengths of electrons and positrons,prespectively. The plasmapfrequency of the cold species of electrons is given by !pc = 4 noce2=me [84]. Equation (5.13) in the absence of rotation and magnetic e¤ects (x =p eff = 0) has the form !=k = (nocThTp) = (nopTh + nohTp) (1)me as reported earlier in Ref. [84]. In the presencepof external magnetic …eld (i.e., x = z = 0; eff = R) and in the limit ! R, kx kz, Eq. (5.13) leads to the dispersion relation !2 = c2sepkz2=(1 + c2sepk2=R2) describing an electron acoustic mode

5**in a magnetized e-p-i-plasma,** and which **for**

much longer wavelength becomes !2 = c2sepk2z, a result similar to the case when both rotation and magnetic …eld were absent. However, in the limits ! R, kz kx, x = z = 0, eff = R, one …nds !2 = R2 + cs2epkz2; i.e., an electron-cyclotron wave. Furthermore, in the presence of slow rotation only (i.e., R = 0, eff = 2 z, x6 = z6 = 0, ! 0), Eq. (5.13) gives !2 = 4 20+c2sepk2, which is also an electron-cyclotron like mode but this time rotational e¤ect plays the role of a magnetic-…eld-like e¤ect. It is evident from the above mentioned linear dispersion relation of EAW that electron acoustic mode signi…cantly gets modi…ed in a rotating

and positrons that we have already explored in Ref. [84]). It is well known that soliton is formed when the dispersion and steepening e¤ects are balanced, thus, its structural properties would also be modi…ed in a rotating magnetized e-p-i-plasma as we shall discuss in the next sections. 5.3 Derivation of kdV Equation In this section, we shall derive the nonlinear kdV equation from Eqs. (5.5),(5.8) and(5.9), we employ the well known reductive perturbation technique, in this regard let us de…ne the stretched variables as [70, 106] = 1=2 (lxx + lzz t) ; = 3=2t; (5.15) where 1 is an expansion parameter and is proportional to the perturbation amplitude, is the normalized speed of the wave, uth = Th=m denoting the thermal speed, lx and lz are the direction cosines of the wave vecptor k; thus l2x + lz2 = 1. Using reductive perturbation method (RPM), expanding the quantities nc, ucj (j = x; y; z), and ' in the power series form, we get nc = 1 + n(c1) + 2n(c2) + 3n(c3) + ; ucx = ucy = ucz = ' = 3=2u(c1x) + 5=2u(c2x) + 7=2u(c3x) + 3=2u(c1y) + 5=2u(c2y) + 7=2u(c3y) + u(c1z) + 2u(c2z) + 3u(c3z) + ; '(1) + 2'(2) + 3'(3) + : ; ; (5.16) Using Eqs. (5.15) and (5.16) in Eqs. (5.6, 5.9-5.12), and collecting di¤erent powers of : The zeroth order in , gives 1 + = + . The next higher order terms gives, nc(1) = nc(1) = (1 +) ' (1), u(c1y) = lx @ '(1), u(c1z) = (lz 2lx)'(1), 1 x ef f ef f 1 2 (l2z 2lxlz)'(1) x (5.17) ef f Using these expression in Eq. (5.16) leads to the following linear dispersion relation, x 1=2 = (1 +) lz2 2lxlz (5.18) r ef f Equation (5.18) gives the normalized modi…ed EAW phase speed in the presence of nonthermal electrons and positrons, as well as due to the presence of external magnetic Figure 5-1: Plot of normalized EAW phase speed with in the presence (dashed curves) and in the absence (solid curves) of magneto-rotating e¤ects at di¤erent positron concentrations. The other parameters are = 0:7; = 10; = 10 ; lx = 0:3, 0 = 0:1. …eld and rotational e¤ects. For parallel wave propagation, one can take lz = 1, lx = 0, and as a result Eq. (5.18) reduces to !=k = !pc Deff = (nocThTp) = (nopTh + nohTp) (1)me (Jilani et al. 2013b). Figure (5-1), shows that thepphase speed of EAW increases with the increase of , and this is true even in the presence (dotted curves) of magnetic …eld. However, the magneto-rotating e¤ects and with the rise of positron concentration reduces the wave phase speed. We note that in the absence of magnetic …eld (R), Eq. (5.18) gives = (1+) (lz2 + lxlz tan)1=2, here if we ignore magnetic …eld also eliminates the Coriolis foqrce e¤ect, and there remains what only is the angle ( ) of rotation axis and the obliqueness of wave propagation with the magnetic …eld axis (z-axis) that encounter the linear dispersion relation. Figure (5-2) displays the variations of the EAW phase speed (Eq. (5.18)), the left most plot shows that the phase speed decreases with the increase of and the angle of wave propagation with respect to external magnetic …eld. The middle plot shows that phase speed enhances with parameter and degrades with increasing rotation. The right most plot shows that the phase speed decreases with and increases with the magnetic …eld strength. It is evident from all these plots that dispersion prop- Figure 5-2: Variation of normalized EAW phase speed with various parameters. Left most plot, (= 0:7; = 10; = 10 ; R = 0:3; = 0:3; 0 = 0:1) middle plot,(= 0:1; = 0:1; = 10; = 10 ; R = 0:3; = 0:3; lx = 0:3), Right most plot, (= 0:1; = 0:1; = 10 ; R = 0:3; = 0:3; lx = 0:3; 0 = 0:1). erties are signi…cantly gets modi…ed with the presence of magneto-rotating e¤ects and consequently the solitary wave structure would also gets modi…ed. Next, we collect the next higher order terms, that is of the order of 2, the Poisson's equation (5.6), the continuity (5.9), and momentum (5.10-5.12) equations gives us the following results, 2 @ 2 '(1) n(c2) (1 +) '(2) (1 2) '(1) 2 = 0; uc(2y) = lx @ '(2), u(c2z) = @ u(c1y), ef f x @ u(c1z) @ u(c2z) + +lzu(c1z)@ u(c1z) + 2 xu(c2y) lz@ '(2) = 0; @ n(c1) @ n(c2) + lz@ (n(c1)u(c1z)) + lz@ u(c2z) = 0; Finally, eliminating n(c2), u(c2(y); z), '(2) and using Eq. (5.16), we obtain the standard KdV equation, @ + A @ + B @3 = 0; (5.19) where = '(1) 4 (2 1) 3 P2 3 A = 2 P , B = 2P with P = lz2 2lx lz x ef f Clearly, these coe¢ cients become similar to the coe¢ cients of Ref. (Jilani et al. 2013b) for the wave propagation parallel to the magnetic …eld (i.e., for lz = 1, lx = 0). Thus, dispersion and steepening of wave with coe¢ cients are vividly a¤ected by rotation and magnetic …eld when the wave propagates at some oblique angle (0 < lz < 1) to the magnetic …eld. 5.3.1 Solution of KdV Equation To …nd a localized solution of Eq. (5.19), we choose a new coordinate de…ned as soliton solution has the form [78] = u , where u is the normalized (by Th=m) speed of nonlinear soliton. The p = '0 sec h2 ; (5.20) 4 where '0 = 3u=A is the amplitude, and 4 = 4B=u is the

localized solitary structure. 5.4 Discussion of Results We have investigate the e¤ects of magnetic …eld, rotation parameters and obliqueness of the wave propagation along-with other normalized physical parameters of interest including = nop=noh, = noc=noh, and 0 = Th=Tp, on the EA soliton structures. To preserve the charge neutrality condition of e-p-i plasma, we choose a slow rotation of plasma frame (i.e., 0 1). Also, to make the background electric …eld (generated due to rotational e¤ect) negligible, we assumed the angle to be small and R 1 (Hussain et al., 2013). We have selected the appropriate range of parameters (noc (0

1**:1 0:4)cm 3,** nop **(1:5 3) cm 3,** noh **(1:5 3) cm 3,** Th **(200 1000) eV,** Tp **(200 1000) eV,**

(0:25 0:6)) to cover a wide variety of system of plasma

1**ranging from laboratory to astrophysical** and **space plasmas**

[89, 106]. As EAW dynamics is linked up with the

1**dynamics of cold electrons and is relatively low-frequency** electrostatic mode **with phase speed** vph **lying in the range**

utc vph utp,uth, to avoid Landau damping and, therefore, allowing the nonlinear soliton structure formation[78]. Figures 5-3(a, b) show how nonlinearity (A) and dispersion (B) coe¢ cients varies with superthermal population parameter. The dashed curves are in the presence of magneto- rotating e¤ects and the solid curves are in the absence of magneto-rotating e¤ects (caused by the elimination of magnetic …eld e¤ect) wherein the wave propagates at some oblique angle to the z-axis. In Fig. (5-3a) we demonstrate that both in the absence (solid curves) and presence (dashed curves) of magneto-rotating e¤ects, there is a transition in the sign of nonlinearity coe¢ cient from negative (A < 0) to positive (A > 0) at a common critical value of nonthermal parameter (0:3) in the presence of

1**positrons, thereby leading to the existence of both dip (A < 0) and hump (A > 0) type solitons.**

However, in the absence of positrons (= 0) we will always …nd A < 0, therefore, in this case only dunk type solitons exist both in the absence and presence of magneto-rotating e¤ects (see Fig. Figure 5-3: (a) Variation of coe¢ cients

1**A; B with parameter in the** presence **of positrons**

(dashed curves R = 0:3; 0 = 0:1) and (solid curves R = 0). The other parameters are = 0:2; = 0:7; = 10; = 10 ; lx = 0:3: (b) Variation of coe¢ cients

1**A; B with parameter in the** presence **of positrons**

(dashed curves R = 0:3; 0 = 0:1) and (solid curves R = 0). The other parameters are = 0; = 0:7; = 10; = 10 ; lx = 0:3: (5-3b)).Figures 5-4(a, b) illustrate the variation of bump and dunk type soliton structures Figure 5-4: (a)

1**Variation of hump type EA soliton structure with** 0(rotation frequency). **The other parameters are**

= 0:1; = 0:7, = 10, = 10 , R = 0:3, = 0:4, lx = 0:3,

1**u = 0:01.** (b) **Variation of dip type EA soliton structure with** 0(rotation frequency). **The other parameters are**

= 0:1; = 0:7, = 10, = 10 , R = 0:3, = 0:25, lx = 0:3, u = 0:01. with rotation e¤ect (0) due to the Coriolis force in the presence of constant magnetic …eld. Clearly, increase in normalized rotation frequency increases the amplitudes of both bump and dunk type structures and there is a degradation in width of these structures. In Fig. 5-5(a) and Fig. 5-5(b) we demonstrate that the amplitudes of both positive and negative potential solitary structures depreciate while the widths of these structures enhance with the increase of normalized electron-cyclotron frequency (R). In Figs. 5- 6(a, b) the obliqueness of the wave propagation along the direction of magnetic …eld is studied. It is shown that the amplitudes of both opposite polarity structures amplify with the increasing values of angle of propagation with the magnetic …eld. Now in the remaining discussions we have compared the results of di¤erent parameters on the solitary waves both in the absence (solid wave pro…les) and presence (dashed wave pro…les) of magneto-rotating e¤ects. In all these discussions the EASWs are assumed to propagate at an oblique angle with z-axis. Figure 5-5: (a)

1**Variation of hump type EA soliton structure with**

R(electron rotation frequency). The other parameters are = 0:1; = 0:7, = 10, = 10 , 0 = 0:1, = 0:4, lx = 0:3,

1**u = 0:01.** (b) **Variation of dip type EA soliton structure with** 0(rotation frequency). **The other parameters are**

= 0:1; = 0:7, = 10, = 10 , 0 = 0:1, = 0:25, lx = 0:3, u = 0:01. Figure 5-6: (a)

1**Variation of hump type EA soliton structure with**

lx(obliqueness of wave propagation along magnetic …eld). The other parameters are = 0:1; = 0:7, = 10, = 10 , 0 = 0:1, = 0:4, R = 0:3,

1**u = 0:01.** (b) **Variation of dip type EA soliton structure with**

lx(obliqueness of wave propagation along magnetic …eld). The other parameters are = 0:1; = 0:7, = 10, = 10 , 0 = 0:1, = 0:25, R = 0:3, u = 0:01. Figure 5-7: (a)

1**Variation of hump type EA soliton structure with parameter** in **the**

presence (dashed curves R = 0:3, 0 = 0:1) and in the absence (solid curves R = 0) of magneto-rotating e¤ects. The other parameters are = 0:7, = 0:4, = 10, u = 0:01, = 10 , lx = 0:3. (b)

1**Variation of dip type EA soliton structure with parameter** in **the**

presence (dashed curves R = 0:3, 0 = 0:1) and in the absence (solid curves R = 0) of magneto-rotating e¤ects. The other parameters are = 0:7, = 0:25, = 10, u = 0:01, = 10 , lx = 0:3. Figures 5-7(a, b) narrate the e¤ects of increasing hot positron concentration relative to hot electrons both in the absence (solid wave pro…les) and presence (dashed wave pro…les) of magneto-rotating e¤ects. It is observed that an increase in positron concentration decreases the amplitude of both bump and dunk type solitons. However, the amplitudes of these structures are enhanced in the presence (dashed pro…les) of magneto-rotating e¤ects. Physically, an increase in hot positrons concentration depletes hot electrons, and as a result, the charge neutrality is maintained by the gain of cold inertial electrons within the localized nonlinear structure which

20**leads to a decrease of** amplitude. Similarly, **the variations in the** wave pro…les **of**

Figs. 5-8(a, b) can be described. Here,

1**the increase in cold** electrons **concentration relative to** that of **hot**

electrons decreases the amplitude of bump soliton whereas the negative potential solitary pro…le ampli… es the same. However, magneto-rotating e¤ects make the structures more spiky. Figure 5-8: (a)

1**Variation of hump type EA soliton structure with parameter** in **the**

presence (dashed curves R = 0:3, 0 = 0:1) and in the absence (solid curves R = 0) of magneto-rotating e¤ects. The other parameters are = 0:1, = 0:4, = 10, u = 0:01, = 10 , lx = 0:3. (b)

1**Variation of dip type EA soliton structure with parameter** in **the**

presence (dashed curves R = 0:3, 0 = 0:1) and in the absence (solid curves R = 0) of magneto-rotating e¤ects. The other parameters are = 0:1, = 0:25, = 10, u = 0:01, = 10 , lx = 0:3. Figures 5-9(a, b) show the

32**e¤ect of** increase in **hot electron temperature**

relative to that of hot positrons on the EASWs. The bump type soliton decreases whereas dunk type soliton enhances in amplitude. Whereas, in both cases magneto-rotating e¤ects amplify the solitary wave pro…les (dashed pro…les) in terms of amplitude. Physically, the decrease in hot positron temperature (or increase in hot electron temperature) causes the e¤ective Debye length to reduce. Under such conditions there is an increase in the leakage of hot electrons from Debye sphere and causes the hot positron concentration to enhance and, hence, an attractive potential is developed among cold dynamical electrons and hot positrons, resulting into a negative potential solitary wave pro…le which ampli…es with hot electrons temperature. Likewise, the bump soliton diminishes because of reduction in repulsive potential among hot and cold electrons in the localized solitary wave. Figure 5-9: (a)

1**Variation of hump type EA soliton structure with parameter** in **the**

presence (dashed curves R = 0:3, 0 = 0:1) and in the absence (solid curves R = 0) of magneto-rotating e¤ects. The other parameters are = 0:1, = 0:4, = 0:7, u = 0:01, = 10 , lx = 0:3. (b)

1**Variation of dip type EA soliton structure with parameter** in **the**

presence (dashed curves R = 0:3, 0 = 0:1) and in the absence (solid curves R = 0) of magneto-rotating e¤ects. The other parameters are = 0:1, = 0:25, = 0:7, u = 0:01, = 10 , lx = 0:3. 5.5 Conclusion In the present study,

1**we have** extensively **investigated the** properties of **electrostatic EA** solitary **waves in** a **collisionless e-p-i**

nonthermal magnetoplasma in a rotating frame under the Coriolis force. We have derived a LDR for the EAWs and rederived various electrostatic modes under various limiting cases from LDR.

1**Regarding the nonlinear analysis of EAWs,** we have **derived** the KdV equation **by using**

a standard

1**reductive perturbation** method. **It is found that in the** presence **of** positrons **both** bump **and dip type**

solitary structures exist. The variations in the structures of these solitary wave pro…les have been studied under various physical parameters of interest and it is found that (a) coupled magneto-rotating e¤ects seem to amplify the nonlinear structures, (b) the omission of magnetic …eld also cancels the rotating frequency, however, there remains the angle of rotation axis that a¤ects the nonlinear structures, (c) the increase in rotation frequency due to Coriolis force in the presence of constant magnetic …eld increases the amplitudes of both solitary structures, (d) the increase in electron cyclotron frequency at constant rotational frequency depreciates these structures, and (e) the increasing value of angle of the wave propagation with the magnetic …eld ampli…es the amplitudes of both opposite polarity structures. In

1**addition, the variations in the soliton** pro…les **with various parameters**

(= noc=noh, = nop=noh, 0 = Th=Tp) of interest are discussed. 5.6 Future Work In most of the laboratory and space plasmas, the plasma beta could exceed the elec- tron to ion mass ratio, necessitating the incorporation of electromagnetic e¤ects on the ITG modes. In future, one should study electromagnetic ITG modes. Furthermore, ITG mode is important in most of the magnetically con…ned thermonuclear fusion plasmas. In magnetically con…ned fusion plasmas, anomalous transport and particle ‡uxes are generally calculated by using mixing length hypothesis. In ITG modes with nonthermal electrons, new expressions for anomalous particle ‡uxes must be calculated. In future one should estimate anomalous heat transport and particles ‡uxes. In this thesis our main focus of attention in ITG mode was under various situations, when the amplitude of ITG driven waves grow can form various

5**types of nonlinear structures such as** dipolar, tripolar **vortices etc.**

To the best of our knowledge, no one has attempted to see the possi- bility of solitons and shock formation in ITG driven modes in the presence of nonthermal Kappa and Cairns distributed electrons using more sophisticated homotopoy perturba- tion method. Furthermore, in magnetosphere and even in tokamak plasma, multi-ions are always present. This work can be extended for multi-ion case

12**in the presence of non- thermal electrons. The**

above mentioned two problems should be investigated in future work. 1 2 3 4 5 6 7 13 17 18 19 20 21 22 23 24 25 26 27 28 29 30 31 32 33 34 35 36 37 38 39 40 41 42 43 44 45 46 47 48 49 50 51 52 53 54 55 56 57 58 59 60 61 62 63 64 65 66 67 68 69 70 71 72 73 74 75 76